AN ABSTRACT OF THE THESIS OF

Robert Keith Lytz for the degree of Doctor of Philosophy

in Chemistry presented on August 28, 1978

Title: X-Ray Structure Studies of Oriented Phospholipid Membranes

Abstract Approved: Redacted for Privacy

H. Hollis Wickman

Lamellar x-ray diffraction was studied from thin films of L-α-1,2-dipalmitoyl lecithin (DPL) and a 1:1 mixture (BrDPL) of L-α-1-palmitoyl-2-(9-bromopalmitoyl) lecithin and its 10-bromo analog. The specimens had high lamellar order, with an upper bound on the mosaicity of 6 mrad (0.4°) for DPL and BrDPL.

With various water contents, BrDPL underwent a broad, thermal transition centered around 0°C. The transition was evidenced by a reduction in lamellar spacing and a reduction in higher-order reflections at higher temperatures. In these respects, the transition was like the gel-liquid crystal transition known to occur in other phospholipids.

An isomorphous replacement procedure was used to find the phase factors needed to synthesize electron-density profiles (assumed symmetric) for DPL and BrDPL. The resulting profile for DPL was similar to profiles which have been reported for phospholipid multilayers. The profile deduced for BrDPL was also similar, with the addition of a peak corresponding to the location expected for bromine if the hydrocarbon chains were

fully extended.

A one-dimensional, position-sensing proportional counter was built and characterized, in order to collect diffraction data from the lipid specimens. Using it, survey scans of the specimens were done in five minutes. Similar scans required several hours when film was used.

X-Ray Structure Studies of Oriented Phospholipid Multilayers

by

Robert Keith Lytz

A THESIS

submitted to

Oregon State University

in partial fulfillment of
the requirements for the
deqree of

Doctor of Philosophy

June 1979

APPROVED:

Redacted for Privacy

Associate Professor of Chemistry
in charge of major

Redacted for Privacy

Chairman of the Department of Chemistry

Redacted for Privacy

Dean of Graduate School

Date thesis is presented 28 August 1978

Typed by Pamela S. Lytz for Robert Keith Lytz

ACKNOWLEDGEMENTS

I wish to thank my wife, Pam Lytz, who has given me all imaginable support and encouragement during my graduate career. In addition to sharing all aspects of graduate-student life, Pam has punched my computer programs, done bibliographic searches and editing, and typed, illustrated, and edited this dissertation.

I would like to thank Hollis Wickman, my thesis adviser, for his generous support of my work, for his many helpful suggestions, and for his concern for my professional development.

Thanks go to Joe Reinert and Bob Lowry for synthesizing and characterizing the lipids upon which this work depended. In addition, I want to thank Joe for some very helpful conversations.

I wish to thank David Shoemaker for graciously allowing me the long-term use of his laboratory and equipment and for his interest in my graduate work.

I would like to thank Margaret Brault, Ted Hopkins, Steve McCann, and Eric Salin for their enriching friendship and for their considerable help.

And I want to thank my parents, who have always encouraged my formal education, and who have waited patiently for it to be completed.

The research described in this dissertation was supported by National Science Foundation Grants DMR 71-01792 and DMR 76-82091. Travel, computation, and equipment grants from the Oregon State University Research Council are also gratefully acknowledged. Finally, I wish to thank the Oregon State University Environmental Health Sciences Center for partial support of this research in the form of a Pilot Project Grant.

TABLE OF CONTENTS

Page

LIST OF FIGURES

LIST OF TABLES

X-RAY STRUCTURE STUDIES OF ORIENTED PHOSPHOLIPID MULTILAYERS

I. INTRODUCTION

Biological membranes take part in a large variety of important physiological functions [1]. Broadly, these include:

1. Selective maintenence and alteration of the concentration of chemical species in cells and organelles;
2. Energy storage and utilization;
3. Communication with the cell environment;
4. Cell defense.

Biomembranes consist largely of proteins and lipids (most often phospholipids and cholesterol) [2]. There have been several general models of membrane structure [3,4], among which the fluid mosaic model, put forth by Singer and Nicolson [5] in 1972, is consistent with current physical, chemical, and biological data (see Figure 1). This model, which differs from earlier ones mainly by taking into account the mobility of membrane constituents [6], depicts a "two-dimensional solution of oriented globular proteins and lipids." The lipids form a biomolecular layer, with the hydrophilic headgroups of the lipids facing outward, toward the aqueous environment, and with the lipid hydrocarbon region forming a fluid within the layer. Proteins may be associated with the hydrophilic exterior (peripheral proteins) or may be embedded partly or fully in the lipophilic interior (integral proteins). In this view, the lipid matrix, being fluid, allows short-range interaction among the proteins, but does not impose long-range,

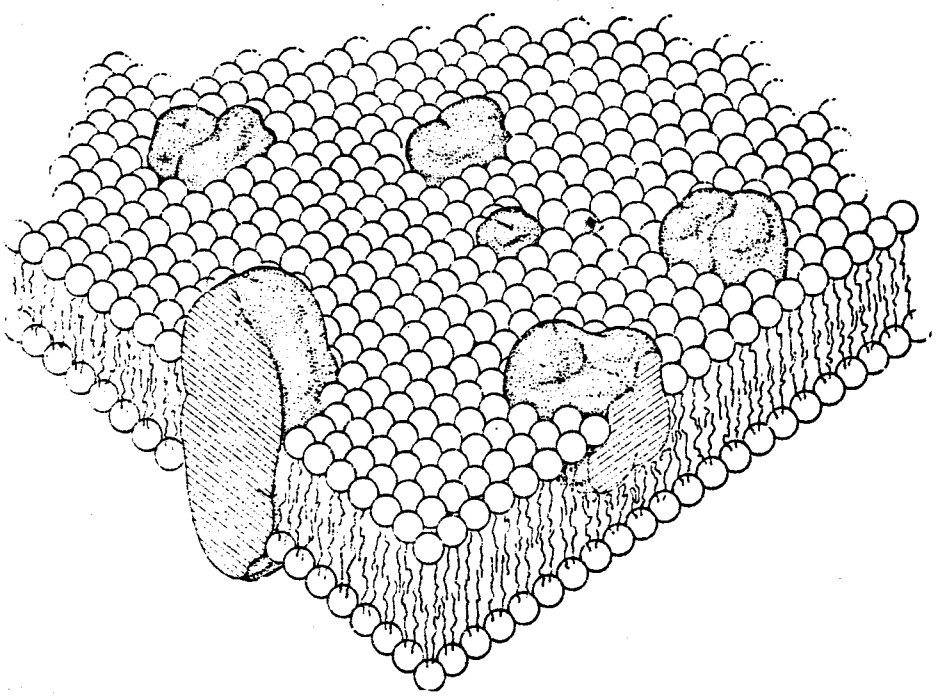

Figure 1. The fluid mosaic model of membrane structure proposed by Singer and Nicolson (from [5]).

lateral order on them.

Phospholipid multilayers, which form spontaneously from mixtures of water and lipid, are easily-prepared analogs of the lipid matrix of natural membranes. These multilayers are known [7-9] to consist of bilayers which undergo an endothermic transition as the hydrocarbon chains melt. Reinert and Steim [10] demonstrated calorimetrically that live Acholeplasma laidlawii undergo this transition and, based on the measured enthalpy change, concluded that most of the Acholeplasma lipid is in the bilayer state. This conclusion supports the use of phospholipid-water multilayers, either unadulterated, or with appropriate additives, as membrane analogs.

Considerable x-ray diffraction has been done on lipid multilayers, multilayers with additives, and natural membranes [11-13]. The wide-angle diffraction peaks are characteristic of the extended (gel) and melted (liquid crystalline) states of the lipids in the bilayers.

In contrast, low-angle diffraction from multilayers, which we have studied, reflects the layer spacing, and contains information about the electron density of the layers projected along a line perpendicular to them. Unfortunately, the information from a single diffraction pattern is not usually sufficient to reconstruct the electron-density distribution which produced it, and stratagems must be used to supply the missing information.

Our approach to this phase problem is the technique of isomorphous replacement [14,15], in which independent sets of data are collected from several (in our case, two) structures which are believed to be identical, except for a difference which is assumed known. Toward

this goal, we have collected and interpreted low-angle diffraction data from multilayers of L-α-1,2-dipalmitoyl lecithin (DPL) and multilayers of a mixture (BrDPL) of equimolar amounts of L-α-1-palmitoyl -2-(9-bromopalmitoyl) lecithin and its 10-bromo isomer (Figure 2). The BrDPL was prepared by J. Reinert and R. Lowry [16].

The immediate purpose of our diffraction study was to determine whether the lipid isomorphs would lead to electron-density profiles consistent with those reported in the literature, which were derived using other phasing methods. There would be several implications of a positive result. First, electron-dense additives to multilayers could be located by a similar phasing scheme. Such additives might be indigenous to biomembranes, such as metal-containing proteins, or they might be exogenous, such as halogenated pesticides. In addition, a multilayer additive with insufficient electron-density contrast to be distinguished in a correct reconstruction of the bilayer profile could be located if an electron-rich atom, such as bromine, were introduced into it.

Finally, the fact that Acholeplasma laidlawii produces phospholipids corresponding to its dietary intake of fatty acids [17] might allow isomorphous methods to be used for phasing diffraction from intact Acholeplasma membranes. This possibility is strengthened by the report of Andrews and coworkers [18] that A. laidlawii thrived on 12,12-dimethyl-12-stannahexadecanoic acid, incorporating up to 39% of the acyl chains in its membrane lipids from this chemical species.

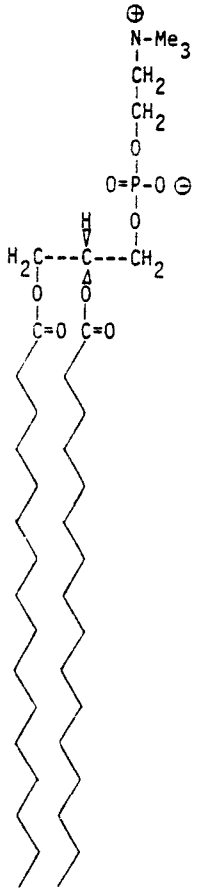

DPL

L-α-1,2-dipalmitoyl lecithin

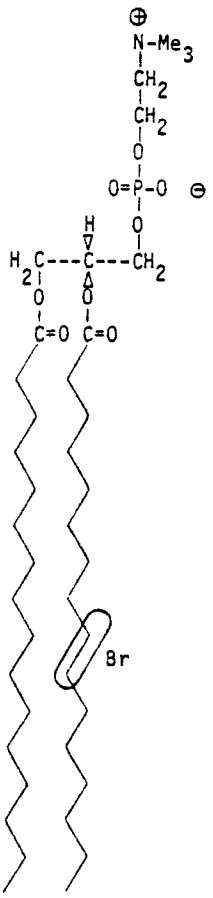

BrDPL

an equimolar mixture of
L-α-1-palmitoyl-2-(9-bromopalmitoyl) lecithin
and
L-α-1-palmitoyl-2-(10-bromopalmitoyl) lecithin

Figure 2. The lipids used in this study.

The phase problem in the context of one-dimensional, centrosymmetric systems is discussed in Chapter IV, below. In broad terms, the types of solution to this problem that have been applied to multilayer diffraction include

1. Isomorphous replacement;
2. Swelling;
3. Deconvolution.

The approach used in our study is isomorphous replacement. Bromine atoms near the center of the hydrocarbon chains of the phospholipids serve as the isomorphous substituents. Our method is an extension of that of McIntosh et. al. [19,20], who determined the structure of fatty acid multilayers, using as substituents dipositive ions saponified to the carboxylate groups. Our implementation differs from that of McIntosh in that (1) our substituent is not at the unit-cell origin and (2) we evaluate all possible combinations of the phase factors. The isomorphous replacement techniques used by McIntosh and by us are based on the 1957 work of Hargreaves [14].

Techniques using swelling depend on the fact that the lamellar spacing of lipids increases with increasing water content. They depend also on the assumption that all the added water goes between lipid layers, causing no change in the layers themselves. Although there are many ways of dealing with the data from such experiments, they are similar to isomorphous replacement in that phases are estimated by taking advantage of several sets of independent data which arise from essentially the same structure. Franks [21] and Levine and Wilkins [22] have used this approach for multilayers of egg

lecithin with and without cholesterol. It has been applied by Stamatoff, Krimm, and Harvie [23] to red blood cell membranes. It has also been used to elucidate the structure of nerve myelin by Blaurock [24], Worthington and King [25], and Stamatoff and Krimm [26].

Deconvolution methods are described by Worthington, King, and McIntosh [27]. They have been applied to retinal photoreceptors (Worthington and Gras [28]) and to nerve myelin (Worthington and McIntosh [29]). These methods may be used only when a substantial fraction of the unit cell has constant electron density, e.g., a water layer in the case of oriented, hydrated membranes.

The x-ray diffraction data in our work has been collected using a linear position-sensing proportional counter similar to one described in 1968 by Borkowski and Kopp [30]. This kind of detector, which has been referred to as "electronic film" [31], allows rapid collection, digitizing, and viewing of an entire diffraction pattern, without motion of the detector. A one-dimensional, or linear, detector is well suited to collect lamellar diffraction data, which arises from a one-dimensional electron-density profile, and which appears along a single line when film is used. DuPont and coworkers have used such a detector to observe low- and wide-angle diffraction from membrane and lipid systems [32]. Schelten and Hendricks [33], have described construction of a facility at Oak Ridge National Laboratory to utilize a two-dimensional detector for small-angle scattering. Using data from a two-dimensional detector, Kraut's group [31,34] has completed models for dehydrofolate reductase and derived electron-density maps

for cytochrome c peroxidase. They report that with the position-sensing detector, data collection is about 30 times faster for a given number of reflections than it would be with a conventional diffractometer.

II. POSITION-SENSING DETECTORS--BACKGROUND

A. Historical Perspective

The position-sensing detectors used in this project are similar to those developed by Borkowski and Kopp in 1968 [30]. These risetime (also called RC-encoded) detectors are akin to the classic gas-ionization chambers originated seventy years ago by Rutherford and Geiger [35], but have the additional, useful ability to provide information about the location of incoming radiation.

Beginning in the early 1950s [36], but especially since the late 1960s, many kinds of position-sensing detector of nuclear radiation have been developed. The wide variation in their operating principles is evident in this brief summary:

I. Gas-ionization detectors
   - A. Digital position output
     1. Multiwire spark chamber [36]
     2. Multiwire proportional chamber [37-50]
   - B. Analog position output
     1. RC-encoded (risetime) [30,51-57]
     2. Charge division [58-64]
     3. Multiwire delay line [65-74]
     4. Backgammon [75]

II. Detectors other than gas-ionization [76]
   - A. Vidicon
   - B. Semiconductor [77]
   - C. Charge coupled device
   - D. Microchannel plate [78-82]
   - E. Image intensifier

B. Principles of RC-Encoded Detectors

A schematic diagram of a detection system using a one-dimensional, RC-encoded, position-sensing proportional counter is shown in Figure 3. This configuration, which was employed in our diffraction experiments, is based on the design of Borkowski and Kopp [30]. The detector itself is similar to gas-filled counters which do not convey position information: an incident photon, through photoionization and gas multiplication in the fill gas [83], generates many electrons and ions. Under the influence of a constant electric field produced by biasing the electrodes, electrons move to the anode, where they are collected, and cations move to the cathode, where they are neutralized. The resultant change in potential between the anode and cathode is sensed at the ends of the anode, signaling the detection of radiation.

In the RC-encoded detector, the position along the anode at which radiation enters is available because a highly resistive anode is used and because the anode and cathode behave as a cylindrical capacitor. In our detector the resistance and capacitance per unit length, R_o and C_o, were typically 8 MΩ/m and 10 pF/m. This arrangement of resistance and capacitance causes the anode and cathode to act together as a distributed RC line, a special case of the well-known RCLG transmission line [84]. As signals pass through an RC line, their shapes are changed, the change increasing with the distance traveled by the signal. This signal-shaping effect is the

basis of the RC-encoded detector: it allows the entry positions of photons to be distinguished according to the shape of the signals that are produced.

The signal-shaping influence of the detector can be seen in Figures 4 and 5 . The detector, behaving as a distributed RC line, is approximated as a ladder network of discrete resistors and capacitors. Each ladder element, consisting of one series resistor and one shunt capacitor, acts as a low-pass RC filter, which selectively attenuates and shifts high-frequency components of the signal more than it does low-frequency components.

Figure 5 illustrates the principle involved. The output voltage $v_{out}(t)$ is calculated for application of a unit voltage impulse (delta function) to 2- and 4-element RC ladder networks, using tabulated transfer functions [85]. The broadening of the impulse in these discrete circuits is analogous to the process which occurs in the distributed line of the detector.

Decoding, the extraction of position information, is illustrated in Figure 3, where encircled numbers refer to typical waveforms found at various points in the instrument network. In this example, radiation enters the detector near the end of the anode from which signal ② is derived (also called the START end for reasons which will become apparent). Signals ① and ② differ in shape as a result of traversing different lengths of the RC line. They are further filtered by the linear amplifiers into bipolar pulses ③ and ④ . The difference, Δt, in the time at which the bipolar pulses cross the baseline

(marked by dots on ③ and ④) can be made a linear function of the entry position of radiation by matching the filter characteristics of the linear amplifiers to the electrical properties of the detector.

Crossover of ③ and ④ triggers timing signals ⑤ and ⑥ from the timing single channel analyzers. These signals start and stop the time to amplitude converter, producing an analog pulse ⑦ whose height is proportional to Δt and therefore proportional to the entry position of the photon. The analog pulse height ⑦ is finally digitized and stored by the multichannel analyzer, which displays a graph of counts versus photon position.

Borkowski and Kopp [54] have derived the transfer function of the RC-encoded detector. From it, they have deduced approximate relations among the distributed resistance and capacitance of the line, the impedance of the line termination, filter characteristics of the linear amplifiers, and S, the spatial sensitivity (= Δposition/Δtime).

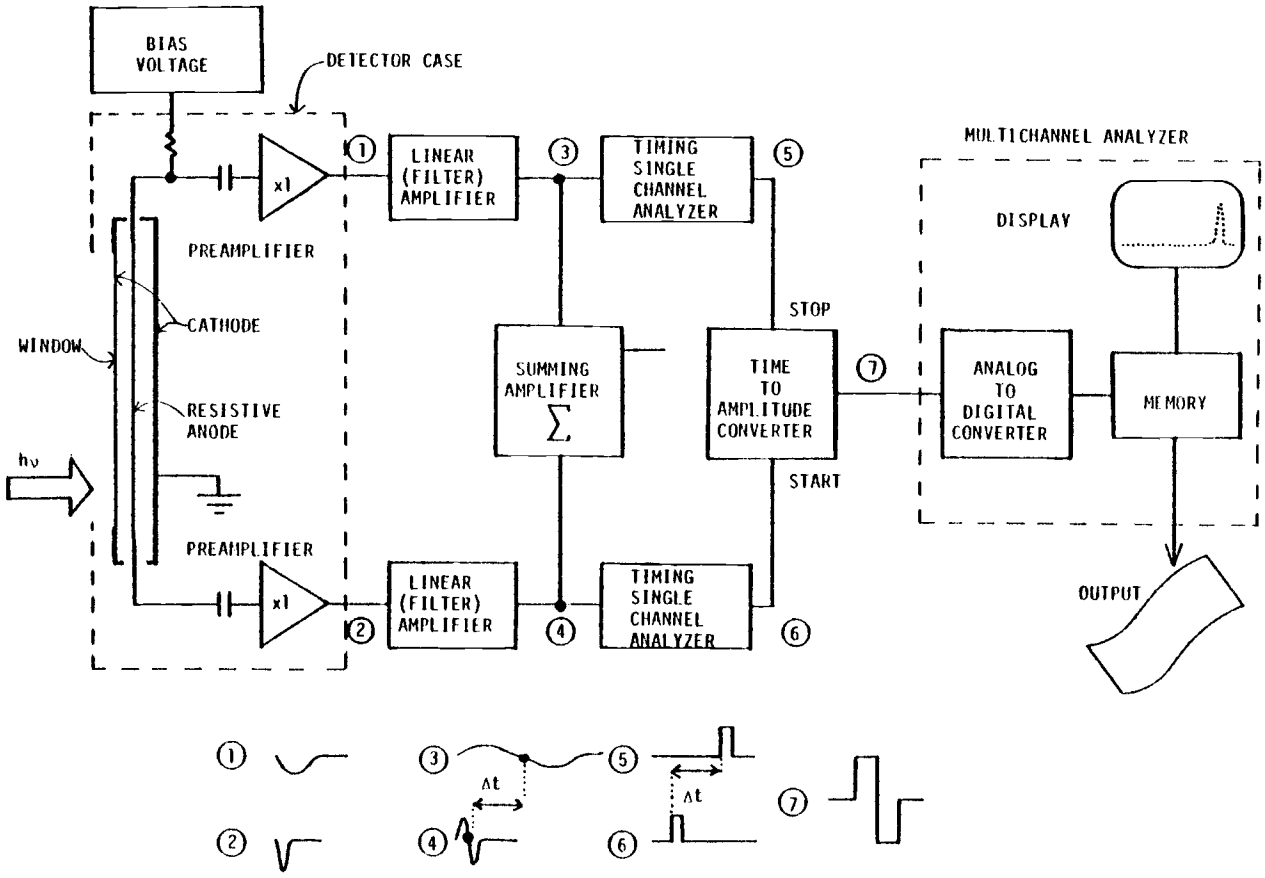

Figure 3. Block diagram of RC-encoded detector system.

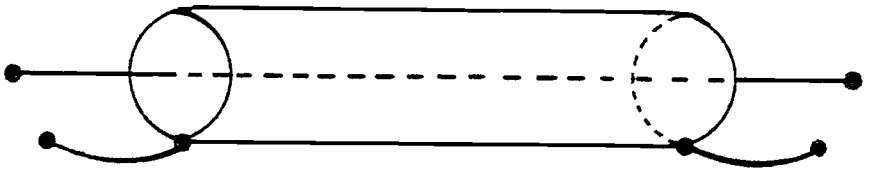

DETECTOR ANODE AND CATHODE

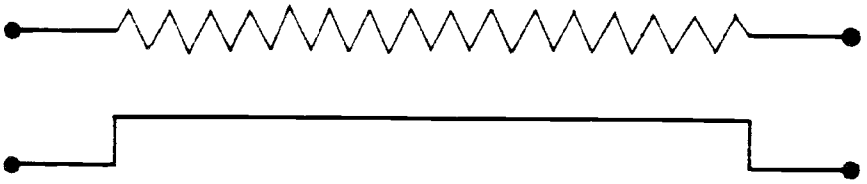

DISTRIBUTED RC LINE

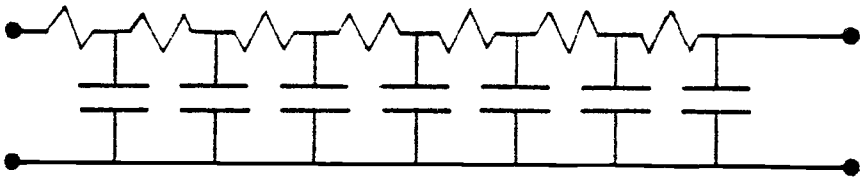

DISCRETE RC LADDER

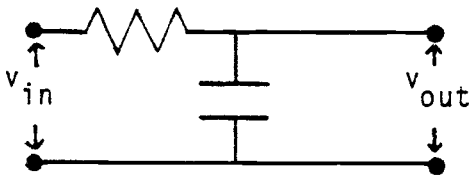

LOW-PASS RC FILTER

Figure 4 . Electrical interpretation of RC-encoded detector.

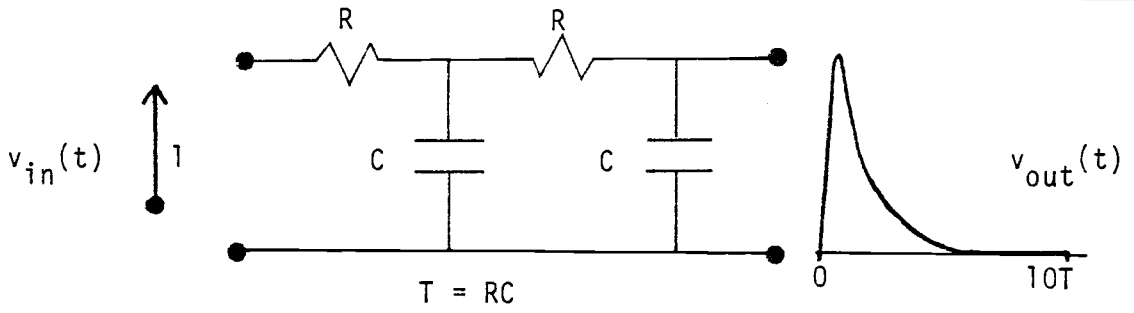

$$\mathcal{V}_{in}(s) = 1$$

$$\mathcal{V}_{out}(s) = [T^2s^2 + 3Ts + 1]^{-1}$$

$$v_{in}(t) = \delta(t)$$

$$v_{out}(t) = T^{-1}[0.22e^{-0.764t/T} - 0.22e^{-5.23t/T}]$$

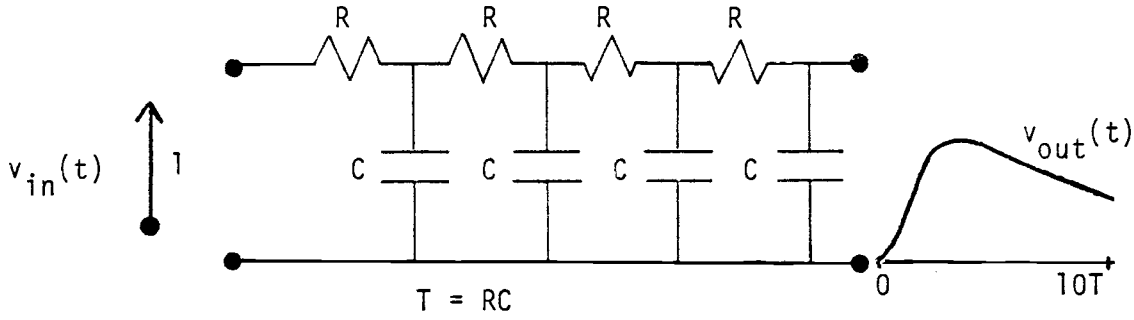

$$\mathcal{V}_{in}(s) = 1$$

$$\mathcal{V}_{out}(s) = [T^4s^4 + 7T^3s^3 + 15T^2s^2 + 10Ts + 1]^{-1}$$

$$v_{in}(t) = \delta(t)$$

$$v_{out}(t) = T^{-1}[-0.099e^{-3.53t/T} + 0.283e^{-2.35t/T} - 0.337e^{-1.00t/T} + 0.152e^{-0.13t/T}]$$

Figure 5. Impulse response of 2- and 4-element RC ladders.

III. EXPERIMENTAL RESULTS FOR DETECTORS

A. Detector Construction and Performance

The two RC-encoded, 1-dimensional, position-sensing detectors built and used in our laboratory are designated D1 and D2. Both employed continuous flow of the fill gas, 90% argon-10% methane. D2, used for the diffraction experiments reported here, was operated at a total pressure around 380 kPa (3.7 atm). D1, designed for use at ambient pressure only, was superseded by D2, which was several times more efficient. Apart from the difference in efficiency, the performance of the two detectors was quite similar. Performance and operating parameters for the pressurized detector, D2, are given in Table 1 .

Table 2 summarizes construction data for the detectors. Figure 6 shows D2, in which o-rings sealed the aluminized mylar windows and anode mounts to the cathode body. The mylar was a gift of Mr. C.J. Gagnon, Metallized Products Division, King-Seely Thermos Company, Winchester, MA. D1 was built similarly, differing mainly by having a beryllium window and no o-rings. The window frame of D1 was pressed to the cathode by the detector housing and sealed with latex cement; anode mounts were held in place with epoxy.

The anode wires used routinely were 20-μm diameter quartz fibers coated with pyrolitic graphite. These fibers, with a resistance of 8 MΩ/m, were purchased from Reuter-Stokes, Inc, Cleveland, OH. For experiments concerning resolution and sensitivity, fibers of solid

pyrolytic graphite (Thornel, trademark) were also used. These fibers had a diameter of 7 μm and a resistance of 0.05 MΩ/m. They were a gift of Ms. S.L. Horniak, Carbon Products Division, Union Carbide, New York, NY.

Before installation in the cathode, the anode was inspected microscopically at a magnification of 100x. Fibers with apparent surface defects were discarded. The cathode and selected anode were carefully rinsed with 2-propanol before and after installation. During installation, the anode was secured at each end to copper leads with both 5-minute epoxy and silver-loaded, conductive epoxy. Each such junction was sealed to its delrin mount at the end of the cathode with 5-minute epoxy, tension [57] being applied with a 10-g weight suspended from one lead while the epoxy set.

The two preamplifiers (Tennelec TC 212), which were on 3.8 cm x 5.5 cm printed circuit boards, were secured in the detector case directly behind the cathode chamber. Lead length from the chamber to each preamplifier was 1-2 cm. The inside of the acrylic detector case was lined with 0.2 mm aluminum sheet, which was electrically connected to the cathode and to the power supply ground.

Table 1 . Performance and operating parameters for detector D2.

Usable length	95 mm
Window width	4.0 mm
Chamber depth	4.0 mm
Anode resistance	8 MΩ/m
Anode-cathode capacitance	12 pF/m
Termination capacitance	0.5 pF
Fill gas	90% argon-10% methane
Pressure	380 kPa
Bias	2200 V
Filter time constant	2 μs (nominal)
Filter passband center	1.4 Mrad/s
Spatial sensitivity	26 μs/m
Point spread	0.4 (0.5)* mm fwhm
Curve fit deviation	
linear	0.9 (1.4) mm
cubic	0.1 (0.2) mm
Drift over 24 hours	0.06 mm
Quantum detection efficiency	0.09
deviations full length	3 (5)%
Energy resolution, 8 keV	18% fwhm

* For entries with two numbers, the first is the mean value, and the second (in parentheses) is the maximum.

Table 2 . Construction data for detectors.

Detector	D1	D2
Cathode		
material	machined aluminum	machined aluminum
≠ length, L (mm)	85	100
≠ height, H (mm)	9.5	3.9
≠ depth, D (mm)	2.5	3.9
Window		
material	beryllium	aluminized mylar
thickness (μm)	50	25
Anode mount	delrin, epoxied to cathode	threaded delrin, with o-ring
Operating pressure	ambient	to 400 kPa
Anode*		
material	quartz, coated with pyrolytic graphite	quartz, coated with pyrolytic graphite
diameter (μm)	20	20
resistance (MΩ/m)	8	8

* typical ≠ cavity

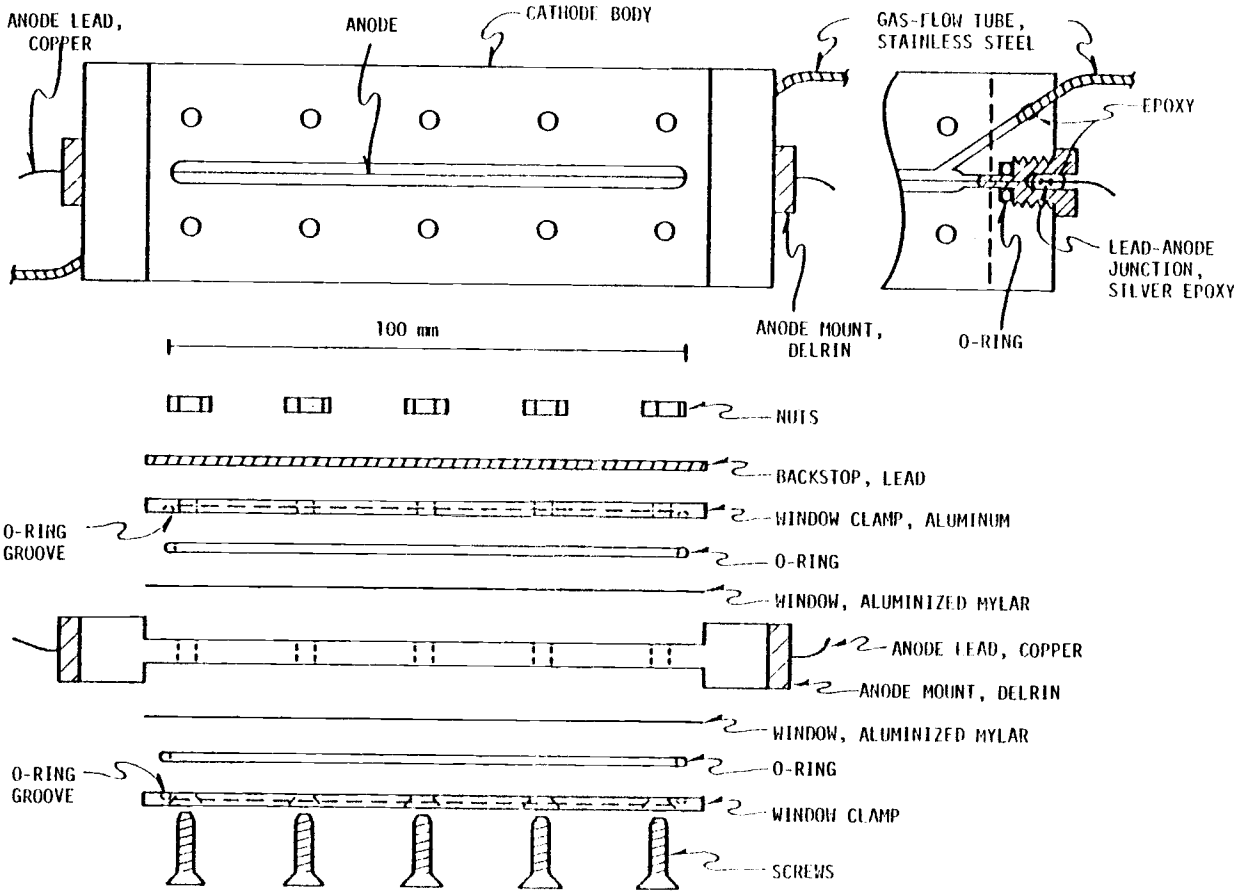

Figure 6(a). Pressurized detector D2 (schematic).

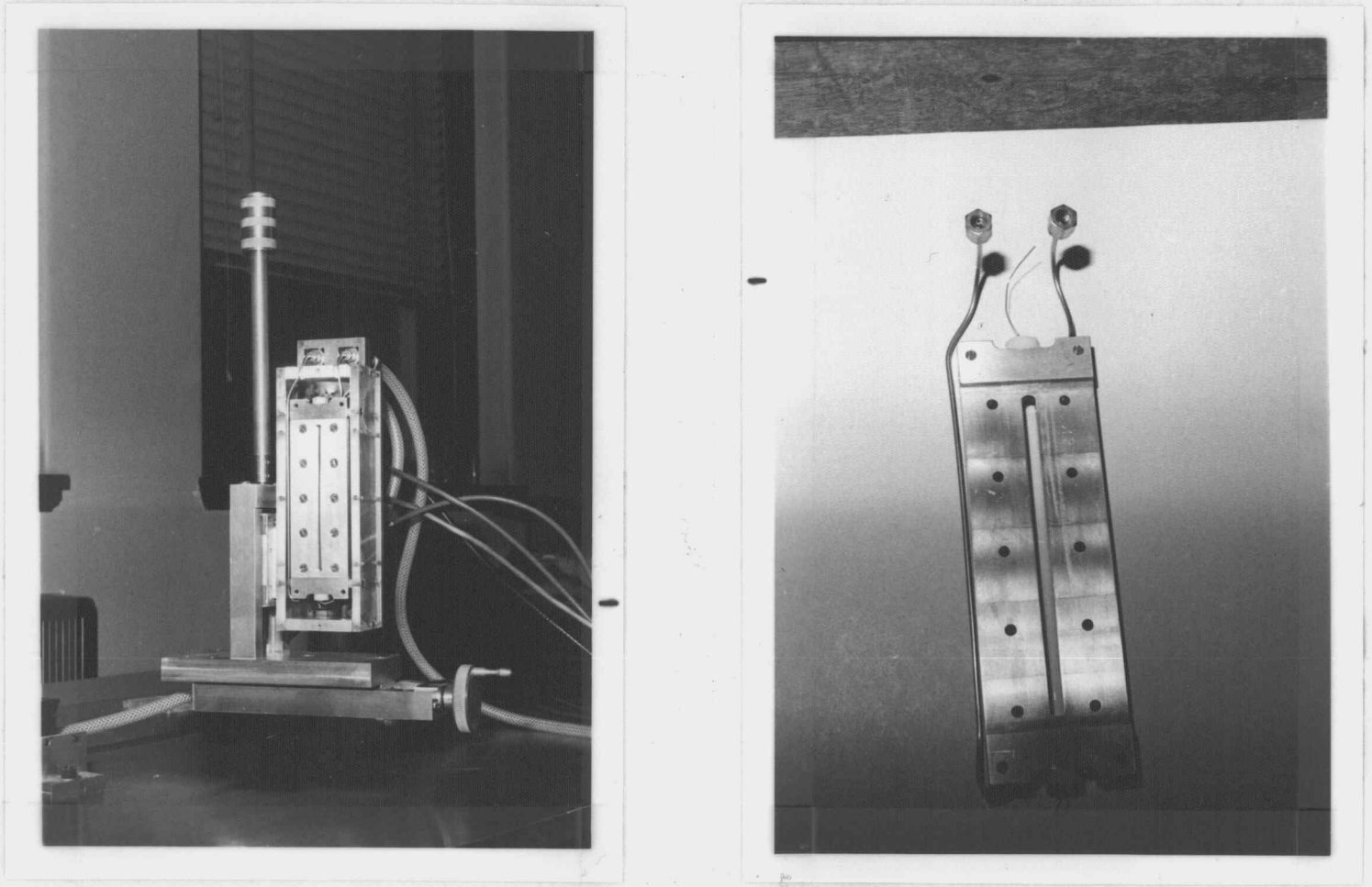

Figure 6(b). Pressurized detector D2.
Left: detector
Right: cathode-anode chamber

B. Stability of Detector and Source

A fundamental requirement for diffraction data to be usable is that neither the intensity of the direct beam at the specimen nor the efficiency of the detector change appreciably with time. Simple counting experiments were used to determine the stability over time of the detector and x-ray generating apparatus employed in subsequent diffraction studies. Both detector D2 and the x-ray source (Picker constant potential generator with copper tube--see Chapter II) were found stable enough for use in diffraction, with a combined error of less than 1%. Using the technique of section D of this chapter, the position calibration for the detector changed by only 0.06 mm rms over a 24-hour period.

Results for repeated counting experiments with the detector and Cu tube are given in Table 3. Interpretation is based on the Poisson distribution, which is expected for a random emissive process whose mean rate does not change over the experimental time span [88]. This distribution requires that $\sigma \simeq M^{1/2}$ for a series of identically performed counting experiments (M = mean counts, σ = standard deviation). This equation is equivalent to $\sigma/M \simeq M^{-1/2}$ for the relative deviation.

Count-rate stability of the detector was established by irradiating a small portion of the detector window with a beam of 6-keV x-rays from a 100-μCi ^{55}Fe source ($t_{1/2}$ = 2.6 y). For the number of counts sampled, variation in the counting rate was explained by the expected statistical variation in activity of the source. This experiment was carried out over ten hours.

The stability of the collimated beam from the Picker Cu tube (14 kV, 2 mA) was determined using a NaI(Tl) scintillation detector, which was assumed to be 100% efficient. The relative deviation for a series of counting experiments was 0.3%, three times the statistically expected value (Table 3). This discrepancy implied a drift in intensity of the source over the 200-minute span of the counting experiments, but this small a drift was not detrimental to interpreting diffraction data.

Table 3. Counting rate variations for detector D2 and for the Picker Cu x-ray source.

	^{55}Fe source with detector D2	Picker x-ray tube with NaI(Tl) detector
Number of samples	9	10
Sample period (ks)	3.600	1.200
Mean rate (counts/s)	19.9	927
M, mean counts	71 680	1 112 852
σ, standard deviation	301	3 167
σ/M (%)	0.4	0.3
$M^{-1/2}$ (%)	0.4	0.1

C. Calibration using Collimated Beam

1) Calibration Parallel to Anode

Ideally, a set of equally intense, equally spaced, finely collimated beams normal to the detector window should produce a comblike display of equally spaced, very narrow peaks, each with the same integral count. Deviations from this ideal are called nonlinearity, point spread, and nonuniformity. If the display peaks are not equally spaced, the detector is said to be nonlinear. If the peaks have different integral counts, it is said to be nonuniform. If the peaks are broadened, the resolution is said to be poor, and the point spread appreciable.

These deviations were estimated by translating the detector in the direction collinear with the anode at equal intervals before a slit-collimated x-ray beam and counting for the same time at each position. Ni-filtered Cu x-rays (14 kV, 2 mA) were further attenuated by a 0.2 mm sheet of aluminum between the generating tube and collimator. Actual beam width at the detector was less than 0.1 mm fwhm, determined photographically. Stability of the x-ray source was better than 0.5%.

The program CALIB (Appendix C) was written to analyze and plot these data. Typical results for detectors D1 and D2 are given in Table 4 and in Figure 7.

Both detectors had a variation of less than 5% in spatial sensitivity (channels/mm) from end to end. Both had a point spread

of less than 0.45 mm fwhm averaged over all positions. For D1, end-to-end variation in integral count was 0.5% mean, 1% average. For D2 this variation was 3% mean, 5% maximum.

2) Calibration Perpendicular to Anode

The variation in relative efficiency as the beam was translated along a line perpendicular to the anode (and to the detector window) was determined. This was done using the calibration technique described in the immediately preceding section, with the detector rotated by $\pi/2$ rad.

This variation, which is plotted in Figure 8, was smooth and symmetric, with a falloff of about 20% 1.5 mm either side of the central (anode) position. The variation was probably due to the observed bulging of the mylar windows under pressure, which resulted in the path length through the fill gas being longer for photons entering centrally than for those entering near the chamber edges.

Table 4. Calibration analysis from program CALIB. Top: unpressurized detector D1. Bottom: pressurized detector D2 at 380 kPa.

0488 22FEB77 UNPRESSURIZED DETECTOR

POSITION (MM)	CENTROID CHANNEL	INTEGRAL COUNT	NORM COUNT	CHANNELS PER MM	FWHM (MM)
15.00	27.50	29340	1.000		
20.00	59.46	29340	1.000	6.439	.560
25.00	91.89	29343	1.000	6.416	.453
30.00	123.62	29371	1.001	6.345	.422
35.00	155.34	29134	.993	6.320	.410
40.00	186.82	29425	1.003	6.260	.424
45.00	217.94	29259	.997	6.205	.391
50.00	248.87	29686	1.011	6.194	.407
55.00	279.98	29436	1.003	6.245	.397
60.00	311.32	29494	1.005	6.352	.413
65.00	343.40	29212	.995	6.451	.415
70.00	375.83	29241	.996	6.524	.408
75.00	408.64	29431	1.002	6.547	.433
80.00	441.30	29215	.995	6.469	.448
85.00	473.33	29346	1.000		
MEAN		29350	1.000	6.367	.430
STANDARD DEV		135	.005	.118	.043
RELATIVE DEV (%)		.46	.46	1.86	10.05
CENTER/END				.954	

F45A 15MAY78 PRESSURIZED DETECTOR

POSITION (MM)	CENTROID CHANNEL	INTEGRAL COUNT	NORM COUNT	CHANNELS PER MM	FWHM (MM)
10.00	57.83	49222	.992		
15.00	82.53	49992	1.006	4.969	.390
20.00	107.52	51115	1.031	4.942	.419
25.00	131.95	48894	.986	4.890	.396
30.00	156.42	52440	1.056	4.932	.443
35.00	181.27	52242	1.052	4.934	.435
40.00	205.76	51214	1.032	4.893	.433
45.00	230.29	50559	1.018	4.880	.432
50.00	254.56	51139	1.030	4.913	.432
55.00	279.33	49913	.999	4.956	.411
60.00	304.12	49977	1.007	5.022	.387
65.00	329.55	49996	1.007	5.075	.396
70.00	354.87	48849	.977	5.132	.374
75.00	380.87	47541	.955	5.258	.423
80.00	407.45	46646	.936	5.217	.379
85.00	433.04	48827	.973	5.156	.430
90.00	459.01	47706	.948		
MEAN		49963	1.000	5.011	.395
STANDARD DEV		177	.036	.125	.033
RELATIVE DEV (%)		3.56	3.56	2.50	9.51
CENTER/END				.969	

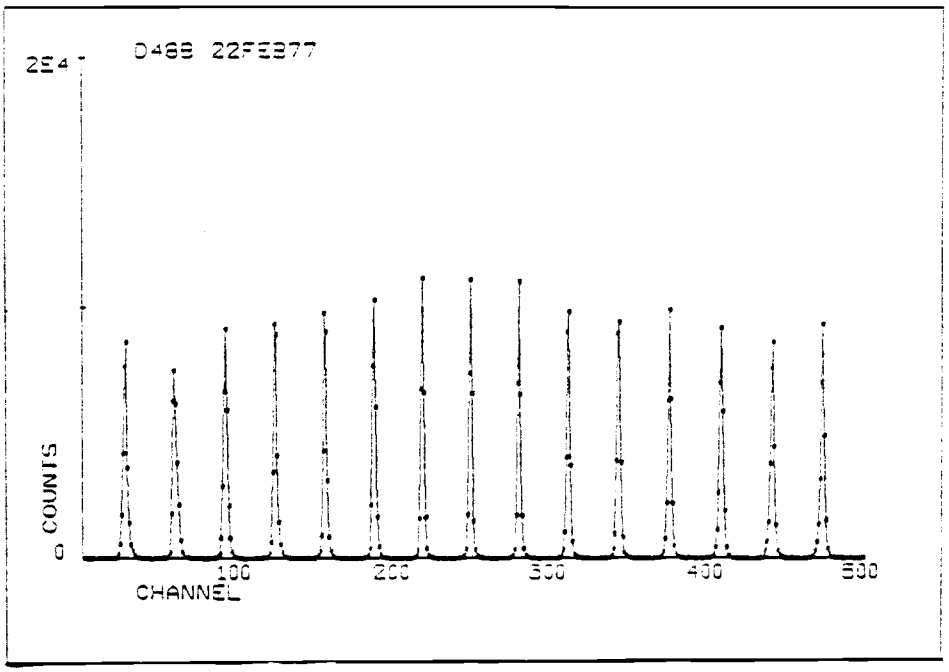

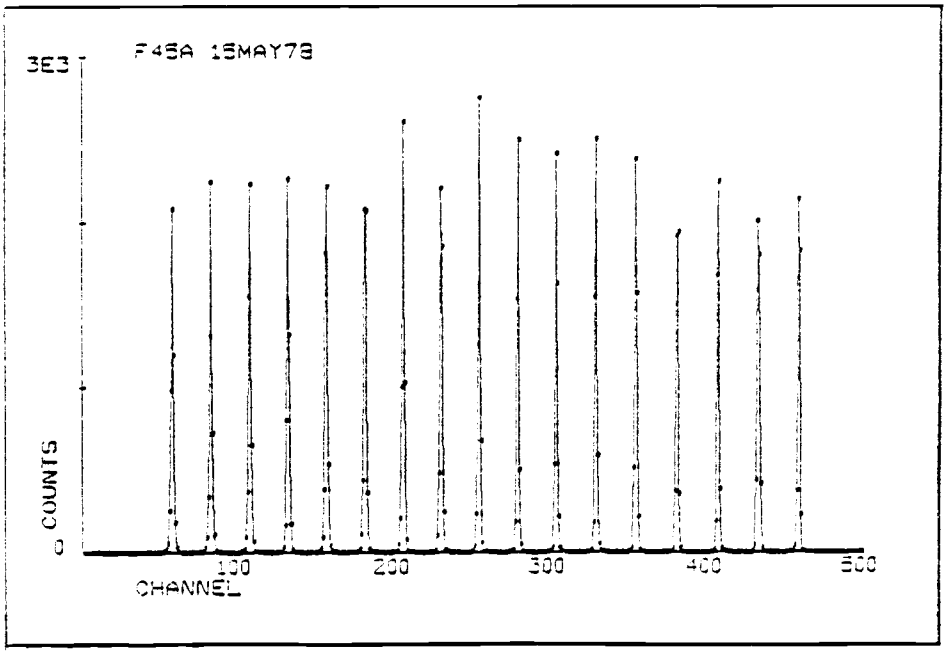

Figure 7(a). Calibration pattern for CALIB--counts vs channel. Top: unpressurized detector D1. Bottom: pressurized detector D2 at 380 kPa.

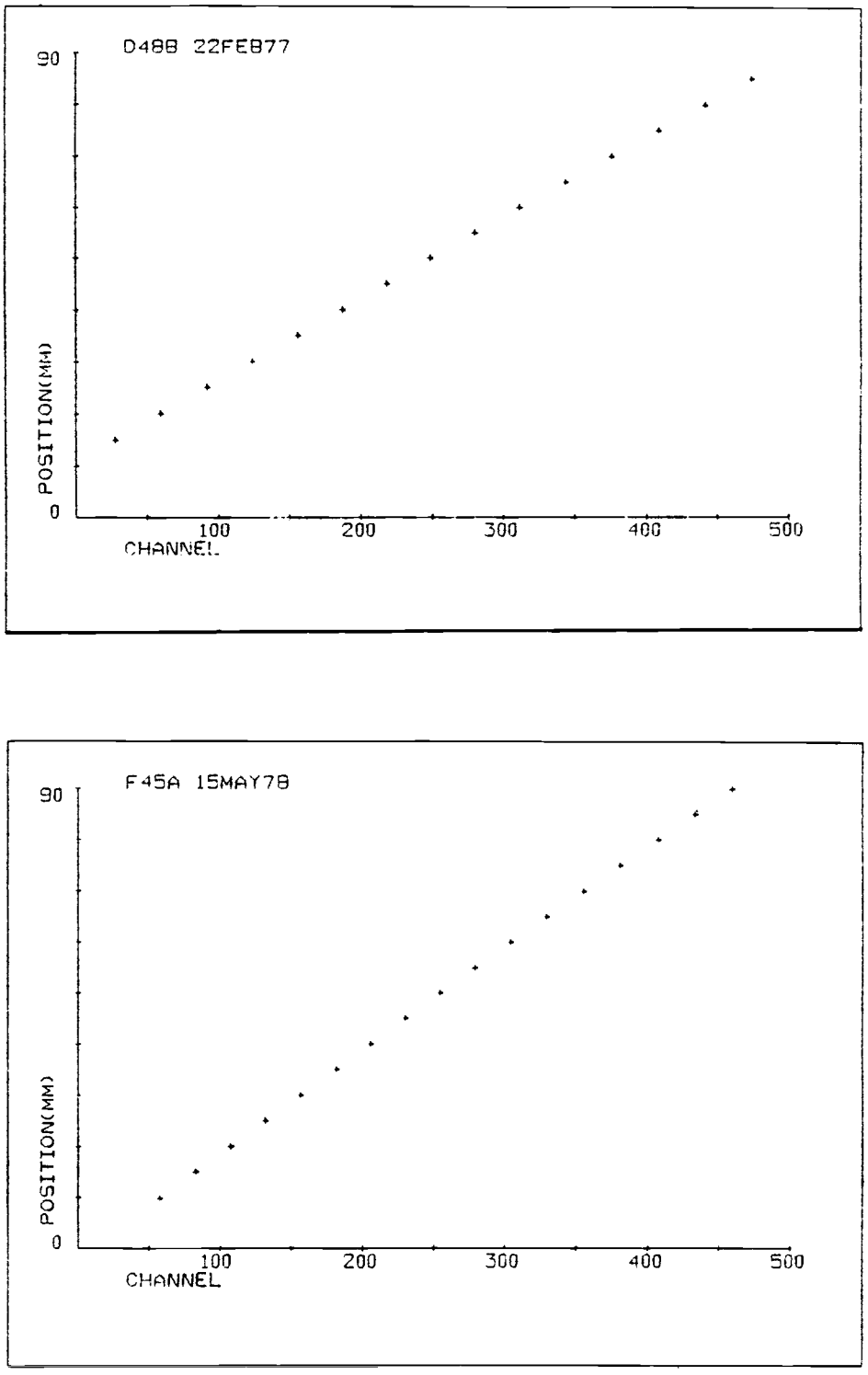

Figure 7(b). CALIB output--position vs channel centroid. Top: unpressurized detector D1. Bottom: pressurized detector D2 at 380 kPa.

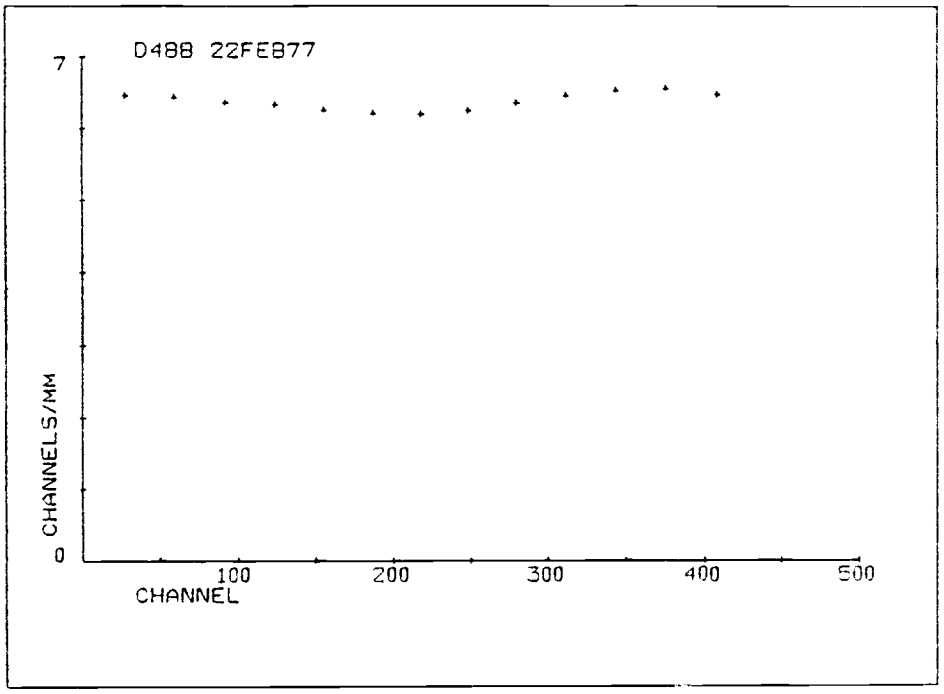

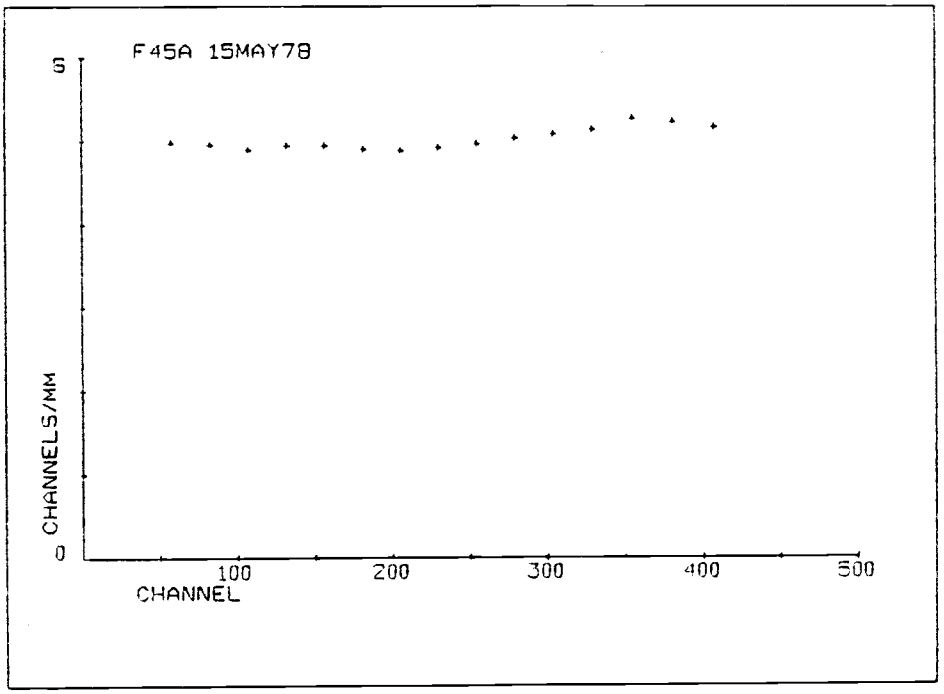

Figure 7(c). CALIB output--channels/mm vs channel centroid. Top: unpressurized detector D1. Bottom: pressurized detector D2 at 380 kPa.

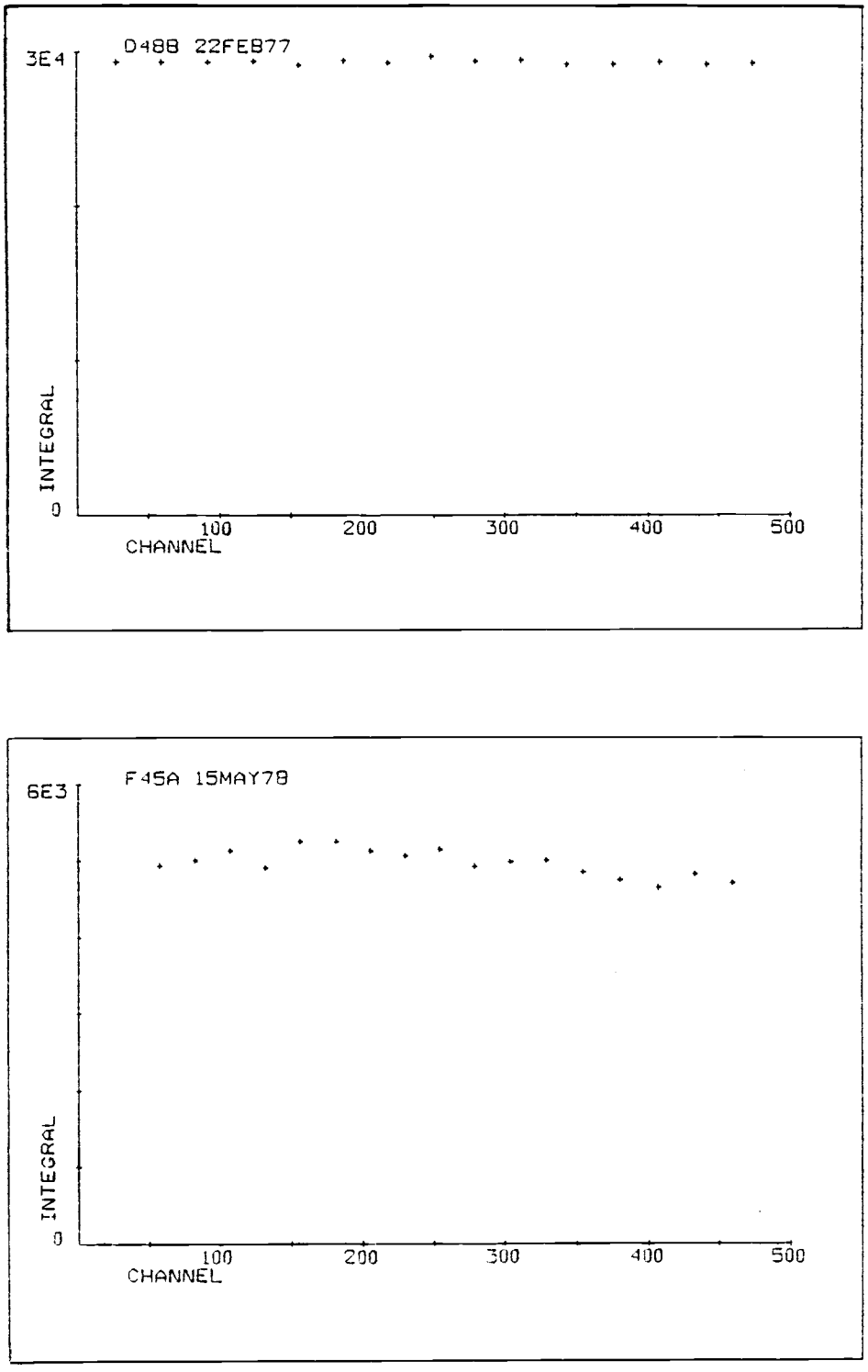

Figure 7(d). CALIB output--peak integrals vs channel centroid. Top: unpressurized detector D1. Bottom: pressurized detector D2 at 380 kPa.

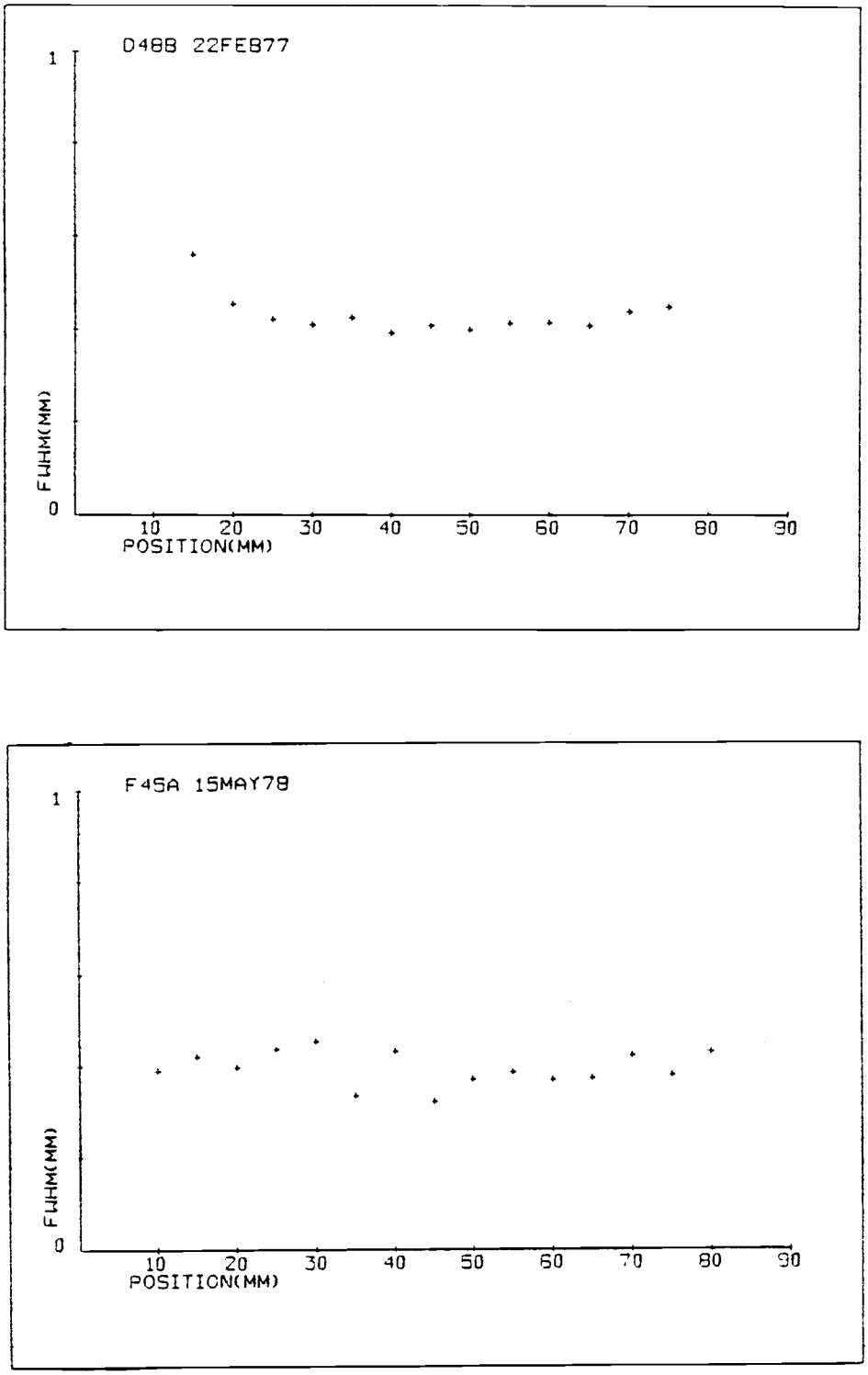

Figure 7(e). CALIB output--point spread (fwhm) vs position. Top: unpressurized detector D1. Bottom: pressurized detector D2 at 380 kPa.

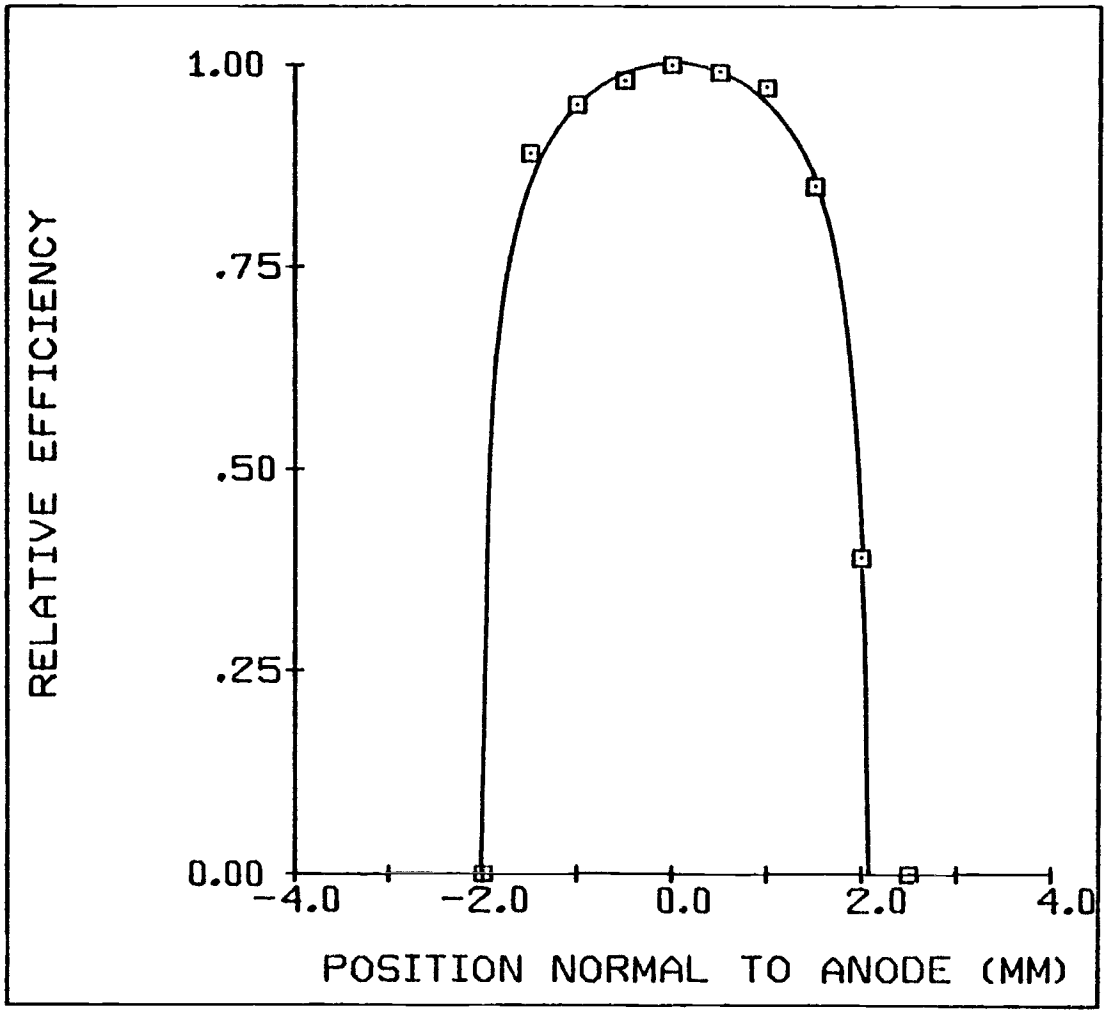

Figure 8. Relative efficiency of detector along axis normal to anode.

D. Calibration using Point Source and Mask

Calibration by translating the detector was too cumbersome and disruptive for routine use with diffraction experiments. Instead, the procedure of White and Naylor was followed, using a point source with a masked detector [86].

A 100-μCi ^{55}Fe point source of 6-keV x-rays was used to bathe the detector in a nearly uniform flux. Linear amplifier gain was multiplied by a factor of 0.7 to provide a pulse height spectrum from the linear amplifiers similar to that obtained for the 8-keV photons used for diffraction. To simulate diffraction geometry (Figure 19), the source was placed at the position normally occupied by the diffraction sample, collinear with the incident beam and ∿240 mm from the detector.

For position calibration, a 1 mm-thick, perforated, aluminum mask was accurately clamped into a recess on the detector exterior 1 cm from the anode. (For calculations involving sample-detector distance, this calibration technique defines the plane of registration to be at the mask, and not at the anode.) The mask holes, 1 mm in diameter, were 5.00 mm center-to-center on a line parallel to the anode.

A computer program, POSIT (Appendix C), was written to analyze the comblike multichannel analyzer pattern obtained on irradiation. POSIT used a third-degree least squares curve fit to find the relation between channel centroid in the display and hole position on

the mask. This relation was interpolated at 1-channel (∿0.2 mm) intervals. Deviation between actual and computed positions over the detector length was 0.09 mm rms, 0.2 mm maximum. Input and output for POSIT are given in Figure 9 and Table 5.

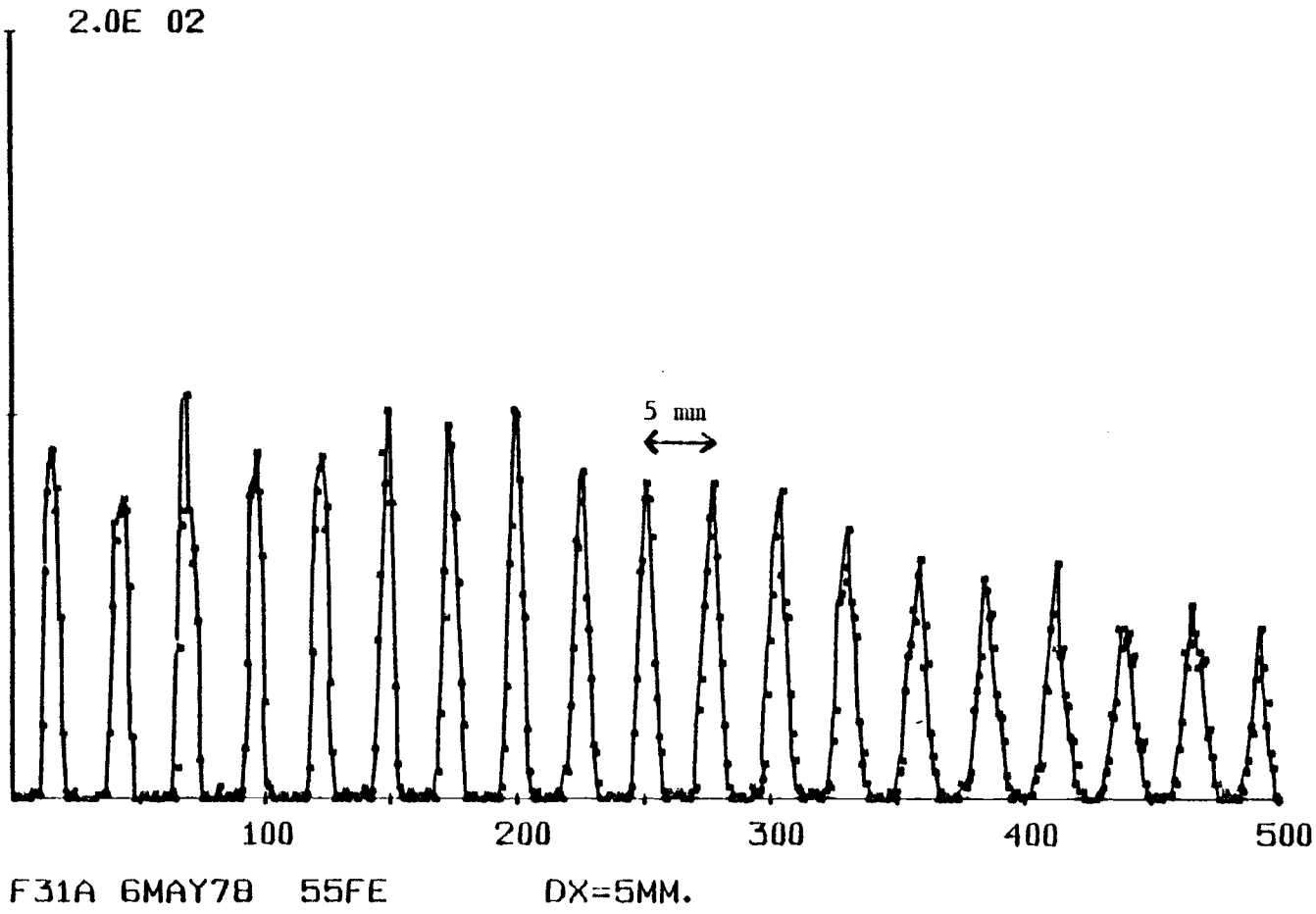

Figure 9. Calibration input for program POSIT.

Table 5. Calibration output from program POSIT.

```
PROGRAM POSIT   --3RD DEGREE CURVEFITFOR DETECTOR POSITION CALIBRATION
F31A 6MAY78
CALIBRATION POINTS= 18

CURVEFIT COEFFICIENTS

X=X(C)=SUM(I=1,4) OF A(I) * C ** (I-1)
A(1)=-2.98587E+00
A(2)= 1.84136E-01
A(3)= 4.59132E-05
A(4)=-8.05249E-08
DEV = 1.12325E-01

C=C(X)=SUM(I=1,4) OF B(I) * X ** (I-1)
B(1)= 1.61112E+01
B(2)= 5.39549E+00
B(3)=-6.46884E-03
B(4)= 6.50632E-05
DEV = 5.68673E-01
```

	ACTUAL POSITION	CALC POSITION	DIFF POSITION	ACTUAL CHANNEL	CALC CHANNEL	DIFF CHANNEL
1	0.000	-.047	.047	15.901	16.111	-.210
2	5.000	4.927	.073	42.555	42.935	-.380
3	10.000	10.000	-.000	69.468	69.484	-.016
4	15.000	15.104	-.104	96.318	95.809	.510
5	20.000	20.107	-.107	122.475	121.954	.521
6	25.000	25.104	-.104	148.482	147.972	.510
7	30.000	30.057	-.057	174.194	173.911	.283
8	35.000	34.976	.024	199.700	199.819	-.119
9	40.000	39.914	.086	225.322	225.745	-.423
10	45.000	44.822	.178	250.846	251.738	-.892
11	50.000	49.852	.148	277.107	277.846	-.739
12	55.000	54.930	.070	303.778	304.120	-.342
13	60.000	59.975	.025	330.478	330.606	-.128
14	65.000	65.097	-.097	357.852	357.355	.497
15	70.000	70.215	-.215	385.537	384.415	1.122
16	75.000	75.135	-.135	412.522	411.834	.688
17	80.000	80.004	-.004	439.668	439.662	.006
18	85.000	84.828	.172	467.359	467.947	-.888

E. Position Linearity

The detector is said to be linear in position when the location of a peak in the output is proportional to the actual location of the beam at the detector. This condition is equivalent to having the spatial sensitivity, S (ns/mm), independent of beam position.

Procedures described in the previous sections were used to find spatial sensitivity and spatial linearity. End-to-end variation in S of less than 10% was achieved by trial-and-error adjustment of the linear amplifier time constants, which determined ω_o, the frequency of the passband center of the amplifier filters [54]. Even gross deviations from linearity did not affect uniformity (countrate per unit length of anode).

For events near the end (S_1) and center (S_2) of a capacitively terminated anode, Borkowski and Kopp have found empirically

$$S_1 = R_o C_{GT}, \qquad (1)$$

$$S_2 = 2(R_o C_o/\omega_o)^{1/2} \qquad (2)$$

where S = spatial sensitivity
= position-time conversion factor = dt/dx

R_o = anode resistance/unit length

C_o = anode-cathode capacitance/unit length

ω_o = passband center of amplifier filter (rad/s)

L = anode length

C_L = termination capacitance

$$C_{GT} = C_o L + 2C_L$$

In Table 6 our values of S found for both low- and high-resistance anodes are compared with values calculated from Equations 1 and 2 . Quartz fiber coated with pyrolytic graphite (8.4 MΩ/m) was routinely used as the anode in both detectors; solid, pyrolytic carbon (0.5 MΩ/m) was also tried in this experiment.

In these calculations, C_o was estimated from the theoretical equation [87] for a coaxial, cylindrical capacitor:

$$C_o = \frac{C}{L} = \frac{2\pi\varepsilon_o}{\ln(b/a)} = \frac{55.6 \text{ pF/m}}{\ln(b/a)} ,$$

where a = outside diameter of inner conductor (anode), and

b = inside diameter of outer conductor (cathode).

Because the cross section of the cathode was rectangular, rather than circular, C_o was approximated by taking for b the average of the two dimensions of the cross section.

For various values of the linear amplifier time constant, ω_o was measured using a Harris-PRD Model 7808 frequency synthesizer. R_o was measured with a Fluke 8000A digital multimeter.

When no additional capacitor was added, C_L, the terminating capacitance, was taken as 0.5 pF, the input capacitance specified by the manufacturer of the preamplifiers. For run D104A, an additional 7.5 pF was placed between each end of the anode and ground.

Agreement between observed and calculated values for S ranged from good to poor (Table 6). Differences between S_{obs} and S_1

could easily be explained by errors in estimating C_L. However, differences between S_{obs} and S_2 could not be explained by errors in estimating C_o. For example, for run F44A, the value of C_o necessary to make Equation 2 agree with the observed value of S is 28 pF/m. For the known anode diameter of 20 μm, this C_o corresponds to a very unrealistic cathode diameter of 0.15 mm.

Table 6. Electrical parameters with theoretical (S_1 and S_2) and experimental (S_{obs}) values for spatial sensitivity.

Data set	D47A	F44A	D62A	D104A
Detector	D1	D2	D2	D2
Anode material	quartz	quartz	carbon	carbon
Anode diameter a(μm)	20	20	7	7
Cathode "diameter" b(μm)	6000	4000	4000	4000
R_o (MΩ/m)	8.4	8.4	0.50	0.50
C_o (pF/m)	9.8	10.4	8.8	8.8
ω_o (Mrad/s)	1.0	1.4	4.2	0.7
L (m)	0.113	0.133	0.133	0.133
C_L (pF)	0.5	0.5	0.5	8.0
C_oL (pF)	1.1	1.4	1.1	1.1
C_{GT} (pF)	3.1	3.4	3.1	18.1
S_1 (μs/m)	18	28	1.6	9.0
S_2 (μs/m)	18	16	2.0	5.0
S_{obs} (μs/m)	17	26	3.2	9.6

F. Pulse Height Spectrum

1) Energy Resolution

Energy resolution [88] of detector D2 (90% argon-10% methane) was studied, using Cu K x-rays from the Picker generating tube and Mn K x-rays produced by electron capture in a 100-μCi ^{55}Fe source. The Picker tube was operated at 20 kV, 2 mA, with a β-filter of 17 μm nickel foil. With x-rays incident on the central 1 mm of the detector, the pulse height spectrum of the Σ signal (Figure 3) was recorded in the multichannel analyzer.

These spectra are shown in Figure 10; they indicate that the detector operates proportionally within an energy error of 5%. Main peaks in the two spectra occur with a voltage (channel) ratio of 1.26, near the expected energy ratio of 1.3 for 8.0-keV Cu K x-rays to 6-keV Mn x-rays [89].

In Figure 7 , a minor peak (the escape peak [88]) is 2.5 keV from the main peak for Mn x-rays, and a shoulder is the same distance from the main peak of the Cu x-rays. These smaller features are attributed to energy lost when some of the 3-keV [89] Ar K x-rays produced during primary ionization escape from the chamber.

Measured energy resolution in both cases was 18% fwhm, ignoring the shoulder in the case of Cu x-rays.

2) Variation of Pulse Height Spectrum with Position

Pulse height spectra of the linear amplifier output signals were collected separately as the detector was translated in 10-mm increments in front of the Ni-filtered Cu x-ray beam. Voltages of the main peaks from these spectra (Figure 11) varied from 1.6 to 2.9 V, and the sum varied from 3.9 V (center) to 4.5 V (ends).

Other settings of voltage and linear amplifier gain gave values proportional to these, as expected.

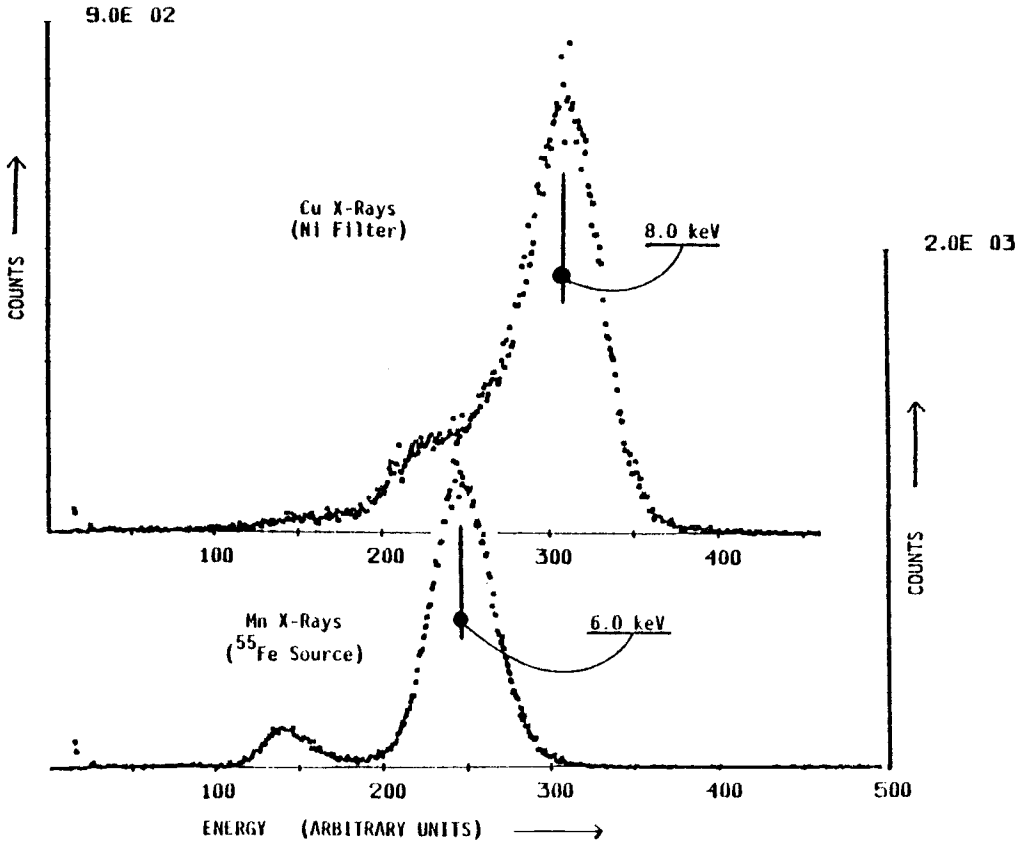

Figure 10. Summed pulse height spectra. Top: 8 keV Cu x-rays. Bottom: 6 keV Mn x-rays.

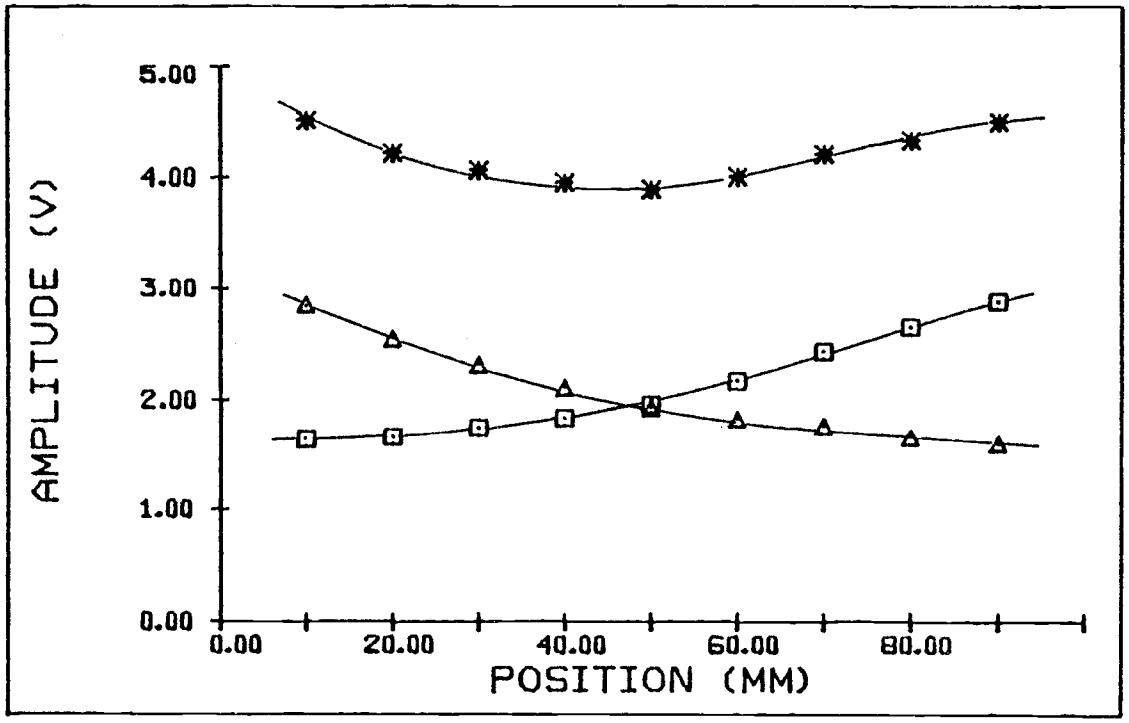

Figure 11. Variation of pulse height centroids with position.

⊡ from START linear amplifier
Δ from STOP linear amplifier
* sum

G. Position Resolution

Measured timing noise in the timing single channel analyzers (TSCAs) (Figure 3) largely accounted for the observed position resolution of 0.4 mm fwhm for a high-resistance (8 MΩ/m) anode and 0.5 mm fwhm for a low-resistance (0.5 MΩ/m) anode.

Measurements of walk (variation of timing output with different input signal amplitudes) and jitter (variation of timing output with a constant input signal) of the TSCAs are given in Figures 10 and 11. These measurements were made with 0.1-fraction timing and with the "walk" adjustment optimized for 1-8 V input. Other fractions gave similar results on readjustment of the "walk" potentiometer.

The effect of this timing noise was roughly estimated. For the high-resistance anode of quartz coated with pyrolytic graphite (diameter=20 μm, R_o=8.4 MΩ/m, S=27 μs/m), the voltage divider effect caused by high R_o put heavy demands on the TSCAs. In order to register 97% of all counts at all positions (Figures 12 and 13), the TSCAs had to accept amplitudes from 1.5-7 V, with 1.5 V chosen as the lower limit to avoid excessive jitter. Over this range, σ_{walk} = 2.2 ns, and σ_{jitter} = 1.1 ns. Approximating the σ to be uncorrelated and normally distributed,

$$\sigma_{total} = [2\sigma^2_{walk} + 2\ \sigma^2_{jitter}]^{1/2}$$

for both TSCAs together.

Thus, σ_{total} = 3.4 ns, equivalent to 8.8 ns fwhm. At S = 27 μs/m, this amounts to 0.34 mm fwhm, near the value of 0.4 mm

fwhm observed with a 0.1 mm beam.

With the anode made from pure, pyrolytic carbon (diameter = 7 μm, R_o = 0.5 MΩ/m, S = 9.6 μs/m), a narrower range of pulse amplitudes was sent to the TSCAs, reducing errors due to walk.

In order to catch 97% of all counts at all positions in this case, the TSCAs needed to respond only between 1.5 and 4.2 V. For this range, σ_{walk} = 1.3 ns, σ_{jitter} = 1.1 ns, and σ_{total} = 2.4 ns (5.7 ns fwhm). With S = 9.6 μs/m, this timing dispersion implies a position spread of 0.6 mm fwhm, to be compared to the observed value of 0.5 mm fwhm for a 0.1-mm beam. Thus, lower anode resistance caused reductions in both sensitivity and walk error, which largely cancelled each other.

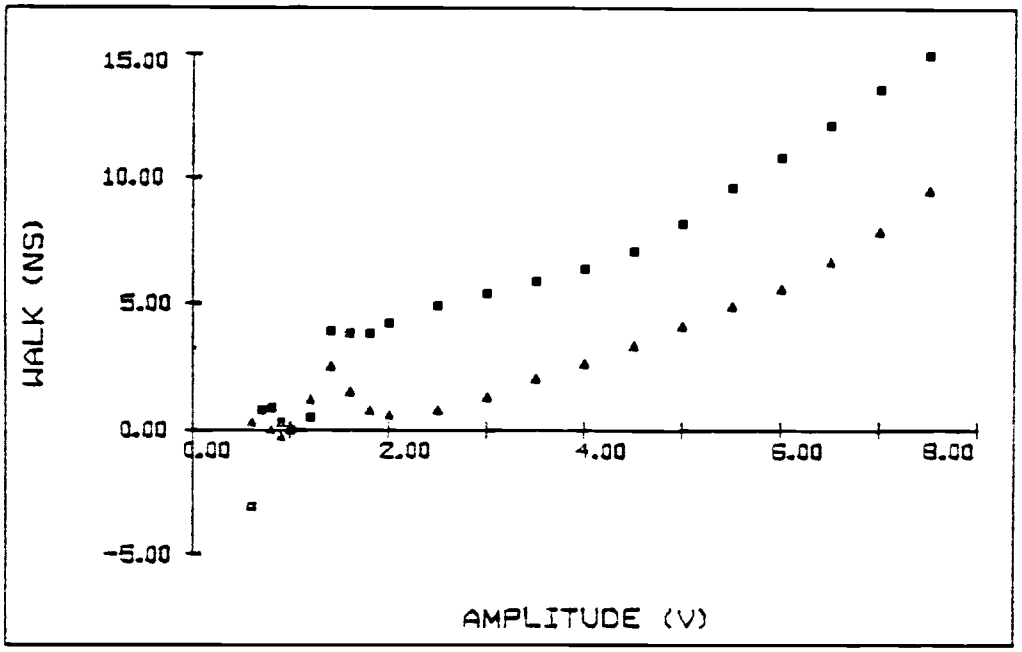

Figure 12. Variation of walk with input amplitude for timing single channel analyzers. (Relative to 1.0 V input.)

□ START analyzer
Δ STOP analyzer

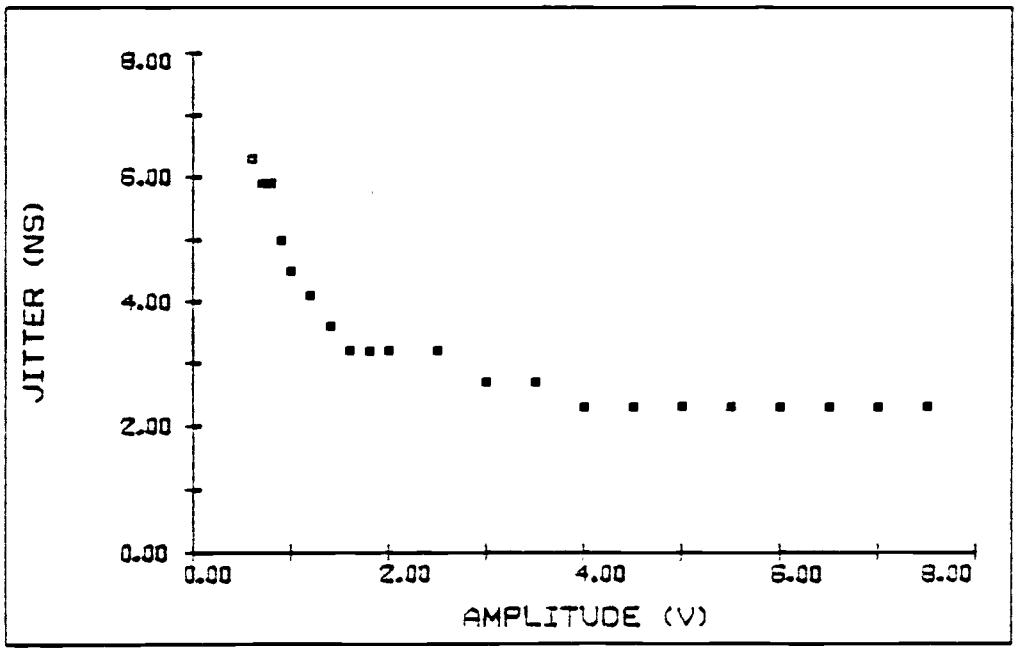

Figure 13. Jitter for timing single channel analyzer.

H. Efficiency vs Pressure

Quantum detection efficiency is the counted fraction of the quanta that are presented to the detector. The relation between efficiency and pressure was determined for detector D2. As expected, efficiency increased with pressure, since the probability of primary ionization [83] is proportional to the number of absorbing atoms per unit volume for a given absorber [89].

Collimated 8-keV Cu x-rays were counted first by a NaI(Tl) scintillation detector, which was assumed 100% efficient [83] and taken as a standard. The same beam was then counted by detector D2, which was operated at several pressures. With the absorbing gas used in all our experiments, 90% argon-10% methane, efficiency ranged from 3% at atmospheric pressure to 10% at 430 kPa (Figure 14). Above 400 kPa, the detector tended to leak around the window seals.

Even in a detector as thin as D2, xenon would have stopped virtually all incoming 8-keV photons, giving nearly 100% efficiency. Since the photoelectric cross section for absorbance in this energy range [89] varies approximately as $Z^4/(h\upsilon)^3$, the cross-section ratio of xenon to argon is about 80. However, xenon, which is $\sim 10^4$ times as expensive as argon, is too costly to use in a flow-through counter.

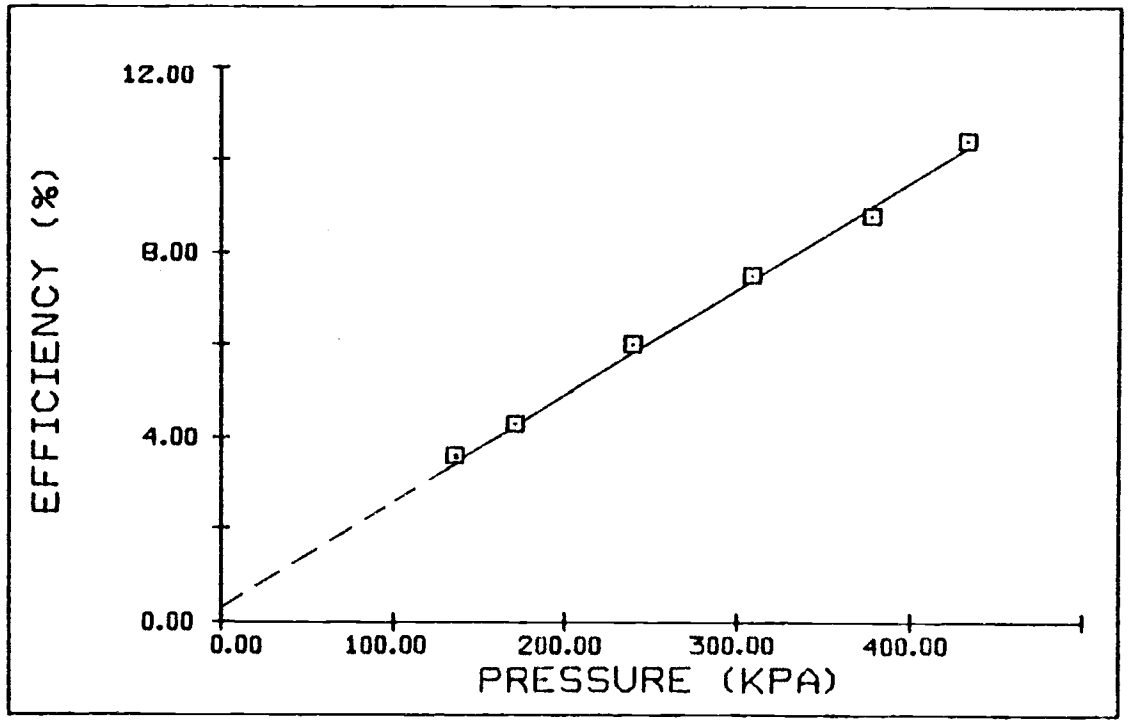

Figure 14. Variation of absolute efficiency with pressure at 8 keV.

I. Oblique Incidence

Borkowski and Kopp [54] found that x-rays entering non-normally to the anode are detected with larger point spreads and higher count rates than those entering normally. This is because photons can cause primary ionization anywhere along their path through the detector, and the path length increases as incidence becomes more oblique. In addition, there is a systematic error in position, since the probability of interaction is greatest where the path enters the detector and decreases exponentially toward the exit position.

This error in position was largely avoided with the calibration technique of White and Naylor [86], described in section E. With a point source at the sample position and a perforated mask on the detector, diffraction conditions, including oblique incidence, are simulated during calibration, and the plane of registration is defined to be at the mask.

For a Cu K x-ray beam, Figures 15 and 16 show variations in position resolution and relative efficiency with angle of incidence, α. We define α as the angle between the beam and the normal to the anode.

For $\alpha = 2\theta = 250$ mrad, corresponding to about the ninth order of lamellar diffraction from phospholipids, the efficiency increase was less than 5% and position resolution was better than 1.5 mm fwhm for both detectors.

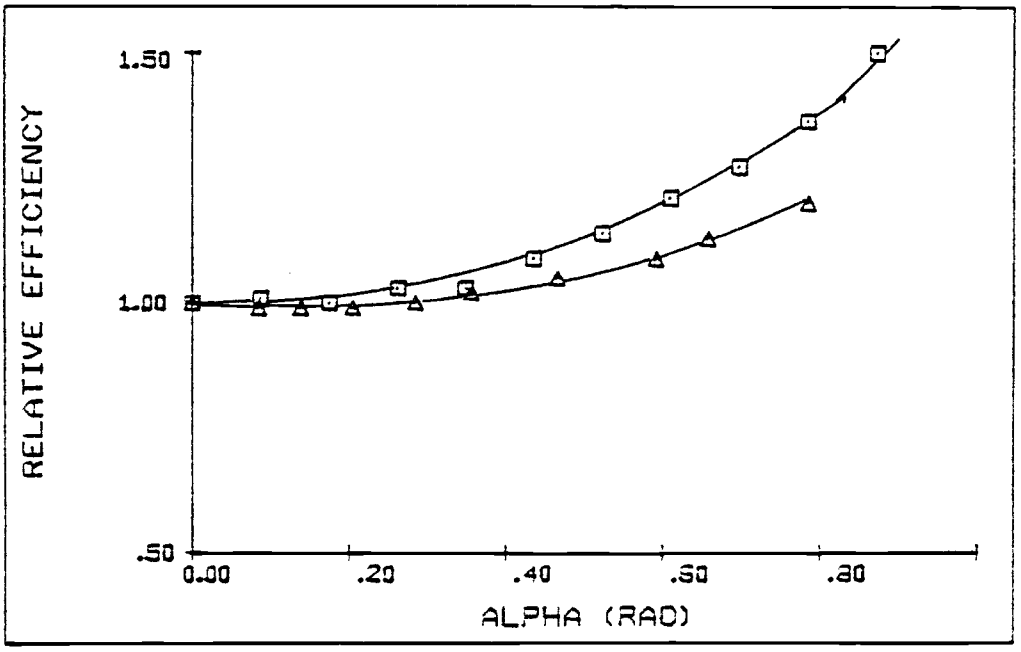

Figure 15. Variation of relative efficiency with angle of incidence: Efficiency (α)/Efficiency (α=0) vs α. α = angle between beam and normal to detector.

⊡ unpressurized detector
Δ pressurized detector, 380 kPa

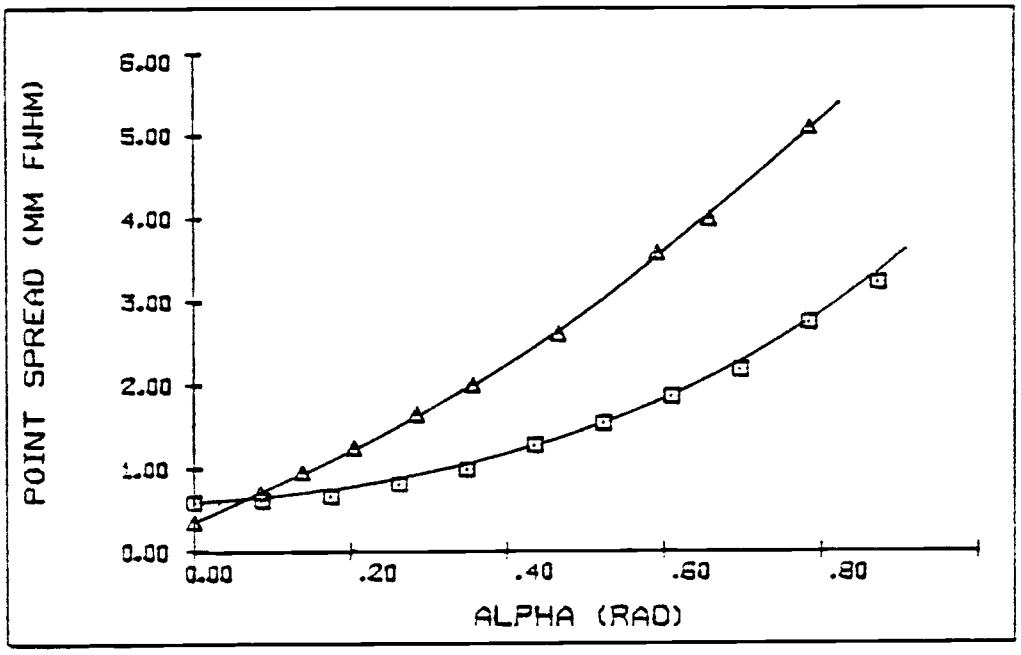

Figure 16. Variation of point spread with angle of incidence. α = angle between beam and normal to detector.

⊡ unpressurized detector
Δ pressurized detector, 380 kPa

IV. DIFFRACTION THEORY

A. X-Ray Diffraction Applied to Multilayers

1) Fundamentals

Since x-ray wavelengths are about the same as interatomic distances, x-ray diffraction is one of the major sources of structural information on the molecular scale. This chapter will briefly review the standard diffraction theory [15,90] as it applies to stacked, lipid multilayers, and outline our approach to the problem of determining the projected electron density of such multilayers. The following notation and relations will be used:

$\bar{F}$ Conjugate of complex number F

$$(F = a + ib) \Rightarrow (\bar{F} = a - ib) \qquad (3)$$

$|F|$ Modulus of complex number F

$$(F = a + ib) \Rightarrow (|F| = \sqrt{a^2 + b^2}) \qquad (4)$$

$\vec{x}$ Direct space position vector

$\vec{s}$ Reciprocal space position vector

$\mathcal{T}$ Fourier transform

$$\mathcal{T}g(\vec{x}) = G(\vec{s}) = \int_{\text{all } \vec{x}} g(\vec{x}) \exp(2\pi i\, \vec{x}\cdot\vec{s})\, dV_x \qquad (5)$$

$\mathcal{T}^{-1}$ Inverse Fourier transform

$$\mathcal{T}^{-1} G(\vec{s}) = g(\vec{x}) = \int_{\text{all } \vec{s}} G(\vec{s}) \exp(2\pi i\, \vec{x}\cdot\vec{s})\, dV_s \qquad (6)$$

* Convolution

$$f(\vec{x}) * g(\vec{x}) = \int_{\text{all } \vec{u}} f(\vec{x})\ g(\vec{u} - \vec{x})\ dV_u \qquad (7)$$

$\Delta_d(x)$ Infinite assembly of delta functions of spacing d (one dimension)

$$\Delta_d(x) = \sum_{k=-\infty}^{+\infty} \delta(x - kd) \qquad (8)$$

Convolution transform theorm

$$T(f * g) = (Tf) \cdot (Tg) \qquad (9)$$

$$T(f \cdot g) = (Tf) * (Tg) \qquad (10)$$

X-ray diffraction depends on the coherent scattering of electromagnetic radiation by atomic electrons in an object and on the subsequent interference of waves scattered from different locations in the object. The classical dipole-oscillator treatment for the interaction of an electron with electromagnetic radiation provides an adequate scattering model, and the Fraunhofer theory of diffraction describes the effect of interference among the scattered waves.

In the classical dipole-oscillator model, a free electron oscillates harmonically in response to the innident electric field, and reradiates energy of the original wavelength in all directions. We express the time-independent part of the electric field magnitude as a complex phasor E, so that $\overline{E} \cdot E$ equals the time-averaged intensity of exiting radiation. For a free electron, this model predicts that

$$f_e(2\theta) = \frac{(E_{out})_{electron}}{E_{in}} = r^{-1} \cdot k \cdot p_e(2\theta) \cdot e^{-i\pi}, \qquad (11)$$

with 2θ = angle between incident and observation axes

r = distance from electron to observer

$k = e^2/(4\pi\varepsilon_o m_e c^2)$

$p_e(2\theta) = (1 + \cos^2 2\theta)/2$ for initially unpolarized radiation

Since the factor $e^{-i\pi}$ is a constant for all electrons in a diffracting specimen, it can be ignored in a description of diffraction.

The free electron model is valid for an atomic electron when the energy of incident radiation is far from any quantum transition of the atomic electron. Otherwise the classical treatment predicts that Equation (11) must be multiplied by the factor

$$\frac{\omega^2}{\omega^2 - \omega_o^2 - i\gamma\omega},$$

where γ is a damping term and ω and ω_o are the input and transition frequencies [90].

The Fraunhofer theory provides the kinematic description of wave interference in x-ray diffraction. It assumes that the distances between source, specimen, and observer are large compared with λ, but it does not require that the specimen consist of repeating units. However, when the latter condition is met, the theory predicts that diffracted intensity will be zero except for certain discrete values of the scattering angle, in agreement with Bragg's law.

If $\vec{x} = (x_1, x_2, x_3)$ is the position vector (on the molecular

scale) in an object with volume electron density $\rho(\vec{x})$, Fraunhofer diffraction requires that for exiting radiation,

$$E(\vec{s}) = \int_{-\infty}^{\infty}\int\int f_e(\vec{s})\ \rho(\vec{x})\ \exp(2\pi i\ \vec{x}\cdot\vec{s})\ dV_x \tag{12}$$

$$= \mathcal{T} f_e(\vec{s})\ \rho(\vec{x}) \tag{13}$$

$$= f_e(\vec{s})\ \mathcal{T}\rho(\vec{x}) \tag{14}$$

These equations are valid for arbitrary ρ, which may be, for example, a unit cell, a crystal, or an amorphous body. The diffraction vector $\vec{s} = (s_1, s_2, s_3)$ specifies the orientation of the incident beam to the direction of observation. We define $\vec{s}$ to be $\vec{k}_{out} - \vec{k}_{in}$, as shown in Figure 17. The $\vec{k}$ vectors, or wave vectors, are collinear with the direction of propagation of the waves (beams). The angle between $\vec{k}_{out}$ and $\vec{k}_{in}$ is 2θ, the diffraction angle, and $|s| = \lambda/(2\ \sin\theta)$. These definitions and Equation (14) ensure that when any two small regions in ρ are situated so that the paths through them from source to detector differ by $(h + 1/2)\lambda$, their pairwise contribution to the diffracted intensity is zero. Furthermore, when the paths differ by $h\lambda$, their intensity contribution takes its maximum possible value.

Conventionally, $f_e(2\theta)$ is removed from Equation (14) by introducing the relative intensity, I, and the relative structure factor F. During data treatment, $f_e(2\theta)$ is reinserted, along with geometric factors related to the mode of data collection.

$$I(\vec{s}) = I_{obs}(\vec{s})/|f_e(\vec{s})|^2 \tag{15}$$

$$F(\vec{s}) = E(\vec{s})/f_e(\vec{s}) \tag{16}$$

$$I_{obs}(\vec{s}) = \overline{E}(\vec{s}) \cdot E(\vec{s}) \tag{17}$$

$$I(\vec{s}) = F(\vec{s}) \cdot F(\vec{s}) \tag{18}$$

$$F(\vec{s}) = T\rho(\vec{x}) \tag{19}$$

Equation (19) can be reduced to one dimension in both $\vec{x}$ and $\vec{s}$, since we are interested in the image of electron density projected onto a single axis perpendicular to lipid bilayer planes. The projected electron density is defined as

$$\rho_p(x_1) = \int_{-\infty}^{+\infty}\int \rho(x_1, x_2, x_3)\, dx_2\, dx_3 \tag{20}$$

It follows [15] that

$$F(s_1) = T\rho(x_1). \tag{21}$$

Suppressing subscripts, and with scalar x and s,

$$F(s) = T\rho(x). \tag{22}$$

The rest of the development will be the 1-dimensional analog of the standard 3-dimensional case.

The specimen may be regarded as a 1-dimensional crystal, composed of a 1-dimensional unit cell translated indefinitely at intervals of d. This is equivalent to generating the crystal as the convolution of the unit cell with an infinite array of evenly spaced delta functions of spacing d.

$$\rho_{cryst}(x) = \rho_{cell}(x) * \Delta_d(x) \tag{23}$$

By the convolution transform theorm, the structure factor for the crystal, which gives the diffracted intensity, is

$$F_{cryst}(s) = (1/d)\, F_{cell}(s) \cdot \Delta_{1/d}(s) \tag{24}$$

$$= (1/d)\, F_h, \tag{25}$$

where $F_h = F_{cell}(h/d)$ for h = integer, (26)

and $F_h = 0$ otherwise.

This result implies that diffracted intensity is seen only for discrete values of $s = h/d$, with integral h. Since $s = \lambda/(2 \sin\theta)$, Bragg's law is obtained: $h\lambda = 2d \sin\theta$.

To find $\rho(x)$, Equation (21) may be inverted. Generally,

$$\rho_{cryst}(x) = \mathcal{T}^{-1} F_{cryst}(s), \tag{27}$$

which reduces in this discrete case to

$$\rho_{cryst}(x) = \sum_{h=-\infty}^{+\infty} F_h \exp(2\pi i h x/d), \tag{28}$$

with $F_h = F(h/d)$.

Furthermore, if the cell has inversion symmetry, so that $\rho(x) = \rho(-x)$, then the F_h are real, and

$$\rho(x) = \sum_{h=0}^{+\infty} F_h \cos(2\pi h x/d) \tag{29}$$

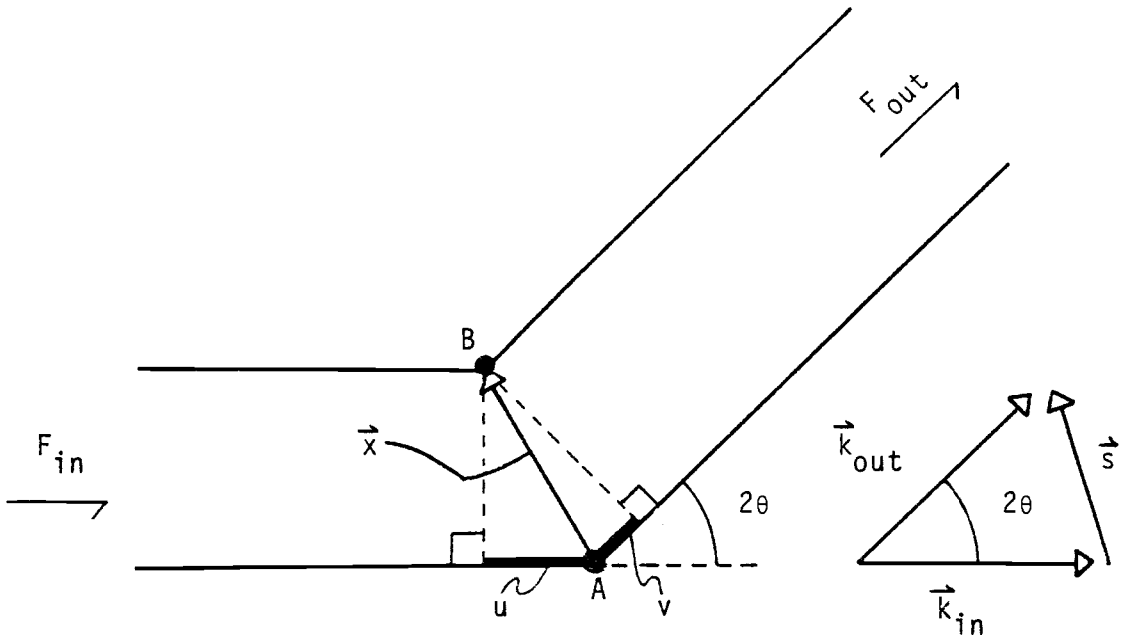

$$F_{out} = F_{in} \cdot e^{i\alpha} = F_{in} \cdot e^{2\pi i \, \vec{s} \cdot \vec{x}}$$

$$\frac{\alpha}{2\pi} = \frac{u + v}{\lambda} = \frac{(\hat{k}_{out} - \hat{k}_{in})}{\lambda} \cdot \vec{x}$$

$$= (\vec{k}_{out} - \vec{k}_{in}) \cdot \vec{x}$$

$$= \vec{s} \cdot \vec{x}$$

Figure 17. Point scattering diagram.

2) Difficulties

If either $\rho(x)$ or the set F_h ($h = 0, \pm 1, \ldots, \pm\infty$) is known, then the other can always be calculated. Unfortunately, experimental determination of diffracted intensity does not allow reconstruction of $\rho(x)$ directly from Equations (27 - 29) for three reasons.

1. $I_o = \overline{F}_o \cdot F_o$ coincides with the direct beam, and is not observed.
2. I_h cannot be observed for $h > (2d/\lambda)$.
3. I_h contains less information than F_h.

The first two factors are not serious. Lack of I_o prevents the zero point of ρ from being fixed. For $d = 6.0$ nm and $\lambda = 0.154$ nm, $h_{max} = 2d/\lambda = 77$, allowing a resolution of $\sim$0.1 nm in the Fourier summation of Equation (29). The third factor constitutes the phase problem, which is the main difficulty in x-ray crystallography:

$$I_h = \overline{F}_h \cdot F_h \tag{30}$$

$$= |F_h| \exp(i\alpha_h) = |F_h| \cdot p_h. \tag{31}$$

Whereas I_h is a positive, real number, the complex F_h is in general represented by two positive real numbers $|F_h|$ and α_h. Even in the centrosymmetric case where $\rho(x) = \rho(-x)$, F_h is represented by a real positive number and a sign factor p_h which may be +1 or -1. In either case, knowing the set I_h is not enough to perform the reconstruction of Equations (27 - 29). Even though we cannot directly perform the synthesis

$$\rho_{cryst}(x) = T^{-1}F_{cryst}(s) = \sum F_h \exp(2\pi ihx/d), \tag{32}$$

the function $P_{cryst}(x)$, defined as

$$P_{cryst}(x) = T^{-1} |F_{cryst}(s)|^2 = \sum |F_h|^2 \cos(2\pi hx/d) \tag{33}$$

is available immediately from the data. $P_{cryst}(x)$, which is called the Patterson function, is identical to the autocorrelation function of ρ_{cryst}, and is related to the autocorrelation function of ρ_{cell}:

$$P_{cryst}(x) = \rho_{cryst}(x) * \rho_{cryst}(-x) \tag{34}$$

$$P_{cell}(x) = \rho_{cell}(x) * \rho_{cell}(-x) \tag{35}$$

$$P_{cryst}(x) = P_{cell}(x) * \Delta_d(x) \tag{36}$$

3) Data Treatment

The phase problem aside, Equation (29) must be modified slightly for use with the integrated intensities of observed diffraction peaks. Since I is defined relative to the scattering for a single electron, the electronic scattering factor $f_e(2\theta)$ or at least its angular dependence $p_e(2\theta)$ must be reintroduced. In addition, I in all the above equations refers to peak intensity at an optimum, fixed scattering angle. The Lorentz factor $L(2\theta)$ compensates for rotation of the specimen and for the fact that integrated intensities $(I_{int})_h$ are used [15, 90]. For the geometry of Figure 19(a),

$$|F_h| \propto \left[\frac{(I_{int})_h}{Lp}\right]^{1/2} \tag{37}$$

$$L = 1/(\sin 2\theta) \tag{38}$$

$$p = (1 + \cos^2 2\theta) \tag{39}$$

For small θ,

$$Lp \propto 1/h \tag{40}$$

For multilayers with inversion symmetry, and assuming the p_h have been found

$$\rho'(x) = \sum_{h=1}^{h'} p_h[h \cdot (I_{int})_h]^{1/2} \cos(2\pi hx/d) \tag{41}$$

This equation gives the projected electron density profile on an arbitrary scale, with an arbitrary ρ-origin, and subject to the limit in resolution caused by use of a finite number of reflections h'.

B. Phasing Methods

1) Survey

The central difficulty in interpreting x-ray diffraction data comes from technological deficiencies. On the one hand, lenses for focusing x-rays have not been found. With light and electron microscopy, as well as vision, the inverse transform analogous to $\rho(x) = T^{-1}F(s)$ is performed on scattered waves by optical or magnetic lenses, resulting immediately in an image, which is not available with x-rays [15]. On the other hand, spatially coherent sources of x-radiation have not yet been developed, so holographic techniques are not possible. Therefore, for x-ray diffraction, the inverse transform giving $\rho(x)$ must be computed.

With repetitive structures, which have discrete, complex structure factors F_h, the problem has traditionally been seen as a search for phase factors p_h or phase angles α_h, which are lost when diffracted waves are detected as time-averaged intensity I_h.

$$I_h = \overline{F}_h \cdot F_h = |F_h| \tag{42}$$

$$F_h = |F_h|\exp(i\alpha_h) = |F_h| \cdot p_h \tag{43}$$

Traditional strategies to obtain the phases from auxiliary data--usually data from similar structures or at several wavelengths-- are called indirect methods. In contrast, direct methods attempt to deduce the structure of a crystal using intensities collected at one wavelength from that crystal alone. Several techniques are often

combined, and iterative refinement is used extensively [96]. Since usage varies for the terms "direct" and "indirect", the following grouping is given arbitratily:

A. Direct methods
   1. Hauptmen-Karle
   2. Patterson deconvolution
   3. Heavy atom
B. Indirect methods
   1. Isomorphous replacement and addition
   2. Anomalous dispersion

Hauptman-Karle methods

The Hauptman-Karle and Patterson approaches result from analyses which show that observed intensities can determine (or actually over-determine) the structure. The algebraic methods of Hauptman and Karle [91] make use of mathematically required relations, either strict or probabilistic, among the structure factors of different reflections in a single crystal. These methods require that the experimental moduli $|F_h|$ of the structure factors be put on an absolute scale with the atomic scattering factors. This scaling is difficult when only a small number of reflections is available [14,92].

Patterson methods

Patterson deconvolution techniques are the direct-space analogs of the Hauptman-Karle methods. They use the overall autocorrelation (Patterson) function P(x), which is easily obtained from observed intensities, since

$$P_{cryst}(x) = \Sigma_h(I_h)\cos(2\pi hx/d). \tag{44}$$

Peaks in the Patterson map represent all possible vectors between pairs of peaks in the structure $\rho_{cryst}(x)$. As an outgrowth of the

long-standing use of the Patterson map as an aid to other approaches, Buerger has devised general image-seeking methods which extract $\rho_{cell}(x)$ from $P_{cryst}(x)$ [93]. These methods require that P and ρ contain distinct maxima corresponding to atomic locations, working best in the hypothetical limit of point atoms. This requirement is apparently not met by oriented membrane and lipid multilayer systems.

Patterson deconvolution techniques have been applied in one dimension to fatty acid multilayers [94] and to oriented membranes [28,29]. In this approach, which is based on the theoretical work of Hosemann and Bagchi [95], the autocorrelation function of the unit cell $P_{cell}(x)$ is deconvoluted, yeilding the cell electron density, since

$$P_{cell}(x) = \rho_{cell}(x) * \rho_{cell}(-x). \tag{45}$$

This requires separation of $P_{cell}(x)$ from the overall Patterson function $P_{cryst}(x)$, which comes directly from intensity data. The separation can be done only in special cases, such as (1) presence in the unit cell of a large region of constant electron density (e.g., a water layer in stacked membranes) [27], or (2) use of a specimen containing a few unit cells [94].

Heavy atom method

The heavy atom method [15] used by itself applies only to centrosymmetric structures, the phase factors being therefore limited to ± 1. The unit cell must contain one or a few atoms which are much heavier--and therefore scatter more strongly--than the rest. The

Patterson map provides locations of the heavy atoms, whose contribution to the structure factor is then calculated. The signs of these contributions are taken as the signs of the overall structure factors, which are assumed to be dominated by the heavy atoms. Since many of these assignments will be wrong, iterative refinement is typically used in finding atomic postions [96].

Isomorphous methods

Isomorphous methods estimate phase factors using intensity data from two or more crystals whose structures are unknown, but differ from each other in a simple way which is known. This is normally done by using two or more crystals which differ only by replacement or addition of one atom in the unit cell. The result is several independent sets of data arising from essentially the same structure. In fortunate cases, the additional information is enough to identify the phase factors, allowing $\rho(x)$ (and at high resolution, atomic locations) to be determined. The main difficulties of the isomorphous techniques are (1) getting replacement atoms into the desired locations and (2) not perturbing the remainder of the structure.

Anomalous scattering

Anomalous scattering methods [97] use several sets of independent data, but the wavelength of incident radiation--rather than the identity of the diffracting species--is varied from one set to another. Normally this would have little effect on the diffraction pattern aside from a linear shift of peak positions. However, when the incident energy is near a quantum transition of an atom in the crystal, Equation (11) is not valid, and the atom is said to scatter anomalously.

Both the magnitude and phase of scattering from an anomalous atom are affected, and the result is evident in typical changes of up to a few percent in diffracted intensity.

The availability of synchrotron radiation as a tunable, nondivergent, intense source of x-rays has increased the utility of--and interest in--anomalous scattering methods [104].

2) Isomorphous Replacement Applied to Multilayers

The indirect phasing procedure used in our studies is a type of isomorphous replacement based on the method first used by Hargreaves in 1957 for hydrated salts of p-toluene sulfonic acid [14]. Hargreaves presented the method as a way of avoiding the need to place isomorphous sets of experimental intensities on an absolute scale with each other and with the atomic scattering factors. The data treatment leads to a so-called Hargreaves plot (described below) which gives a straight line only if the right phase factors are chosen for all reflections of the different isomorphs.

This method was adapted in 1976 by McIntosh and coworkers [19,20] to infer the 1-dimensional electron density in dipped multilayers of behenic (C_{22}) acid and its salts. McIntosh got isomorphous differences by varying both the cation and the degree of saponification of the fatty acid, thus altering the electron density at the unit cell origin (carboxyl end). Rather than testing permutations of phase factors, McIntosh combined his intensity data with phase factors which Lesslauer and Blasie [94] obtained for barium stearate (C_{18}) by other means. The result was a linear Hargreaves plot for nine reflections and electron density profiles which were physically reasonable for various salts of behenic acid in several degrees of saponification.

Although our procedure is a special case of Hargreaves's, it is an extension of that of McIntosh, allowing the substituted atom to be at a general position in the unit cell. In addition, in our implementation, all possible combinations of phase factors

(which are limited to ±1, since the unit cell is assumed symmetric) are searched to determine the set which gives the best Hargreaves plot.

For the two isomorphous structures A and B, we call the projected electron densities $\rho^A(x)$ and $\rho^B(x)$, and let their difference be $\Delta\rho(x)$. Superscripts A and B will represent species and not exponents. We assume (1) that the unit cell length is d for both isomorphs, (2) that $\rho(x) = \rho(-x)$, and (3) that $\Delta\rho_{cell}(x)$ is a gaussian function of height q and halfwidth at half-maximum w, which is displaced a distance t from the cell origin.

$$\Delta\rho_{cell}(x) = \rho^B_{cell}(x) - \rho^A_{cell}(x) \tag{46}$$

$$= q\cdot\exp[-(x+t)^2\ (\ln 2)/w^2] + q\cdot\exp[-(x-t)^2\ (\ln 2)/w^2] \tag{47}$$

Then
$$T\Delta\rho_{cell}(x) = \Delta F(s) \tag{48}$$

$$= F^B(s) - F^A(s) \tag{49}$$

$$= \{k\ \exp[-(\pi sw)^2/\ln 2]\} \cdot \{\cos\ (2\pi st)\} \tag{50}$$

$$= \{\text{Gaussian envelope}\} \cdot \{\text{ripple}\}, \tag{51}$$

where $k = qw\sqrt{\pi \ln 2}$.

Due to the repetitive structure of the crystals, diffracted intensity is zero unless s = h/d, h = 0, 1, 2, ... Therefore

$$T\Delta\rho_{cryst}(x) = \Delta F_h \tag{52}$$

$$= F_h^B - F_h^A \tag{53}$$

$$= \{k \exp[-(\pi hw/d)^2/\ln 2]\} \cdot \{\cos(2\pi ht/d)\} \tag{54}$$

$$h = 1, 2, 3, \ldots .$$

The transform $\Delta F(s) = T\Delta\rho(x)$ is the product of a gaussian envelope and a ripple function. The width of the envelope varies inversely with that of $\Delta\rho_{cell}$. The ripple function oscillates as s varies, the frequency of oscillation increasing with t/d. When t = 0 or t = d/2, the observed intensity and discrete structure factors have their maximum possible differences between A and B.

Introducing undetermined scale factors C^A and C^B for the two sets of data,

$$F_h^A = p_h^A |F_h^A| = C_h^A p_h^A [h(I_{int}^A)_h]^{1/2} \tag{55}$$

and

$$F_h^B = p_h^B |F_h^B| = C_h^B p_h^B [h(I_{int}^A)_h]^{1/2}, \tag{56}$$

with values of p limited to ±1. Equations (55 and 56) may be rearranged to the form

$$k = C^A p_h^A M_h^A + C^B p_h^B M_h^B, \quad h = 1, 2, 3, \ldots , \tag{57}$$

where

$$M_h^A = [h(I_{int}^A)_h]^{1/2} \Big/ \{\exp[-(\pi hw/d)^2] \cos(2\pi ht/d)\} \tag{58}$$

and

$$M_h^B = [h(I_{int}^B)_h]^{1/2} \Big/ \{\exp[-(\pi hw/d)^2] \cos(2\pi ht/d)\}. \tag{59}$$

The M_h depend on measured values of I_{int} and d and on assumed values of w and t, the halfwidth and position of the replacement atom. When $p_h^B M_h^B$ is plotted against $p_h^A M_h^A$, Equation (57) predicts a straight line only if t, w, and all the phase factors p_h are chosen correctly.

$$p_h^B M_h^B = -(C^A/C^B) p_h^A M_h^A + k/C^B \tag{60}$$

The slope of this Hargreaves plot, $-(C^A/C^B)$, gives the scaling factor for the sets of data, and the intercept k/C^B increases with the scattering power of the isomorphous atom.

In the search for the phases, we let g_h^A and g_h^B be arbitrary trial values for p_h^A and p_h^B. The sets of g^A and g^B are cycled through all possible permutations of ±1 for each h, while the (straight) regression line of $g_h^B M_h^B$ vs $g_h^A M_h^A$ is found for each permutation. Values of $(F_h^B)_{calc}$ are then computed by determining $(M_h^B)_{calc}$ from the regression line for each actual value of $g_h^A M_h^A$. The goodness-of-fit measure for each permutation is defined as

$$\delta = \frac{1}{N} \sum \frac{(F_h^B)_{obs} - (F_h^B)_{calc}}{(F_h^B)'} \tag{61}$$

$(F_h^B)'$ is a scale factor defined so that δ reflects relative, rather than absolute deviations. If $(F_h^B)_{obs} \neq 0$, $(F_h^B)'$ is defined as $(F_h^B)_{obs}$. If $(F_h^B)_{obs} = 0$, then $(F_h^B)'$ is assigned the value of the estimated detection limit for F_h^B--that is, the estimated, largest value F_h^B might actually have and still be undistinguishable from zero experimentally.

The permutation that minimizes δ is taken as the correct set of phases (p_h^A, p_h^B).

If t and w, the position and radius of the substituent, are not known, then the permutations can be carried out for several values of t and w, with the combination of t, w, g^A, and g^B that minimizes δ taken as the correct combination.

The program PHASE was written to implement this procedure, and the program PREDICT written to test PHASE (Appendix C). PHASE allows the electron density of the substituent, $\Delta\rho$, to be either a gaussian function or a rectangular strip function. Normally the gaussian was used. PREDICT finds the diffracted intensity expected from a given, 1-dimensional, centrosymmetric distribution of electron density $\rho_{in}(x)$. PREDICT allows $\rho_{in}(x)$ to be expressed as a sum of gaussians or as a sum of rectangular strips. PHASE successfully reconstructed each isomorphous pair $[\rho_{in}^A(x), \rho_{in}^B(x)]$ with which it was tested. Figure 18 shows the flow of information for PHASE (1) with artificial "data" from PREDICT and (2) with real data.

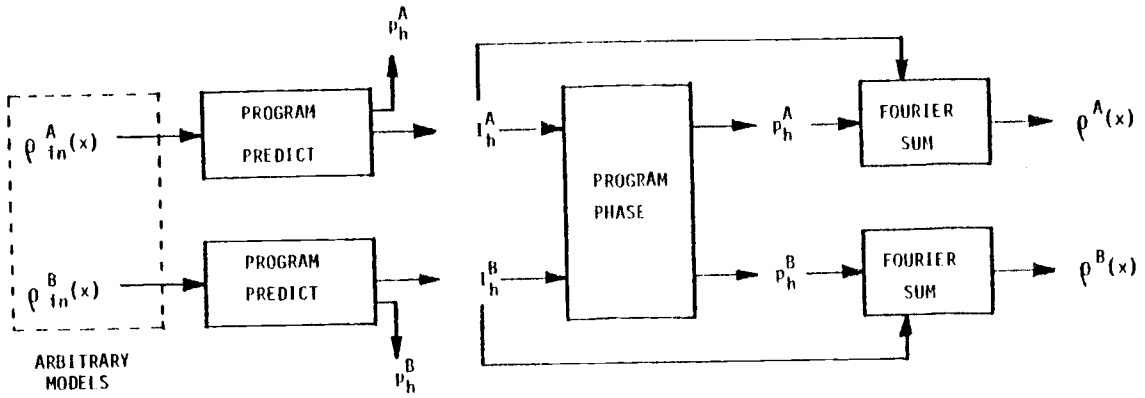

Data flow for verification of program PHASE

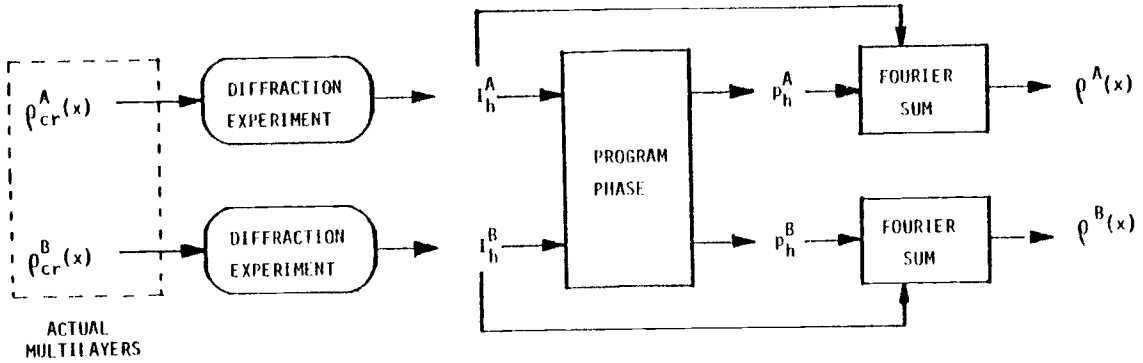

Data flow for diffraction experiment

Figure 18. Use of the program PHASE.

V. X-RAY DIFFRACTION FROM PHOSPHOLIPIDS - EXPERIMENTAL

A. Specimen Preparation

The phospholipids investigated were L-α-1,2-dipalmitoyl lecithin (DPL) and a mixture (BrDPL) of equal amounts of L-α-1-palmitoyl-2-(9-bromopalmitoyl) lecithin and its 10-bromo analog. The DPL was used as purchased from Supelco (4-6017: 99+% purity). The BrDPL was synthesized by J.C. Reinert and R.R. Lowry, of the Environmental Health Sciences Center at Oregon State University, according to their published procedure [16]. Their analyses found

1. 9.7% Br and 3.4% P (theoretical: 9.85% and 3.8%);
2. palmitate : monobromopalmitate = 51.5 : 49.5;
3. 95% of fatty acid at 2-position = monobromopalmitate.

Each diffraction sample consisted of a lipid film (3 mm x 1 mm x ∿3 μm) on the surface of a piece of glass (15 mm x 4 mm x 0.1 mm), which had been made hydrophobic. The hydrophobic glass supports were made from 18 mm x 18 mm x 0.1 mm microscope slide covers. The slide covers were cleaned and treated with the hydrophobic surfactant N,N-dimethyl-N-(3-trimethoxysilylpropyl) octadecyl ammonium chloride [98]. They were then cut to size using a diamond-tipped scribe. The surfactant was a gift of Dr. Mary Daniels of the Dow Corning Company, Midland MI. The glass was cut to size after, rather than before, surfactant treatment, so that the cut edges would be hydrophilic, thereby preventing lipid solution from flowing over the edges. The following procedure was used for the glass supports.

1. Rinse in distilled water.
2. Sonicate 1 hr in alcoholic KOH.
3. Rinse in distilled water.
4. Sonicate 30 minutes in dilute HCl.
5. Rinse several times in distilled water.
6. Sonicate 30 minutes in distilled water.
7. Rinse in ethanol (100%).
8. Soak 1 hr in 0.5% (v/v) solution of silane surfactant in ethanol.
9. Rinse in ethanol.
10. Soak in distilled water.
11. Cut to size.

For each specimen, 150 μL of a 1 g/L solution of lipid in chloroform was put dropwise on the glass surface, allowing partial evaporation between drops. This was done in room air and at room temperature. After the specimen had dried in air for one hour, it was placed over calcium chloride at a reduced pressure of ∿3 kPa for eight hours.

The lipid film which covered the glass was then trimmed to an area of 3 mm x 1 mm by scraping the unwanted portion away with a clean knife blade. The exposed area of the glass was wiped with a folded piece of chloroform-dampened filter paper, with care taken not to moisten the remaining lipid. This trimming was done to ensure that a uniform amount of lipid would be exposed to the x-ray beam throughout the range of diffraction angles used ($0 \leq \theta \leq 0.15$ rad). The trimmed specimen was then heated in a drying oven at 100°C for 12 hours.

About 25% of our specimens produced intense, lamellar diffraction of four to ten orders. Among these successful samples, the number and relative intensity of the orders were consistent from specimen to specimen for a given lipid, and depended on the temperature and degree of hydration during diffraction. This dependence was quite pronounced for DPL (especially at low hydration) and less strong for BrDPL. The

unsuccessful 75% of the specimens gave only a broad, weak peak where the first order was expected. These specimens were discarded.

The visual appearance of the lipid films ranged from clear to cloudy. There was no correlation between visual appearance and intensity of diffraction.

B. Diffraction Apparatus and Geometry

The geometry used to obtain lamellar diffraction from our lipid specimens is illustrated in Figure 19. A diffractometer (Picker 6283F), which was kindly loaned to us by Professor D.P. Shoemaker, was modified for use as an x-ray source. The x-ray tube had a copper target, whose projected area normal to the beam was 0.4 mm x 1.0 mm. A 17 μm-thick, nickel β-filter was used as a monochromator to give radiation with λ = 154.2 pm. The stability of the power supply was specified by the manufacturer to be 0.1% for voltage and 0.02% for current. We found the variation in beam flux to be well under 0.5%. The tube was normally operated at 32 kV, 10 mA (full-wave).

The beam was collimated to propagate in the y-direction, with a rectangular cross section in the xz-plane (see Figures 19 and 20). The beam was defined in the z-direction by two parallel, quartz optical flats, which were 5.5 cm long and which were separated by 0.1 mm spacers. Thin (0.13 mm), polished tantalum slits with apertures of 0.5 mm were used to define the beam in the x-direction. In addition, similar tantalum slits were used as a vertical guard aperture at the end of the collimator nearer the specimen. The tantalum was a gift of Mr. Robert Garon, Teledyne Wah Chang, Albany, OR.

The specimen was mounted in a temperature-controlled holder (Figure 20), described below, in which it was precisely rotated in the beam and about the θ-axis, which was parallel to the x-axis. The beam cross section at the specimen location was measured with the position-sensing detector to be 0.7 mm (x) by 0.4 mm (z), fwhm. Since

the projection of the lipid specimen onto the z-axis was less than 0.12 mm at the largest diffraction angles used, the beam flux on the specimen was essentially constant during diffraction experiments.

On its way to the detector, radiation diffracted from the specimen was passed through a 20 cm-long, rectangular chamber, whose 5 cm (x) by 13.5 cm (z) ends were sealed with windows of 50 μm-thick Kaptan film (Trademark, DuPont). A flow of helium was maintained through this chamber to reduce scattering and absorbance due to air.

For diffraction experiments, the detector was usually 242 mm from the sample, as measured with a rule. The detector was shielded from the direct beam by a sheet of 0.13 mm tantalum, backed with 0.1 mm lead foil. This beamstop was attached to the front of the detector, about 1 cm from the anode.

The width, in the x-direction, of the collimated, direct beam was 2 mm at the detector. This was determined photographically by placing film at the usual detector position. The first four orders of diffraction had the same width, 2 mm, and appeared on film as straight lines which looked similar to--but much weaker than--the image of the direct beam. Since these diffraction lines were shorter than the 4 mm-width of the detector window, all diffraction for each order was collected by the detector.

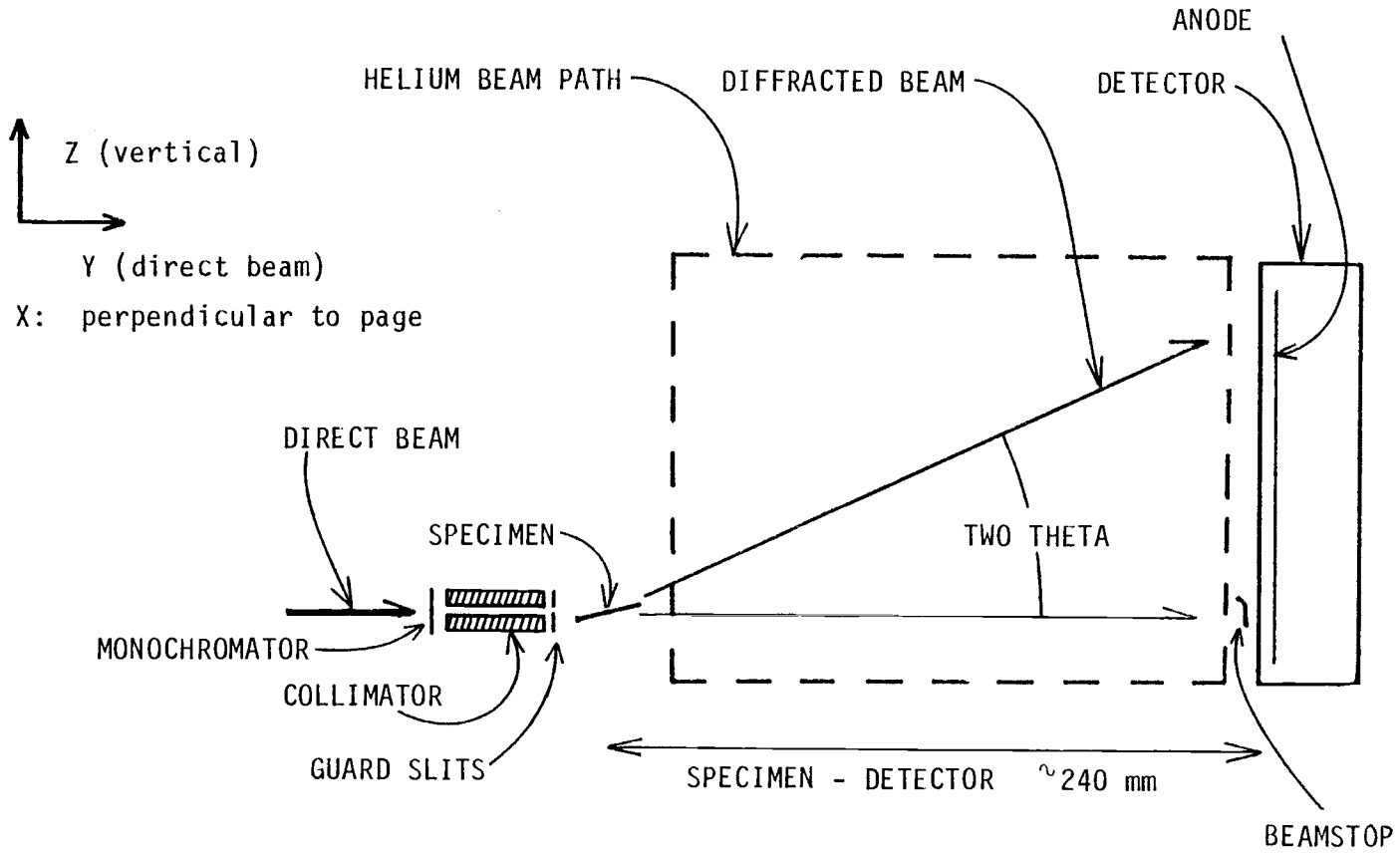

Figure 19(a) Diffraction apparatus (not to scale).

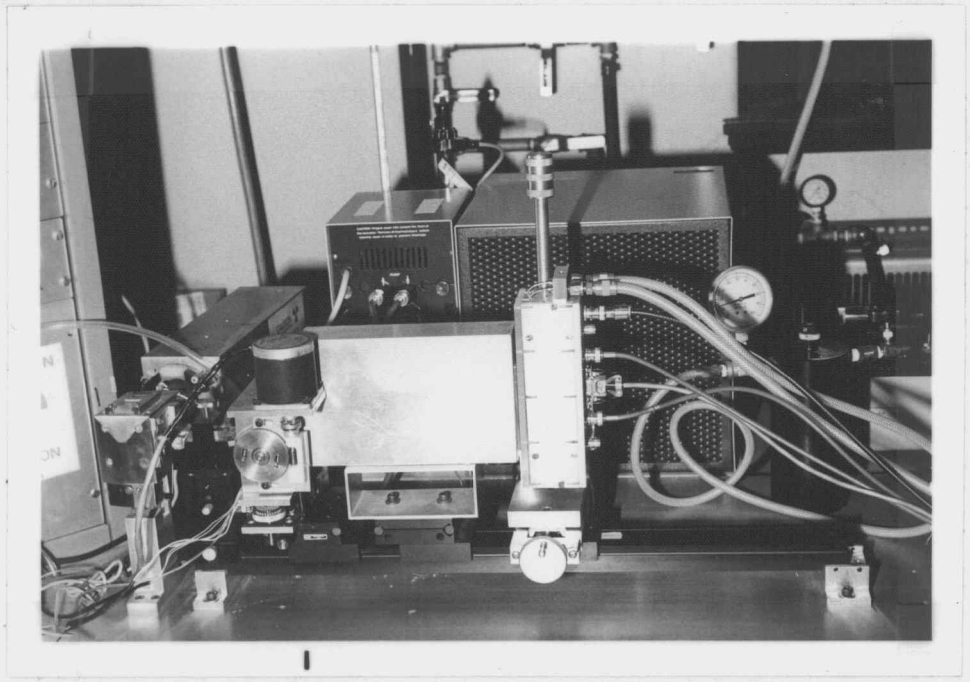

Figure 19(b). Diffraction apparatus.

C. Specimen Holder for Lamellar Diffraction

Specimens described in the previous section were mounted for diffraction in an aluminum specimen holder which we designed. A diagram and photographs of this sample holder are shown in Figures 20 and 21. This device allowed control of specimen temperature to an estimated precision and accuracy of ±0.1 and ±0.2°C over the range -15 to +100°C. At the same time, it allowed the sample to be rotated in the direct beam about an axis parallel to the glass support and passing through the specimen. In addition, since the chamber was sealed, the atmosphere about the specimen could be controlled. The chamber support, shown in the photographs, could be translated in three directions (x, y, and z of Figure 19) for positioning the sample in the beam.

Window units, which are shown in the photographs, but not in the diagram, consisted of 50 μm-thick aluminized mylar sandwiched between delrin and aluminum frames. Small tubes through the frames were included for gas flow through the sample compartment. With flat rubber gaskets and silicone grease used for leak resistance, the window units were easily attached to and detached from the specimen chamber with #4-40 screws.

Coolant was pumped by a Lauda K-2/R refrigerated circulator through a cavity in the chamber block, as shown in the diagram of Figure 20. Above 0°C, 1,2-ethanediol was used as the coolant. For runs which went below 0°C, 2-propanol was used. For these runs, a helical copper heat exchanger in a 2-propanol dry ice bath was used

in the coolant line between the circulator and the sample chamber. At low temperatures, a thin polyethylene shroud filled with dry helium was placed over the chamber and the stages to prevent condensation on the windows and to help prevent convective heat transfer.

The temperature was maintained with an Artronix 5301 temperature controller. This unit drove a resistance heater, which was embedded in the chamber as shown in Figure 20. The heating coil was made from 5.7 m of 120 μm-diameter Cu-Be wire with a resistance of 6.6 Ω/m (California Fine Wire Co.). It was potted with thermally-conductive epoxy resin (Emerson and Cuming Eccobond 285). With this coil and controller, the maximum power available was 65 W, which was enough to raise the sample temperature to over 100°C in a few minutes.

Temperature was monitored with small thermistors, which were embedded near the specimen position with thermally-conductive epoxy. These thermistors (Yellow Springs Instruments 44006 and 44007) were specified by the manufacturer to conform to the supplied temperature-resistance data to 0.2°C. This agreement was verified by immersing the specimen chamber and a calibrated mercury thermometer in a controlled-temperature bath at several temperatures. One of the thermistors was used as a sensor for the temperature controller; the other was used for readout.

The specimen chamber was rotated by a stepping motor (Rapid-Syn 23H503), driven by a controller of our design (Appendix B). A precision pulse generator (Tektronix 115) was used as a timebase. The motor was connected to the θ-axis of the sample chamber through a 1:100 anti-backlash worm drive. The rotational increment (step) was 4° at the

motor, and 0.04° (0.698 mrad) at the specimen.

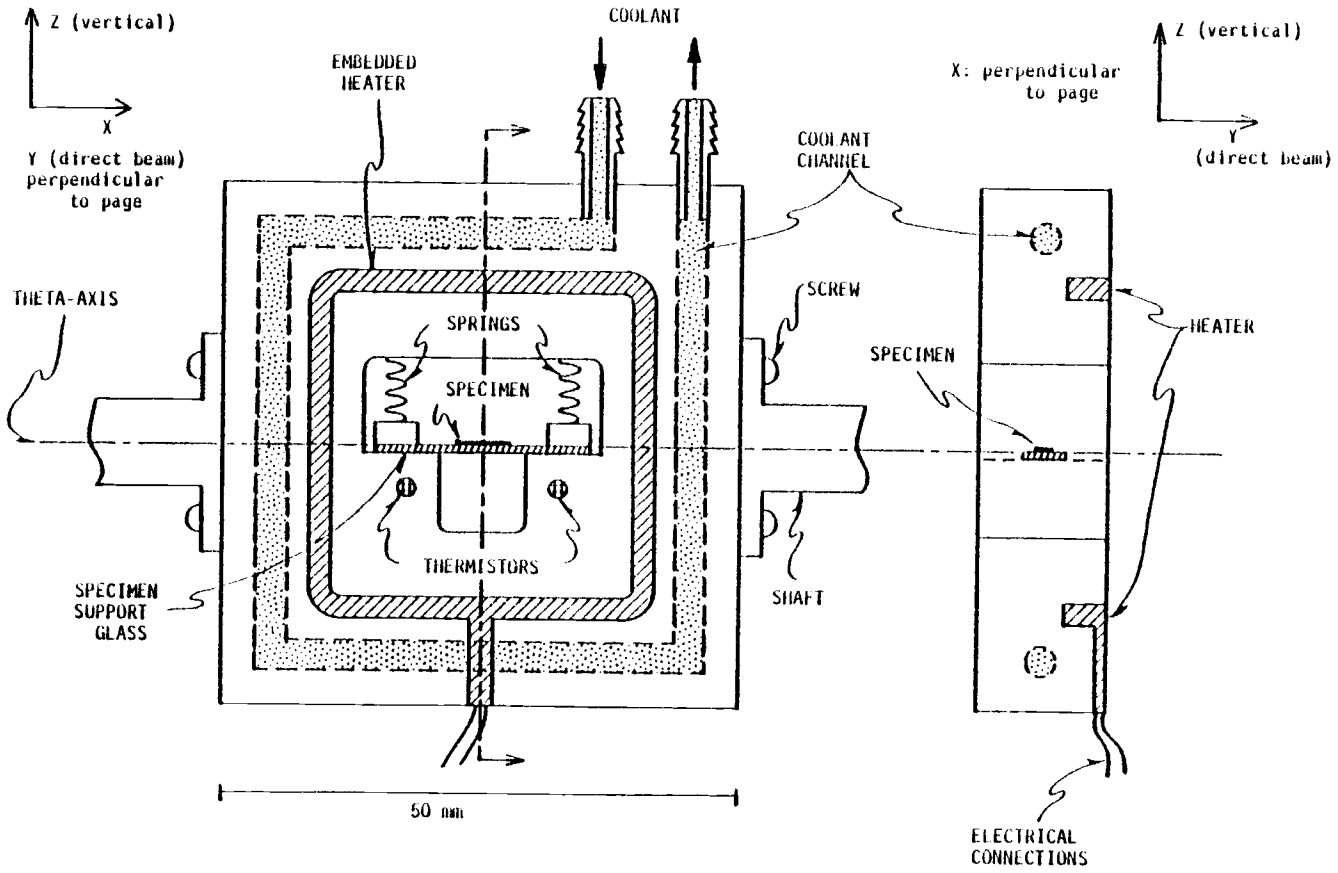

Figure 20. Specimen holder.

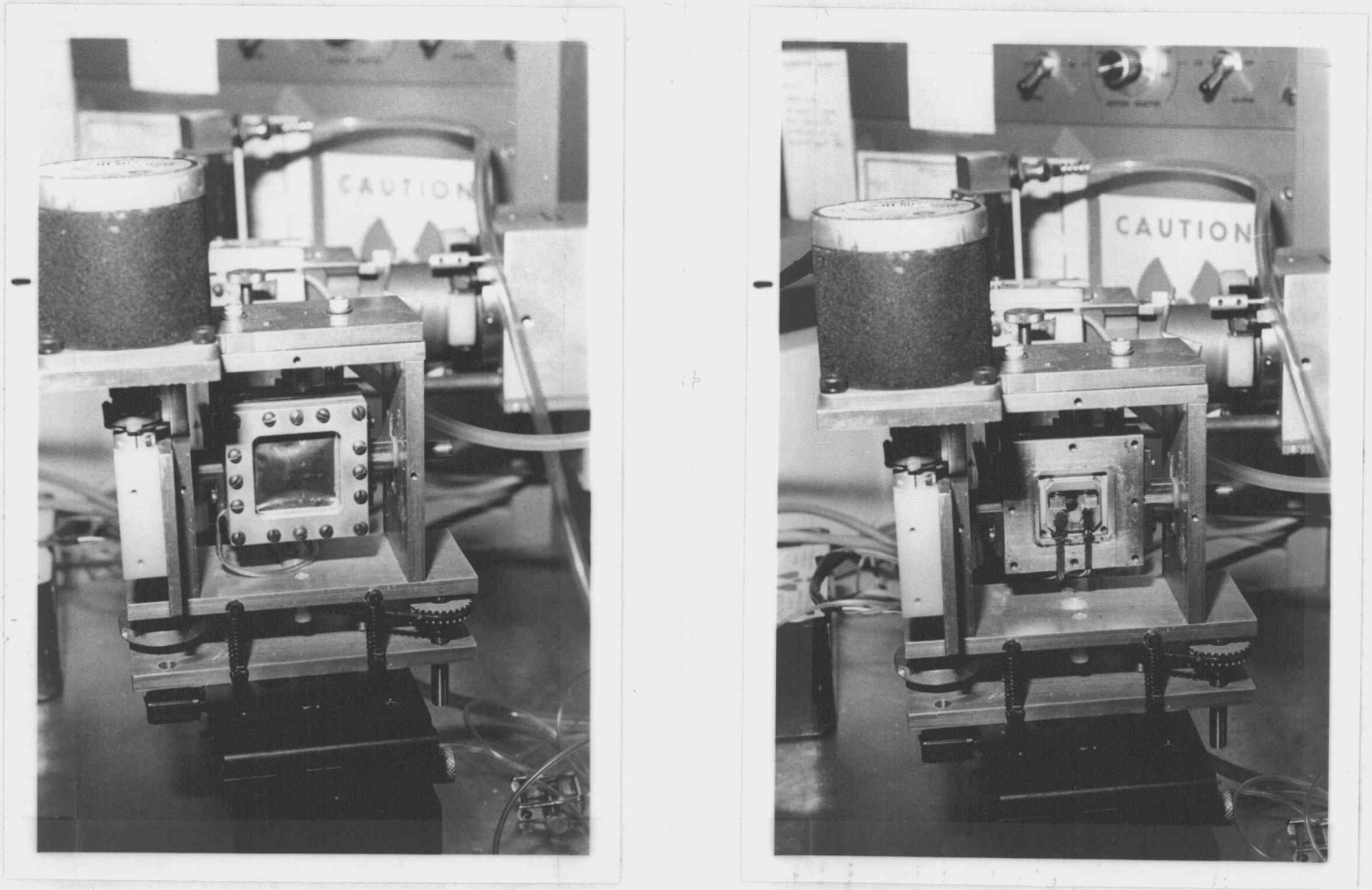

Figure 21. Specimen holder.
Left: windows in place
Right: windows removed

D. Lamellar Diffraction from DPL and BrDPL

1) Hydration Technique and DPL Results

DPL and BrDPL specimens were hydrated by sealing them in the sample holder along with a small tray of water. Additional, inner windows of Kaptan film were clamped between the window-frame gaskets and the holder body. Hydration was effected by heating the holder to 80°C for 90 minutes and then cooling it to room temperature or below. When the chamber was cool, the inner windows, which were covered with condensed water, were removed, and the chamber was quickly resealed.

Specimens were dehydrated by flowing dry nitrogen through the holder while the temperature was kept at 90°C. After 90 minutes, the nitrogen entry and exit were clamped, and the holder was cooled to room temperature or below. Partial dehydration was accomplished by heating to lower temperatures for shorter times or by flowing dry nitrogen through the chamber at room temperature.

For DPL, the degree of hydration was inferred using Chapman's data relating water content to lamellar spacing in the gel state [99]. We refer to our values of this spacing as "d_4", because they were based on the prominent h=4 diffraction peak, which was easily monitored. For DPL at 20.0°C (gel), we found d_4 values of 5.6 and 6.3 nm for the dehydrated and hydrated states defined above. These compare well with Chapman's limiting values of 5.6 nm for anhydrous DPL and 6.4 nm for DPL with excess (above 30 weight percent) water.

As discussed in the next section, corresponding values of d_4 at -15°C for BrDPL prepared in these dehydrated and fully hydrated states were 5.8 and 6.3 nm. We assumed that for identical degrees of hydration, the structure and spacing of BrDPL at -15°C were the same as for DPL in the gel state. Therefore, Chapman's data for DPL were used to estimate the water content of BrDPL also.

Specimens were maintained at nearly constant water content by keeping the chamber sealed. For DPL below 25°C, d_4 did not change by more than ±15 pm (0.15 Å) over several hours. Above 25°C, hydrated specimens tended to dry out even in the sealed chamber, as indicated by reductions in d_4 on return to the reference temperature of 20°C. The rate of dehydration increased with temperature.

Due to this effect, we could not follow the chain-melting (gel-liquid crystal) transition of hydrated DPL. This transition is known to occur at ∿41°C for fully hydrated DPL, and at higher temperatures for DPL with lower hydrations [99].

By increasing the temperature of a dry DPL specimen, we observed a reduction in d_4 from 5.6 to 4.3 nm at 75°C. According to Chapman's data, this corresponds to the chain-melting transition of DPL containing 2% water.

Figure 22 shows the 11-order diffraction pattern we obtained in a 210-minute scan of DPL in its lowest hydration at 20°C. The lamellar spacing was 5.6 nm. The relative peak intensities were qualitatively the same as those obtained by Stamatoff [100] for a DPL specimen made with 2% water by the method of Powers and Clark [98].

Stamatoff's pattern had a higher signal/noise ratio than ours, and included orders 5 and 7, which were about 10% as intense as 2 and 3.

To find the effect of changing the temperature of a partially hydrated DPL specimen in the gel state, we cycled the temperature in the sequence +20.0, -10.0, +20.0, -8.0°C. The lamellar spacing, d_4, changed reversibly from 6.18 nm to 6.03 nm at the high and low temperature extremes. The relative intensities in the diffraction pattern did not change appreciably. Based on the data of Nagle and Wilkinson for thermal expansivity of DPL [101] this change of 0.15 nm is about three times larger than would be expected if the expansion were isotropic.

2) BrDPL Results

The mixture of brominated lecithins exhibited a broad transition in lamellar spacing centered around 0°C, as shown in Figure 23. The diffraction patterns from which these curves are derived (Figure 24 (a) - (c)) were obtained in about five minutes each. The variation in beamstop spillover--the sharp peaks near the origin--is due to starting the scans at slightly different values of θ. The lamellar spacing was calculated from the position of the easily-monitored h=4 peak.

The high and low hydration states of BrDPL were prepared in situ in the same way as the hydrated and dehydrated DPL, above. The intermediate hydration state was prepared from fully hydrated BrDPL by flowing dry nitrogen through the specimen chamber for one hour at room temperature.

For these three hydration states, the lamellar spacing appeared to be approaching maximum values at the lowest temperature we could obtain, -15.0°C. At this temperature, the highest and lowest spacings were 6.2 and 5.8 nm. These are to be compared with our values at 20°C of 6.3 and 5.6 nm for DPL (gel) prepared similarly. Based on the assumption of a similarity of structure and lamellar spacing between gel DPL at room temperature and BrDPL at -15°C, the low, intermediate, and high hydrations discussed here and pictured in Figures 23 and 24 correspond to about 20, 24, and 28% water by weight.

To examine the stability of hydration of BrDPL when the temperature was changed, the intermediate-hydration BrDPL was cycled in temperature from +20.0 to -15.0 to +20.0°C in 5.0°C increments. At these temperatures, d_4 was reproducible to 10 pm (0.1 Å) for the descending and ascending runs. This fact, along with results for DPL over a similar temperature range, were taken as evidence that the hydration of the lipids did not change over this 35° temperature interval. Changes in temperature above 25°C did produce hysteresis in d_4, amounting to about 0.2 nm when the specimen was taken to 40°C and returned to 20°C. This apparent dehydration requires that the curves of Figure 23 be interpreted cautiously above 20°C.

3) Degree of Lamellar Orientation

By monitoring the intensity of a fixed (in this case h=4) diffraction peak as θ was varied, the rocking curves of Figures 25 and 26

were obtained. For partially hydrated DPL at 25°C and BrDPL at +10 and -15°C, we found rocking curve widths of under 6 mrad (0.4°), fwhm. If a perfectly fine, nondivergent primary beam had been used, this number would roughly give the average angular deviation of the lamellae from planarity. Since the measured value was about the same as our beam divergence, it is an upper bound on the actual lamellar disorder in the specimens.

E. Attempted Wide-Angle Diffraction from DPL and BrDPL

In addition to lamellar diffraction, which is obtained in the low-angle region, phospholipids exhibit wide-angle x-ray diffraction, which indicates the distribution of acyl chains in planes parallel to the bilayer lamellae. In the chain-melting transition, the sharp 0.42 nm peak is replaced by a diffuse 0.46 nm band, indicating an increase in the disorder of the chains [99]. With the detector 4 cm from the specimen, and oriented with its anode parallel to the theta axis, wide-angle diffraction was not observed as the specimen was oscillated about $\theta=0$.

Wide-angle diffraction is normally observed from bulk lipid specimens. The fact that it was not observed here may be due to the thinness ($\sim$3 μm) of our specimen.

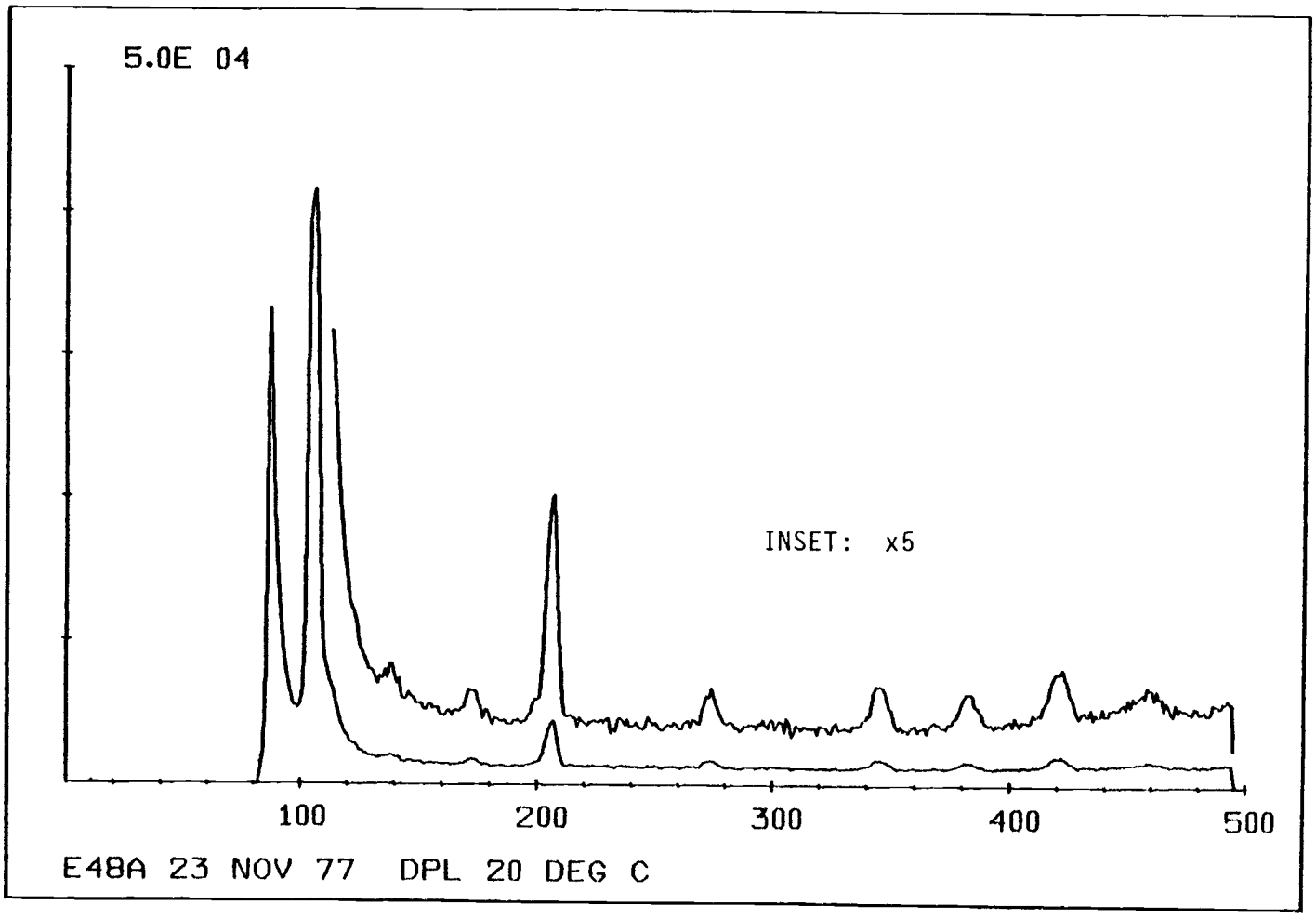

Figure 22. DPL lamellar diffraction at low hydration.

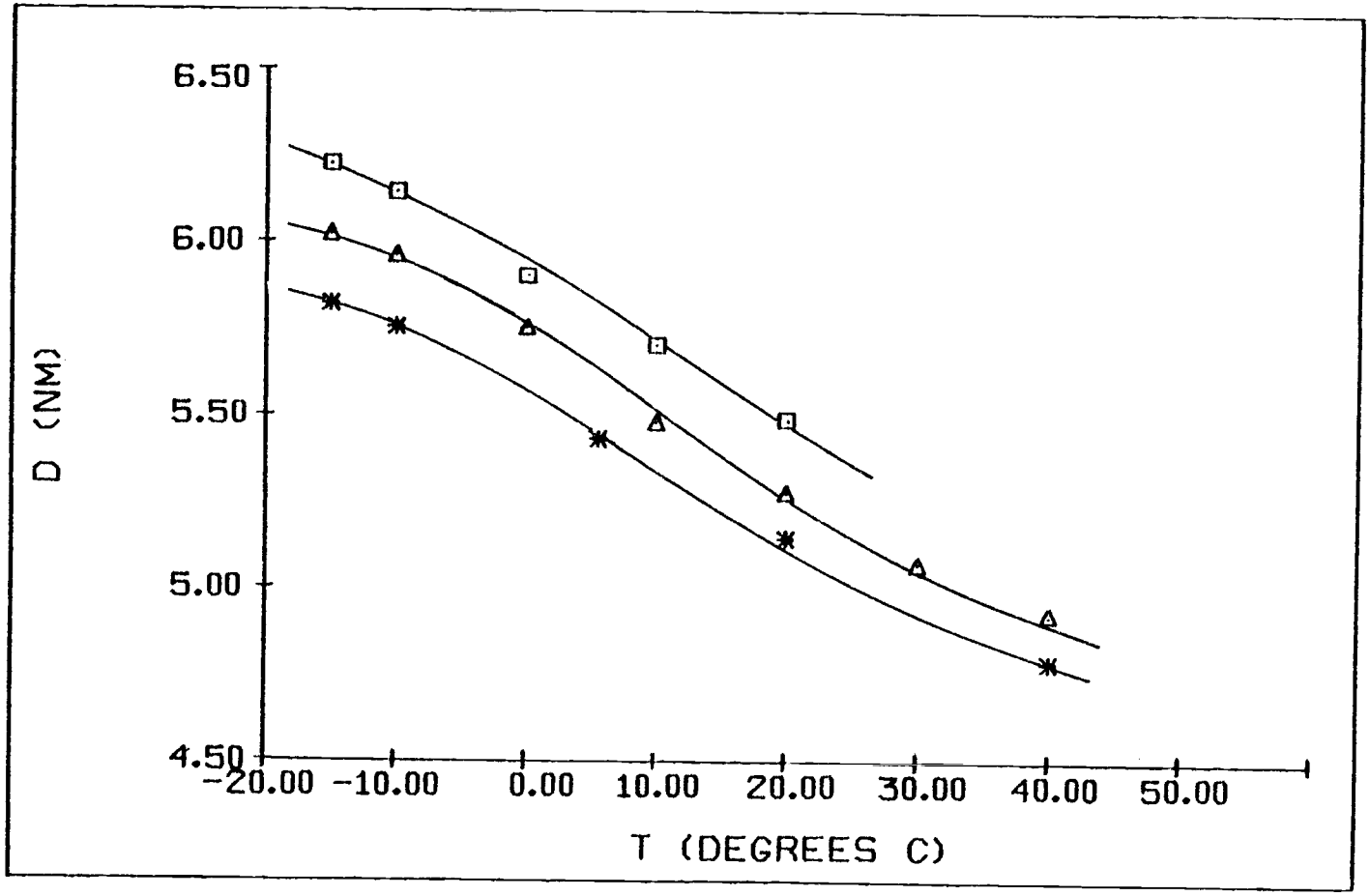

Figure 23. Lamellar spacing vs temperature for BrDPL

Estimated water contents:
- ⊡ 28% water
- Δ 24% water
- * 20% water

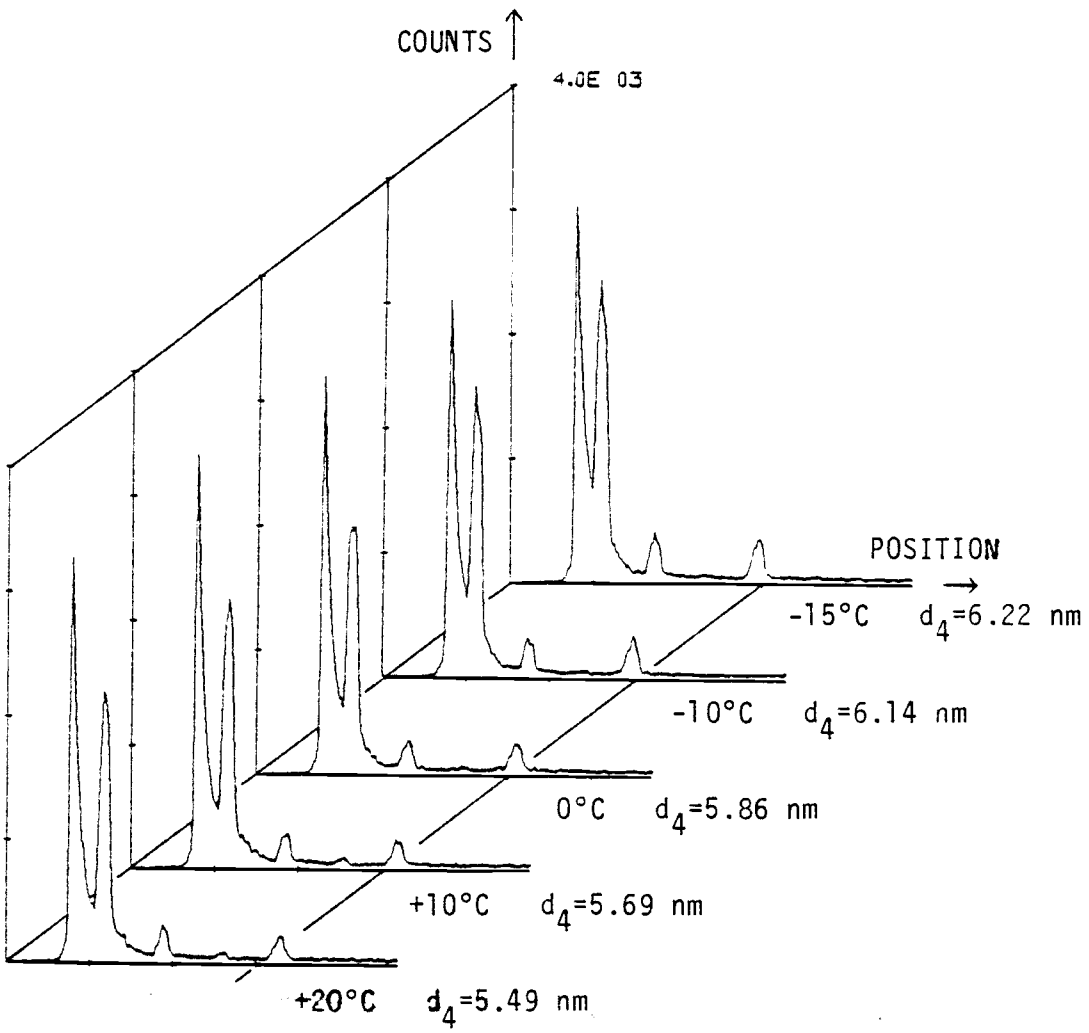

Figure 24(a). Temperature--and hydration--dependence of BrDPL diffraction patterns.

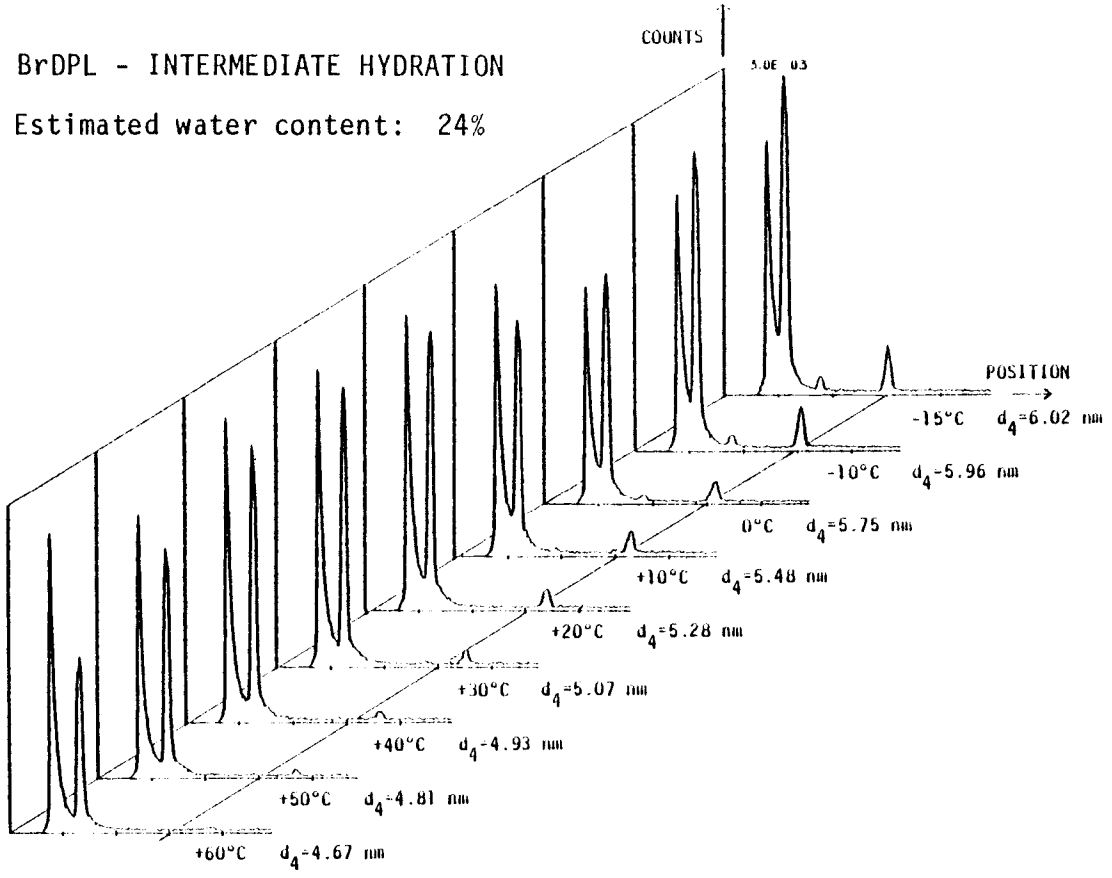

Figure 24(b). Temperature--and hydration--dependence of BrDPL diffraction patterns.

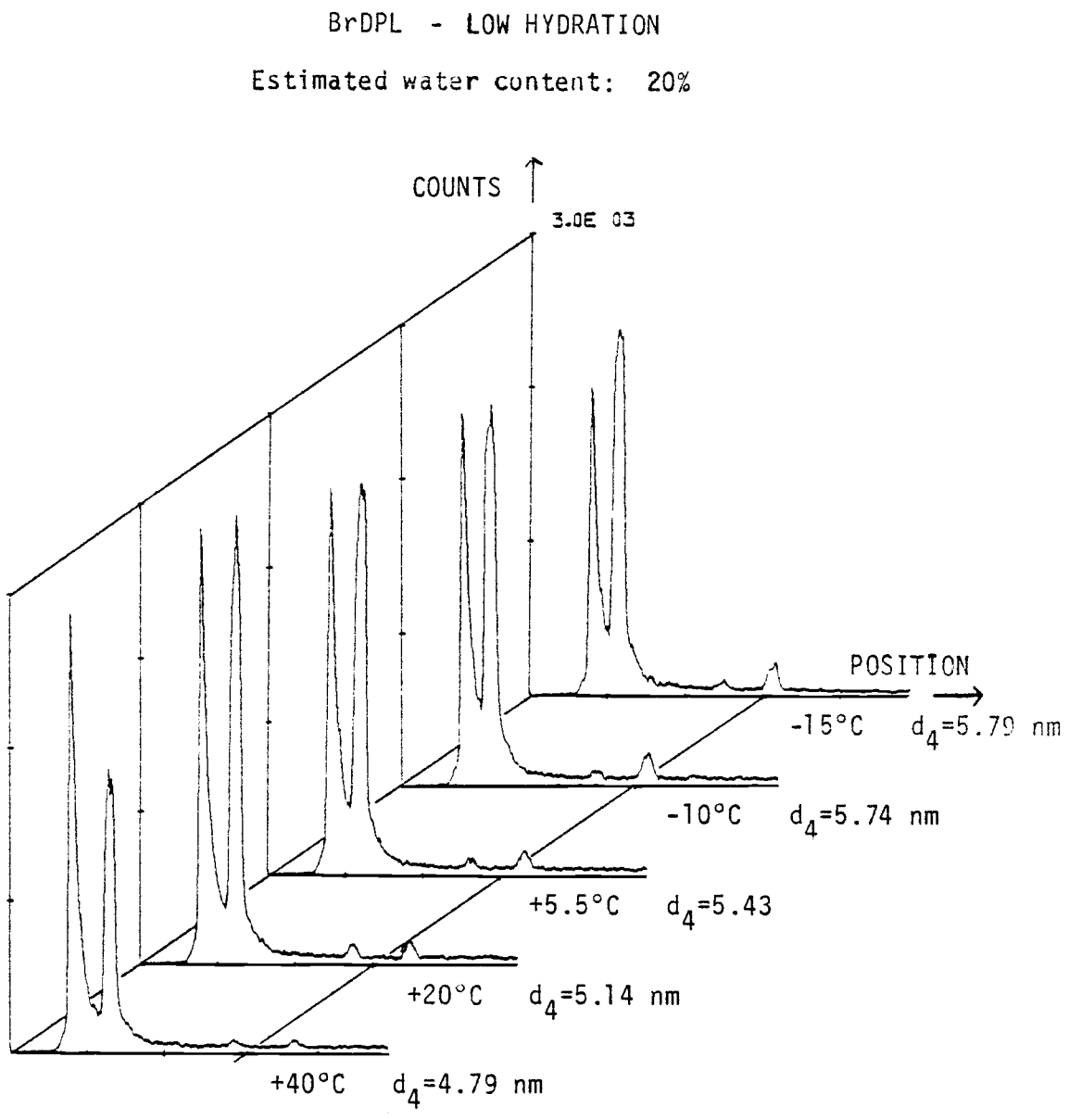

Figure 24(c). Temperature--and hydration--dependence of BrDPL diffraction patterns.

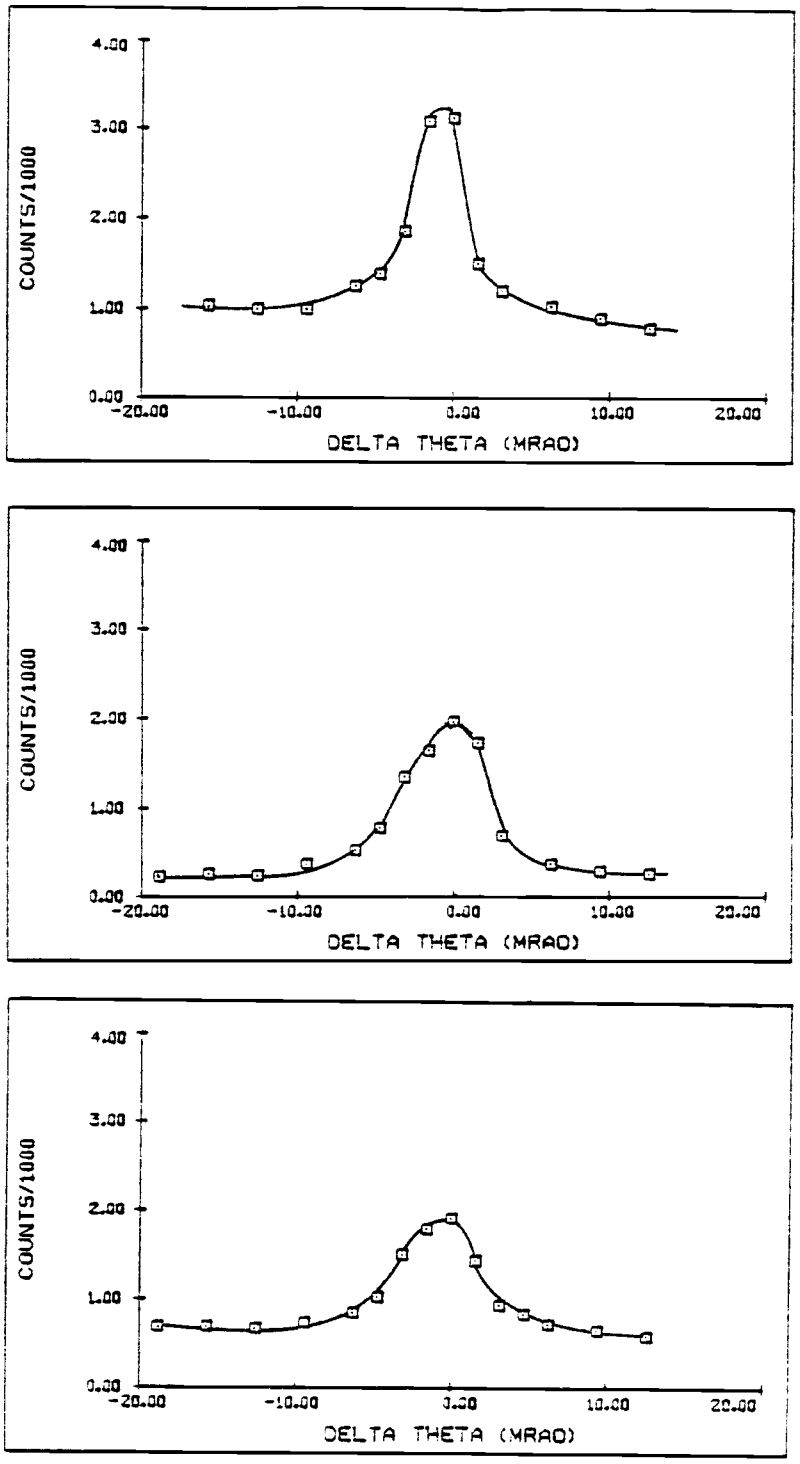

Figure 25. Rocking curves for fourth-order lamellar reflection.

Top: DPL, +25°C
Center: BrDPL, -15°C
Bottom: BrDPL, +10°C

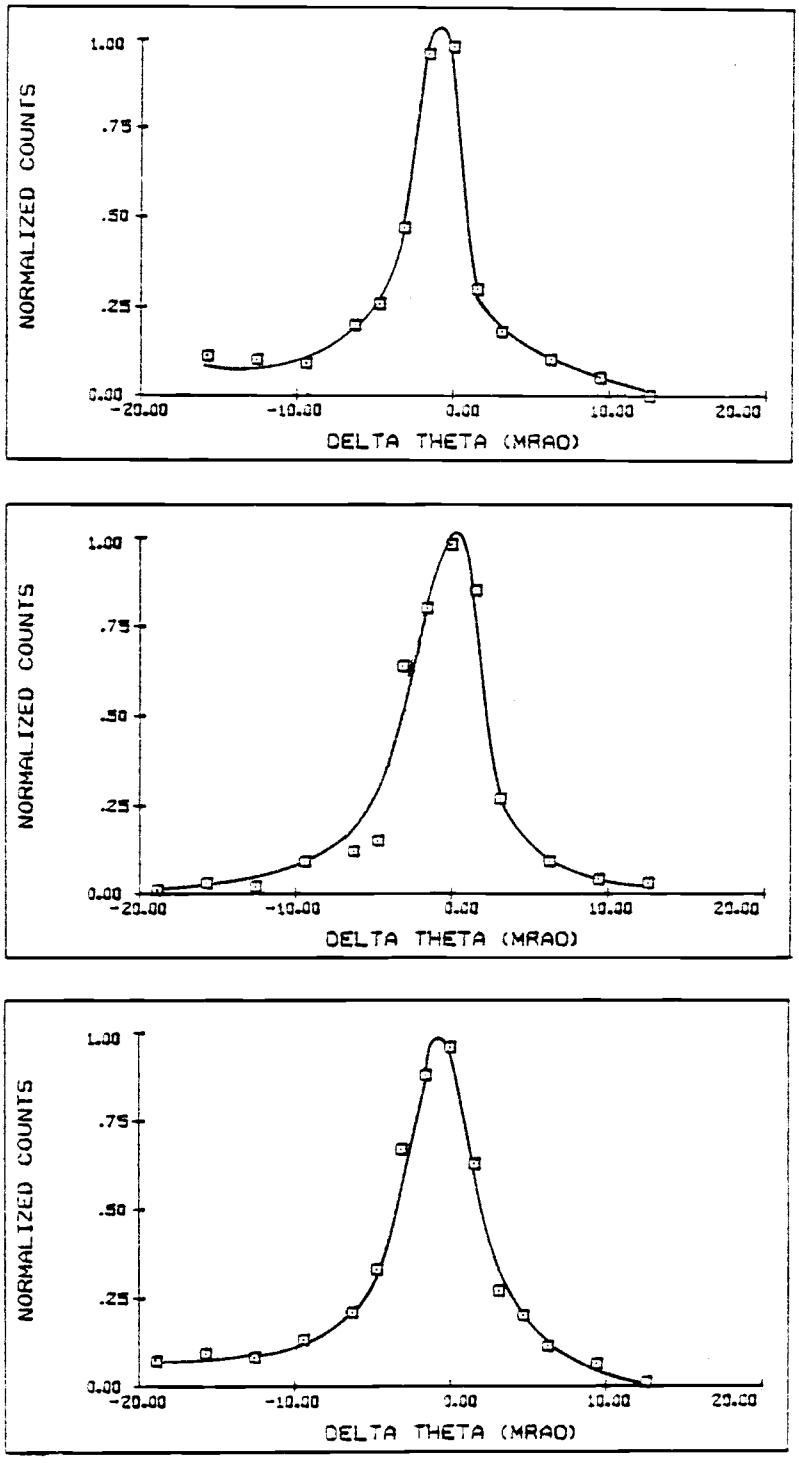

Figure 26. Rocking curves for fourth-order lamellar reflection, normalized, with background subtracted.

Top: DPL, +25°C
Center: BrDPL, -15°C
Bottom: BrDPL, +10°C

F. The Isomorphous Replacement Experiment

1) Rationale

In order to use an isomorphous replacement technique for phasing, the structures must be isomorphous. For determining electron-density profiles of DPL and BrDPL, isomorphicity entails at least that:

1. the lamellar spacings be the same
2. the water contents be the same
3. the chain orientations be the same.

The observed transition in lamellar spacing that occurs over a broad temperature range in BrDPL complicates the situation. In order to proceed with a phasing attempt, the following assumptions were made.

1. The transition in BrDPL is nearly complete at -15°C.
2. The BrDPL chains approach full extension at low temperature.
3. Specimens of BrDPL and DPL which have the same lamellar spacing in the gel state have the same water content.

Assumption one is based on Figure 23 . The fact that the change in lamellar spacing on cooling BrDPL is similar to the change for DPL supports assumption two. Also, the loss of higher orders (Figure 24) on heating BrDPL is consistent with a chain-melting transition for BrDPL.

The lamellar spacings observed for BrDPL and DPL in our hydrated state are both 6.3 nm and are close to Chapman's value for DPL in excess water (6.4 nm). Furthermore, the specimens could be dehydrated from this value, as evidenced by changes in lamellar spacing on heating. These facts support assumption three.

2) Data

Due to considerations discussed in the previous section, BrDPL at -17.0°C and DPL at 20.0°C were used for the isomorphous replacement experiment. A specimen of BrDPL with the arbitrary choice of d_4 = 5.81 nm was used. Dry nitrogen was blown over a hydrated DPL specimen at 20°C until its lamellar spacing had the same value, 5.81 nm. The diffraction patterns used for the isomorphous replacement experiment are shown in Figure 27. The DPL (20°C) and BrDPL (-17°C) patterns were each collected in 80 minutes.

The program DIFRAX (Appendix C) was written and used to strip background from the patterns, compute peak integrals, and perform the Lorentz correction indicated in Equation 40. The output from DIFRAX was two sets of tentatively isomorphous values of $|F_h|$ to be used in the phasing program PHASE.

Background to be stripped consisted mainly of specular reflection and scattering from the glass sample supports. This background was intense in the low-angle region of the patterns, where it was sharply cut off by the beamstop. Attempts to directly subtract the background, using data from a blank sample support, were not successful. This is because the low-angle background depended very strongly on support size and position and on the initial value of θ for the scan.

The stripping portion of DIFRAX computed a sum-of-exponentials background curve based on data points (channel values) between the diffraction peaks and below the first order peak. Typically, the distance between peaks was 35 channels, and the number of points used in

the fit was five between each peak and 15 below the h=1 peak.

This procedure removed most of the background, but the values at the midpoints between peaks still deviated somewhat from zero. The deviation was offset order-by-order by fitting points near the midpoints on either side of a peak to a straight line, which was then subtracted from the peak. The final results of this stripping are shown in Figure 27 as the "background subtracted" patterns.

To remove noise from the patterns, the channel values Z_i were subjected to a three-channel averaging routine, to give smoothed values $\overline{Z}_i$:

$$\overline{Z}_i = (1/3)\ (Z_{i-1} + Z_i + Z_{i+1}) \qquad (62)$$

These smoothed values are shown in the bottom patterns of Figure 27.

The integrated intensity $(I_{int})_h$ was found for each discernible peak by adding the Z_i, using the midpoints between peak centroids as limits. For each peak h, $|F_h|$ was found from

$$|F_h| \propto \sqrt{h \cdot (I_{int})_h}\ , \qquad (63)$$

normalized so that

$$\sum_h F_h^2 = 100\ . \qquad (64)$$

The values of $(I_{int})_h$ and $|F_h|$ for DPL and BrDPL are listed in Table 7.

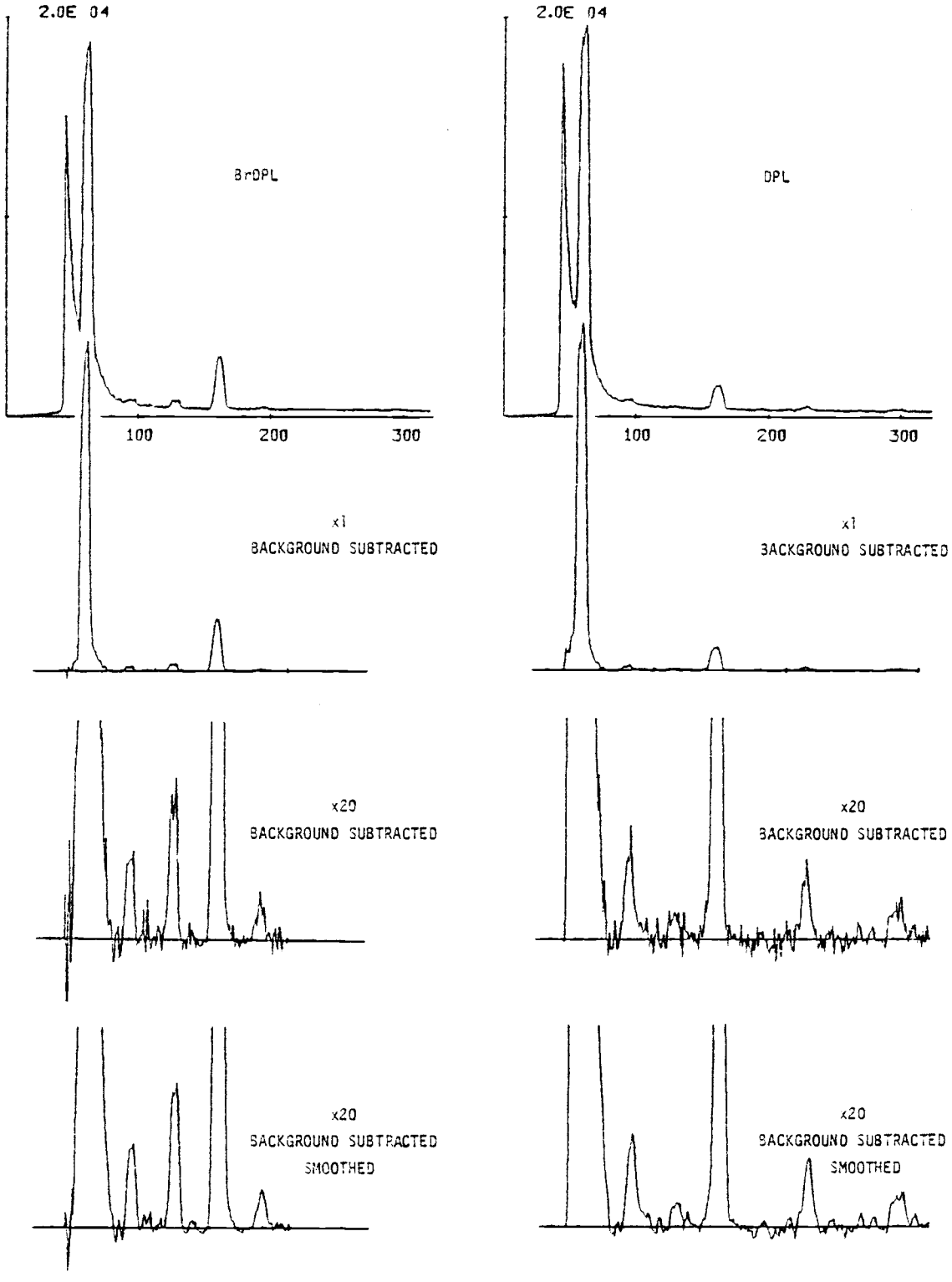

Figure 27. Diffraction patterns used for isomorphous replacement.

Table 7. Integrated intensities and $|F|$ for DPL and BrDPL.

	BrDPL d = 5.81 nm T = -17.0°C			DPL d = 5.81 nm T = 20.0°C	
h	$(I_{int})_h$	$\|F_h\|^{\ddagger}$	h	$(I_{int})_h$	$\|F_h\|^{\ddagger}$
1	127 471	7.67 ±.03	1	150 485	8.46 ±.04
2	1 952	1.34 ±.03	2	2 093	1.41 ±.02
3	2 681	1.93 ±.02	3	489	0.84 ±.02
4	18 475	5.84 ±.02	4	9 984	4.36 ±.02
5	675	1.25 ±.02	5	*	*
			6	1 292	1.92 ±.02
			7	*	*
			8	934	1.89 ±.02

‡ relative
* no distinguishable peak

Confidence intervals estimated as

$\pm 4\delta F$, with

$$\frac{\delta F}{F} = \frac{1}{2h} [(I_{int})_h]^{-1/2}$$

3) Interpretation

The program PHASE (discussed on pages 68-72 and listed in Appendix C) was used to find, for each reflection h, the phase factors most consistent with an isomorphous relationship between DPL and BrDPL. This relationship is characterized by a model in which the projected electron-density profiles differ by a Gaussian function of half-width w and position in the unit cell t.

The data environment of PHASE, for validation and for actual use, is diagrammed in Figure 18. Using the measured values F_h(DPL) and F_h(BrDPL), the program finds the "best" set of phases based on a figure of merit δ. The figure of merit is the mean relative deviation between actual and calculated values of F_h(BrDPL).

The results of Appendix A, based on arbitrary models, and corresponding to the top portion of Figure 18, show that when t is cycled through a range of values including the correct one, δ is minimized for the correct t. This is the approach we used here, since t was not known.

The half-width of the isomorphous substituent, w, was estimated from known molecular geometry. Since the covalent radius of Br is 114 pm [102] and the 9 and 10 positions on the hydrocarbon chain are displaced from each other by about 160 pm, the projected width of Br on the hydrocarbon chains should be about 390 pm. The value of w used in PHASE was therefore 200 pm (2.0 Å).

The F values of Table 7 were used in PHASE, with several trial

values of t. Assuming the conventional view of lipid bilayers [5], and taking the plane midway between the hydrophilic headgroups as the unit cell origin, the minimum possible value for t is 1.9 nm if d = 5.81 nm. This is the position the Br substituent would occupy if the hydrocarbon chains were fully extended from the plane x = d/2 and perpendicular to it.

Table 8(a) gives the results from PHASE for five reflections from BrDPL and six from DPL, over the range t = 1.6 to 2.3 nm at 25 pm increments, and with w = 0.20 nm. The three lowest values of δ were 0.14, 0.20, and 0.23, at t = 2.115, 1.925, and 2.275 nm. The Fourier syntheses for these phase choices are shown in Figure 28 . The first and third choices, corresponding to the top and bottom profiles, are unacceptable, since they require the substituent to have negative electron density. The second choice looks reasonable, and is very much in accord with profiles derived by other phasing methods [19, 21]. For this set, the computed scale factor by which the F_h(BrDPL) must be multiplied is 1.08.

The result of using w $\neq$ 0.20 nm is shown in Table 8(c) For t = 11.850 to 2.025 nm and w = 0.10 to 0.30 nm, the lowest δ was still the one for w = 0.20 nm and t = 1.925 nm.

Figure 29 is the Hargreaves plot [14] for the δ = 0.20 phase set discussed above (DPL ++--0-, BrDPL +-+--). Neither of the points (Δ) corresponding to the F_8 reflection, which is absent in BrDPL, fits the phasing line. Figure 30 shows the profiles based on the 6-order results from PHASE, along with the two arbitrary choices for the 8th

order of DPL. Of the two, the bottom one (DPL +--0-0-) appears the more reasonable. Difference Fouriers corresponding to these profiles are given in Figure 31.

The Patterson maps for the two lipids are reproduced in Figure 32. The Patterson function, which is the overall autocorrelation function of $\rho(x)$ for the crystal, is defined as

$$P_{cryst}(x) = \sum_{h=1}^{h'} F_h^2 \cos(2\pi hx/d) \quad . \tag{65}$$

The distance from the origin to a maximum in $P_{cryst}(x)$ corresponds to a vector between electron-rich points in the crystal. In light of the structures proposed above, the peak in the BrDPL Patterson marked with an arrow (x = 1.4 nm), could easily correspond to a composite of the headgroup-Br (1.2 nm) and Br-Br (1.9 nm) distances.

Table 8(a). PHASE results for DPL and BrDPL -- substituent position varied.

SAMPLE A E1513 DPL
SAMPLE B E1464 BRDPL

REFLECTIONS 6
D-SPACING * 58.100
MODEL GAUSSIAN

INPUT DATA--AMPLITUDES

A	8.4600	1.4100	.8400	4.3800	0.0000	1.9200
B	7.6700	1.3400	1.9300	5.8400	1.2900	0.0000

BEST RESULTS * *

	WIDTH	POSITION	DEVIATION		A	1	2	3	4	5	6	B	1	2	3	4	5	6
1	2.0000	16.0000	.3536			+	-	-	-	0	-		+	+	-	-	+	0
2	2.0000	16.2500	.5274			+	-	-	-	0	-		+	+	-	-	+	0
3	2.0000	16.5000	.6635			+	-	-	+	0	-		+	+	-	+	+	0
4	2.0000	16.7500	.6632			+	-	-	-	0	+		+	+	-	-	+	0
5	2.0000	17.0000	.4998			+	-	+	+	0	-		+	+	-	+	+	0
6	2.0000	17.2500	.7393			+	-	+	+	0	+		+	+	-	+	+	0
7	2.0000	17.5000	.7756			+	+	+	-	0	+		+	-	+	+	-	0
8	2.0000	17.7500	.6468			+	-	+	-	0	+		+	+	-	-	+	0
9	2.0000	18.0000	.7162			+	+	-	+	0	-		+	-	+	+	-	0
10	2.0000	18.2500	.5527			+	+	-	-	0	-		+	-	+	-	-	0
11	2.0000	18.5000	.3721			+	+	-	-	0	-		+	-	+	-	-	0
12	2.0000	18.7500	.2891			+	+	-	-	0	-		+	-	+	-	-	0
13	2.0000	19.0000	.2332			+	+	-	-	0	-		+	-	+	-	-	0
14	2.0000	19.2500	→.1990	(2)		+	+	-	-	0	-		+	-	+	-	-	0
15	2.0000	19.5000	.2533			+	+	-	-	0	-		+	-	+	-	-	0
16	2.0000	19.7500	.3191			+	-	+	+	0	+		+	-	-	+	+	0
17	2.0000	20.0000	.4043			+	+	-	-	0	-		+	+	+	-	-	0
18	2.0000	20.2500	1.2486			+	-	-	-	0	-		+	+	+	+	-	0
19	2.0000	20.5000	.5582			+	-	+	-	0	+		+	-	-	-	-	0
20	2.0000	20.7500	.3970			+	-	+	+	0	+		+	-	-	+	-	0
21	2.0000	21.0000	→.1363	(1)		+	+	+	+	0	+		+	+	-	+	-	0
22	2.0000	21.2500	.1889			+	+	+	+	0	+		+	+	-	+	-	0
23	2.0000	21.5000	.5383			+	+	+	+	0	+		+	+	-	+	-	0
24	2.0000	21.7500	.8386			+	-	+	-	0	+		+	+	-	+	-	0
25	2.0000	22.0000	.6554			+	+	-	+	0	-		+	+	-	+	-	0
26	2.0000	22.2500	.3276			+	-	+	+	0	-		+	-	-	+	-	0
27	2.0000	22.5000	.2450			+	-	+	+	0	-		+	-	-	+	-	0
28	2.0000	22.7500	→.2250	(3)		+	-	-	+	0	-		+	-	-	+	-	0
29	2.0000	23.0000	.2383			+	-	-	+	0	-		+	-	-	+	-	0
30	2.0000	23.2500	.2578			+	-	-	+	0	-		+	-	-	+	-	0
31	2.0000	23.5000	.3016			+	-	-	+	0	-		+	-	-	+	-	0
32	2.0000	23.7500	.4517			+	-	-	+	0	-		+	-	-	+	-	0

* ANGSTROMS

Table 8(b). PHASE results for DPL and BrDPL -- substituent at 1.925 nm, halfwidth 0.20 nm.

SAMPLE A E1518 DPL
SAMPLE B E146A BRDPL

REFLECTIONS 6
D-SPACING * 58.100
WIDTH * 2.000
SHIFT * 19.250
MODEL GAUSSIAN

INPUT DATA--AMPLITUDES

A	8.4600	1.4100	.8400	4.3500	0.0000	1.9200
B	7.6700	1.3400	1.9300	5.8400	1.2500	0.0000

RELATIVE STRUCTURE FACTORS FOR SUBSTITUENT

A	-2.0474	-2.0763	3.6554	-1.4812	-1.5460	2.3129

RAW HARGREAVES COEFFICIENTS

A	-4.1321	-.6791	.2298	-2.9436	0.0000	.8301
B	-3.7462	-.6454	.5290	-3.9428	-.8086	0.0000

BEST RESULTS

INDEX	DEV	A 1	2	3	4	5	6	B 1	2	3	4	5	6	SLOPE	INTERCEPT	PEAK
1	.199	+	+	-	-	0	-	+	-	+	-	-	0	1.0813	.8907	.3018
2	.303	+	+	+	+	0	+	+	+	-	+	+	0	.8531	-.6599	-.2236
3	.399	+	+	+	-	0	-	+	-	+	-	-	0	1.0670	.8020	.2717
4	.411	+	+	-	+	0	-	+	-	+	+	-	0	1.2966	.9536	.3231
5	.417	+	-	+	+	0	+	+	+	-	+	+	0	.8178	-.8935	-.3028
6	.432	+	+	-	-	0	-	+	+	+	-	-	0	1.0913	.6803	.2305
7	.443	+	-	-	+	0	+	+	+	-	+	+	0	.8165	-.8230	-.2789
8	.448	+	-	+	+	0	+	+	-	-	+	+	0	.8986	-.5973	-.2024
9	.465	+	+	-	+	0	+	+	+	-	+	+	0	.8752	-.5682	-.1925
10	.497	+	-	-	-	0	-	+	-	+	-	-	0	1.0543	.6388	.2165
11	.556	+	-	-	+	0	+	+	-	-	+	+	0	.9160	-.5119	-.1734
12	.580	+	+	+	-	0	-	+	+	+	-	-	0	1.0804	.5923	.2007
13	.584	+	-	+	+	0	+	+	+	+	+	+	0	.8601	-.6702	-.2271
14	.615	+	-	+	-	0	-	+	-	+	-	-	0	1.0491	.5571	.1888
15	.649	+	+	-	+	0	-	+	+	+	+	-	0	1.2237	.6314	.2140
16	.680	+	+	+	+	0	-	+	-	+	+	-	0	1.2296	.7610	.2579
17	.682	+	+	-	-	0	-	+	-	-	-	-	0	1.0707	.7095	.2404
18	.713	+	-	+	+	0	+	+	+	-	+	-	0	.8724	-.5664	-.1919
19	.722	+	+	-	+	0	+	+	+	-	-	+	0	.1252	-.1483	-.0503
20	.756	+	+	+	+	0	+	+	+	-	-	+	0	.1129	-.1716	-.0581

WORST RESULTS

256	2.559	+	-	+	-	0	-	+	+	+	+	+	0	.0734	-1.4222	-.4819

* ANGSTROMS

Table 8(c). PHASE results for DPL and BrDPL -- halfwidth and position of substituent varied.

SAMPLE A E1519 DPL
SAMPLE B E146A BRDPL

REFLECTIONS 6
D-SPACING * 5a.100
MODEL GAUSSIAN

INPUT DATA--AMPLITUDES

A	8.4600	1.4100	.8400	4.3500	0.0000	1.9200
B	7.6700	1.3400	1.9300	5.8400	1.2500	0.0000

BEST RESULTS

	WIDTH *	POSITION *	DEVIATION	A 1	2	3	4	5	6	B 1	2	3	4	5	6
1	1.0000	18.5000	.3965	+	+	-	-	0	-	+	+	+	-	-	0
2	1.0000	18.7500	.3107	+	+	-	-	0	-	+	+	+	-	-	0
3	1.0000	19.0000	.2570	+	+	+	+	0	+	+	+	-	+	+	0
4	1.0000	19.2500	.2413	+	+	-	-	0	-	+	+	+	-	-	0
5	1.0000	19.5000	.2474	+	+	-	-	0	-	+	+	+	-	-	0
6	1.0000	19.7500	.2362	+	+	-	-	0	-	+	+	+	-	-	0
7	1.0000	20.0000	.3643	+	-	+	-	0	-	+	-	+	-	-	0
8	1.0000	20.2500	.9379	+	-	+	-	0	-	+	+	+	+	-	0
9	1.5000	18.5000	.4105	+	+	-	-	0	-	+	-	+	-	-	0
10	1.5000	18.7500	.3481	+	-	+	+	0	+	+	+	-	+	+	0
11	1.5000	19.0000	.3369	+	+	+	+	0	+	+	+	-	+	+	0
12	1.5000	19.2500	.2813	+	+	+	+	0	+	+	+	-	+	+	0
13	1.5000	19.5000	.2952	+	+	-	+	0	+	+	+	-	+	+	0
14	1.5000	19.7500	.3093	+	+	-	-	0	-	+	+	+	-	-	0
15	1.5000	20.0000	.3173	+	-	-	-	0	-	+	-	+	-	-	0
16	1.5000	20.2500	1.0769	+	-	+	-	0	-	+	+	+	+	-	0
17	2.0000	18.5000	.3721	+	+	-	-	0	-	+	-	+	-	-	0
18	2.0000	18.7500	.2891	+	+	-	-	0	-	+	-	+	-	-	0
19	2.0000	19.0000	.2332	+	+	-	-	0	-	+	-	+	-	-	0
20	2.0000	19.2500	.1990	+	+	-	-	0	-	+	-	+	-	-	0
21	2.0000	19.5000	.2533	+	+	-	-	0	-	+	-	+	-	-	0
22	2.0000	19.7500	.3191	+	-	+	+	0	+	+	-	-	+	+	0
23	2.0000	20.0000	.4043	+	+	-	-	0	-	+	+	+	-	-	0
24	2.0000	20.2500	1.2486	+	-	-	-	0	-	+	+	+	+	-	0
25	2.5000	18.5000	.4893	+	+	-	-	0	-	+	-	+	-	-	0
26	2.5000	18.7500	.4085	+	+	-	-	0	-	+	-	+	-	-	0
27	2.5000	19.0000	.2525	+	-	+	+	0	+	+	+	-	+	+	0
28	2.5000	19.2500	.2409	+	-	+	+	0	+	+	+	-	+	+	0
29	2.5000	19.5000	.3292	+	+	+	+	0	+	+	+	-	+	+	0
30	2.5000	19.7500	.4077	+	+	-	-	0	-	+	-	+	-	-	0
31	2.5000	20.0000	.4660	+	+	-	-	0	-	+	-	+	-	-	0
32	2.5000	20.2500	1.4063	+	+	-	-	0	-	+	+	+	+	-	0
33	3.0000	18.5000	.5869	+	+	-	-	0	-	+	-	+	-	-	0
34	3.0000	18.7500	.5131	+	-	+	+	0	+	+	+	-	+	+	0
35	3.0000	19.0000	.3605	+	-	+	+	0	+	+	+	-	+	+	0
36	3.0000	19.2500	.2702	+	-	+	+	0	+	+	+	-	+	+	0
37	3.0000	19.5000	.2416	+	-	+	+	0	+	+	+	-	+	+	0
38	3.0000	19.7500	.3949	+	-	+	+	0	+	+	+	-	+	+	0
39	3.0000	20.0000	.6120	+	+	-	-	0	-	+	-	+	-	-	0
40	3.0000	20.2500	1.6447	+	+	-	-	0	-	+	+	+	+	-	0

* ANGSTROMS

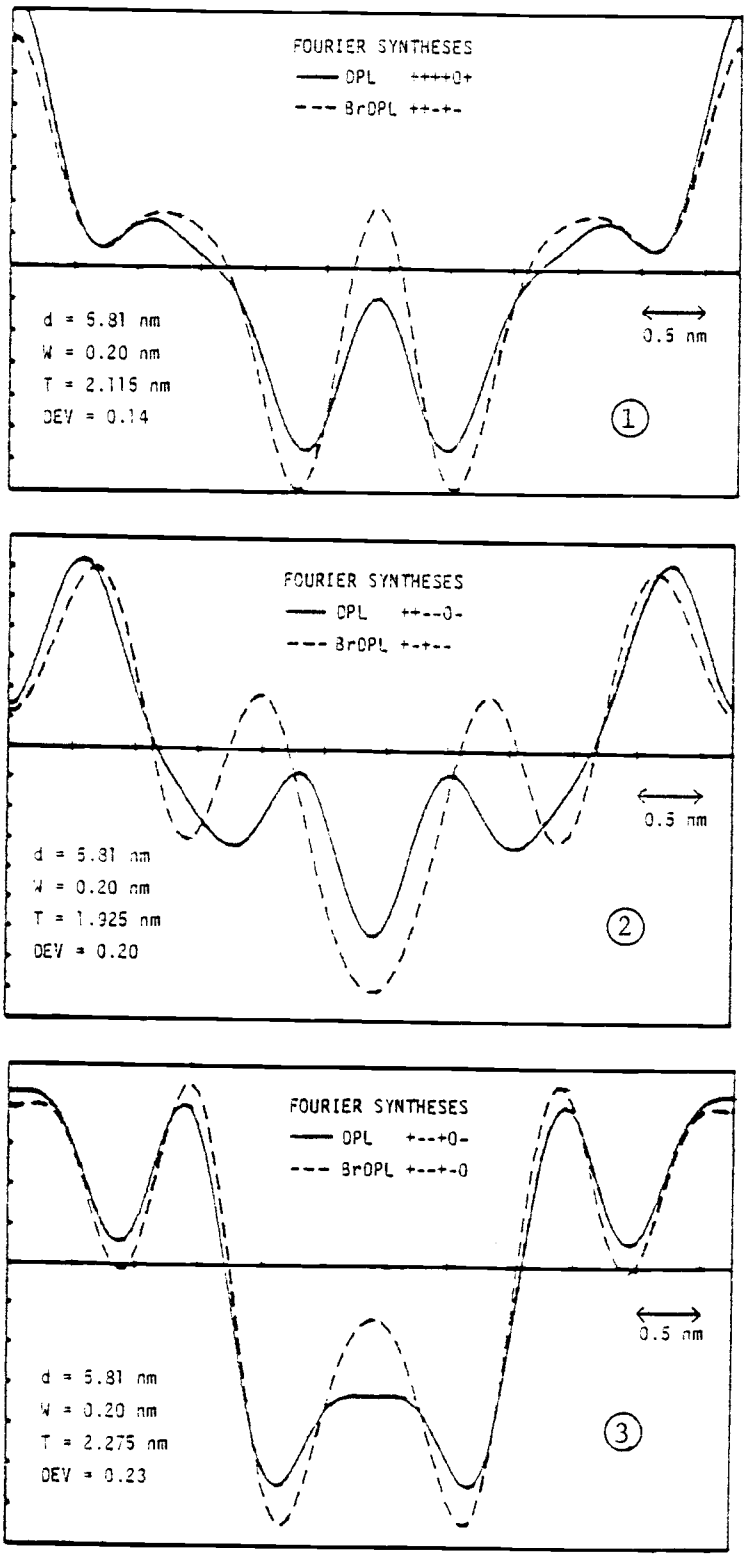

Figure 28. Three top results from program PHASE, using six orders.

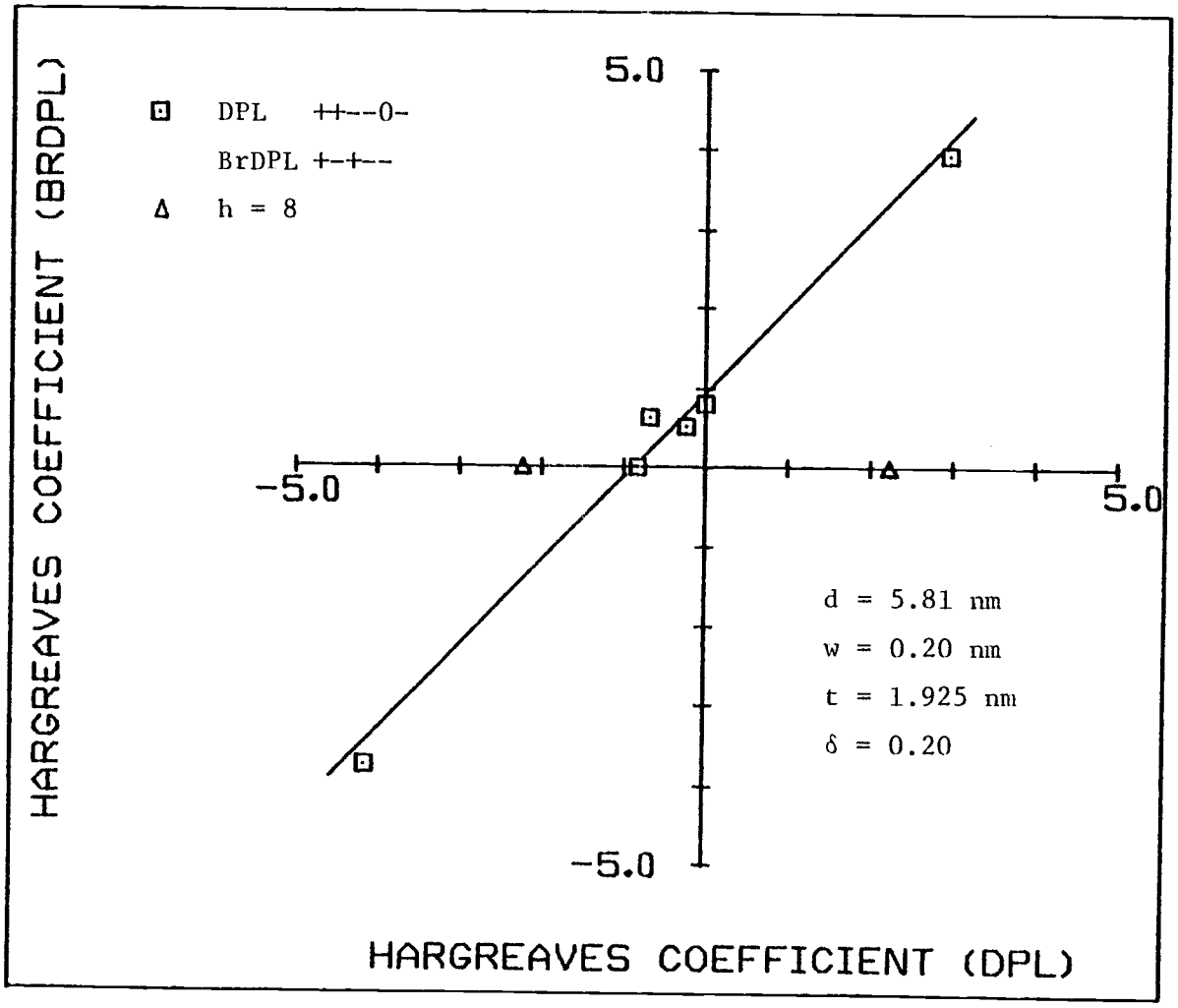

Figure 29. Hargreaves' plot for DPL and BrDPL.

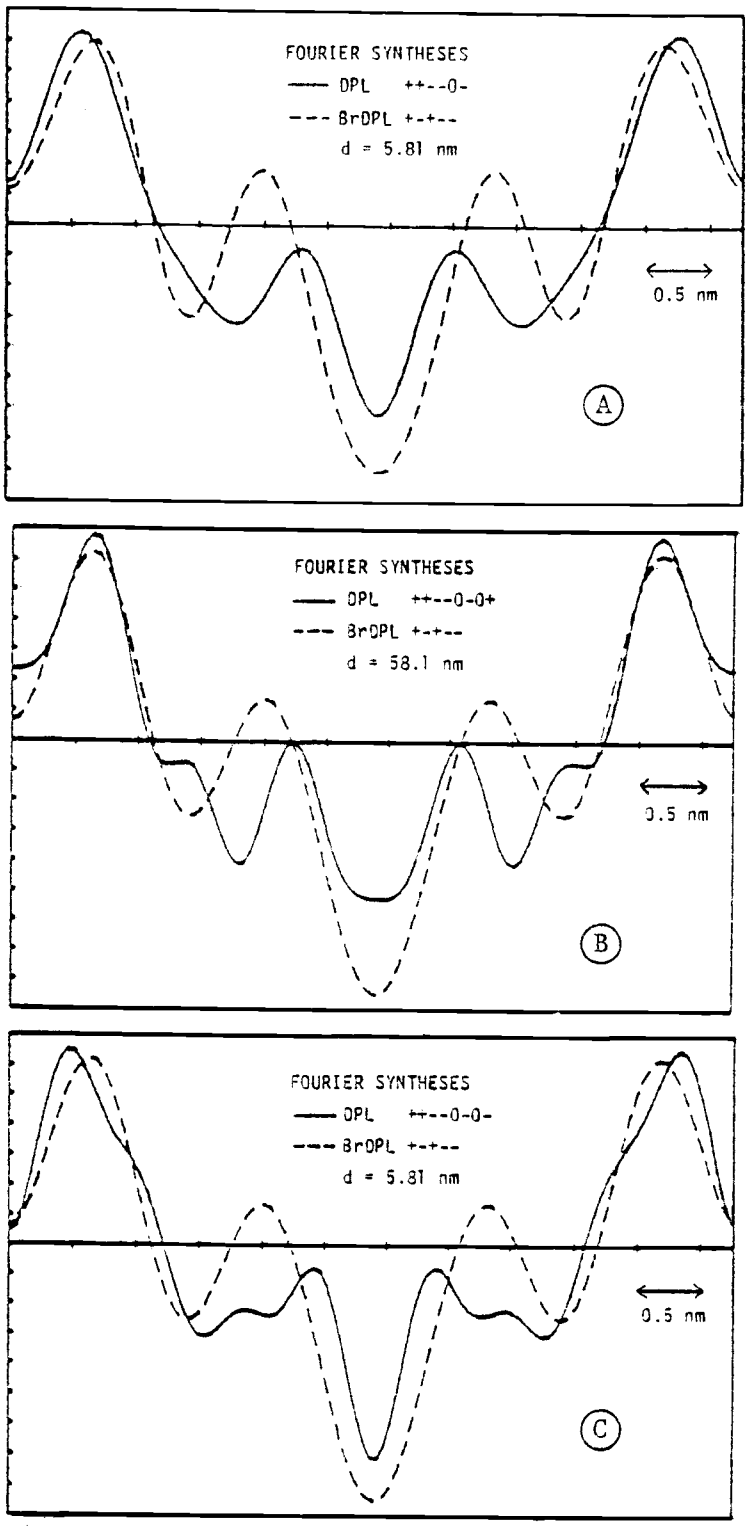

Figure 30. Fourier syntheses with two choices for 8th order of DPL.
Top: 8th order omitted
Center: 8th order +
Bottom: 8th order -

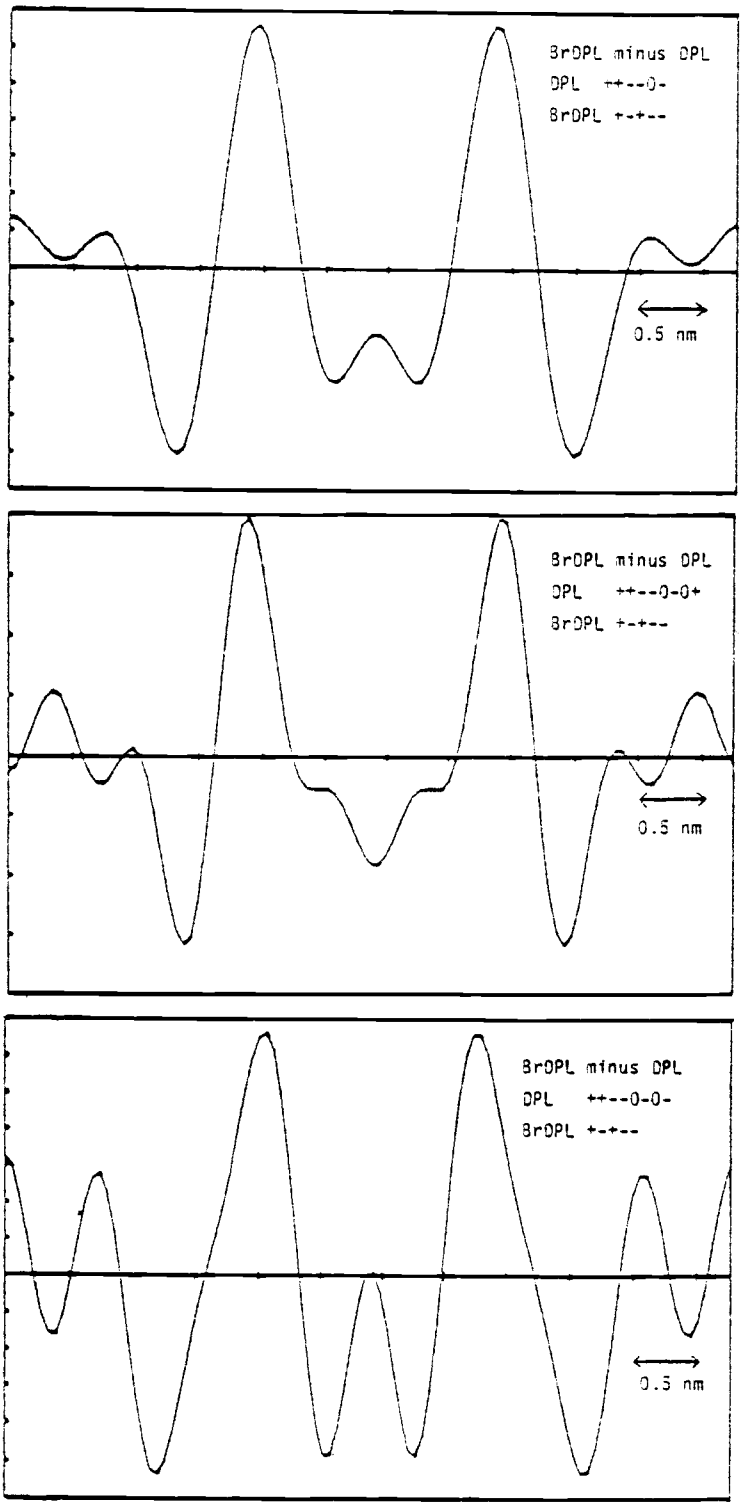

Figure 31. Difference Fourier syntheses with two choices for 8th order of DPL. Top: 8th order omitted
Center: 8th order +
Bottom: 8th order -

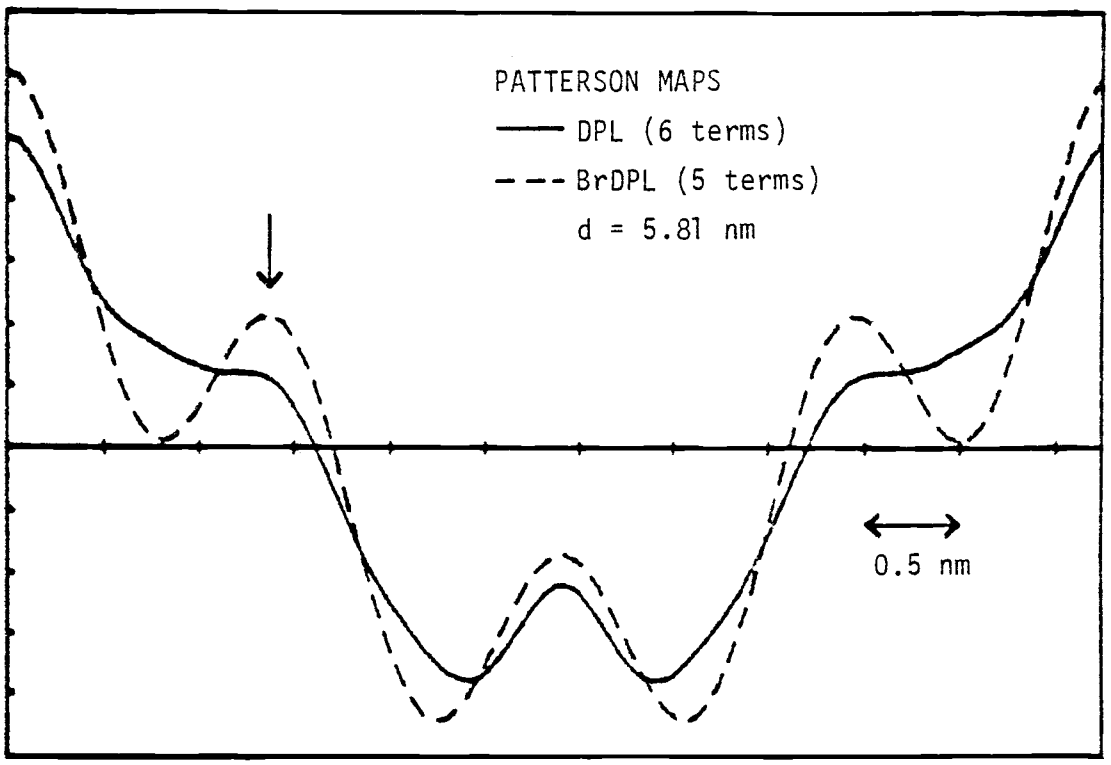

Figure 32. Patterson maps for DPL and BrDPL.

VI. CONCLUSIONS

A. Position Sensing Detector

The position sensing detector allowed diffraction patterns to be collected quickly. For example, the lamellar scans of BrDPL at various temperatures (Figure 24) were collected in about five minutes at each temperature. Using film (Polaroid type 57) in a cassette with a fluorescent screen, about ten hours were needed to obtain good resolution in the h=4 peak in a similar scan.

Another significant advantage of the position sensing detector was its usefulness for positioning specimens in the incident beam.

B. Electron Density Profiles

We have obtained electron-density profiles for DPL that are consistent with those found for phospholipid multilayers by other investigators [21,22], who have used phasing techniques different from ours. Figure 30 shows the result derived from six diffraction orders, based on the hypothesis of isomorphous replacement. Inclusion of eight orders reduced the goodness-of-fit index of our phasing program, leaving a choice between (b) and (c) in Figure 30. We rejected (b), since it indicated features in the chain portion of DPL which are not consistent with other studies. The difficulty with the 8th order could be due to a lack of isomorphicity, which is expected to have a more severe effect in the higher orders [14].

In Figure 30 (a) and (c) the peaks near the edges of the unit

cell are similar to those usually interpreted as the glyceryl-fatty acid ester of the phospholipids. These peaks are 2.2 nm from the center of the unit cell in our syntheses, in agreement with the value of 2.2 nm for hydrated egg lecithin/cholesterol multilayers [21,22].

The trough in the center of electron-density profiles of lipids has been attributed to disorder of the terminal methyl groups of the phospholipid molecules [22]. Deuterium magnetic resonance studies [103], using decanoic acid with various locations deuterated, support this view. The difference between our DPL and BrDPL profiles in this region may be due to relatively greater chain motion for BrDPL.

The location found for the bromine substituent in BrDPL was 1.92 nm from the unit-cell origin, equivalent to 0.98 nm from the center of the unit cell. The latter number is the average distance of the 9 and 10 positions from the end of a C_{16} chain. This fact indicates that the position found for the bromine is reasonable.

C. Location of the Isomorphous Substituent

Other locations might be preferred to the 9 and 10 positions for the heavy-atom substituent. For example, if bromine replaced a hydrogen on the terminal carbon of a C_{15} chain, the result would be sterically identical to a C_{16} chain. Use of such an isomorph might circumvent the broad transition in lamellar spacing we observed, and might result in specimens which were more isomorphous from crystallographic and biological points of view.

D. The Chain Transition of BrDPL

Although the breadth in temperature of the chain transition observed for BrDPL complicated the experimental aspects of isomorphous replacement, this breadth is interesting in its own right.

Techniques which characterize the chain-melting transition of phospholipids are well-established [99]. In addition to low-angle x-ray diffraction, which we have successfully performed on BrDPL, principal techniques include wide-angle diffraction and calorimetry. The experimental signs of chain melting, as temperature is increased, are as follows.

1. Lamellar spacings in low-angle x-ray diffraction patterns are reduced by about 15%, and higher-order diffraction peaks vanish.
2. In the wide-angle diffraction pattern, which monitors chain distribution parallel to the lamellar plane, the sharp 4.2 Å peak is replaced by a diffuse 4.6 Å peak.
3. A calorimetric endotherm is observed.

In accordance with (1), our low-angle data indicate that BrDPL undergoes a chain-melting transition (Figure 24). Data for BrDPL corresponding to (2) and (3), which would be highly desirable, are pending in the work of H.H. Wickman and J.C. Reinert.

Our low-angle results for BrDPL are unusual in that the transition, centered near 0°C, had a breadth of 20°C. One-component phospholipid preparations generally have a sharp chain transition, whereas multi-component lipids have broad transitions [105]. Although our specimens

were thin, flat, highly oriented multilayers, and most phase transition work to date has been performed on bulk lipids, it is not apparent that this difference should affect the phase transitions. In addition, our BrDPL was a mixture of two nearly identical species. However, an explanation of the transition breadth simply in terms of a two-component, thermodynamic phase diagram is elusive, since there was no evidence in our diffraction for the coexistence of melted and unmelted phases.

Although our understanding of the BrDPL transition is incomplete, and needs to be supplemented by data from wide-angle diffraction and calorimetry, several points may be emphasized at this time.

1. From -17 to +60°C, BrDPL formed a highly-oriented, lamellar structure. Our diffraction results gave an electron-density profile for low-temperature (-17°C) BrDPL having the essential features (headgroup peak and central trough) obtained by others for nonbrominated phospholipids in the gel (unmelted) state. In addition, the profile showed bromine where it would be expected if the acyl chains were fully extended. At all temperatures studied, the observed lamellar structure put constraints on the location of bromine that would not apply, for example, in the case of analogous, brominated hydrocarbons.

2. From examination of space-filling, molecular models, it is clear that the presence of bromine should seriously disrupt van der Waals forces that hold the acyl chains together. For example, if the distance between acyl chains were doubled, as is reasonable near the bromine atoms, then the van der Waals attraction, which varies as r^{-6}, should be reduced by a factor of about 50.

3. The steric effect of bromine should also seriously reduce the excluded volume interaction. In other words, rotational isomers of the acyl chains, which could not form if the chains were packed tightly together, could freely form and interconvert.

The situation with bromine is different from that with cis double bonds, which do not cause the chain transition to be broad [106], but which might be expected to be as disruptive sterically as bromine. Actually, space-filling models of long chains with cis double bonds may be packed together with the chains fully extended quite as well as models of fully-extended, unsaturated hydrocarbons. The packing geometry which allows this is consistent with the fact that phosphatidyl ethanolamines (gel) with one cis double bond have lamellar spacings 0.3 nm shorter than do their unsaturated homologs in the gel state [106].

In contrast, it is not possible to pack the acyl chains tightly in a BrDPL model, unless gauche rotamers are introduced. Even then, registry of hydrogen atoms is not nearly so good as it is with unsubstituted chains, either unsaturated or cis-double bonded.

Considerations of positional constraints, van der Waals attractions, and excluded volume repulsions are central to current theories [105,107, 108] of phospholipid phase transitions. BrDPL is structurally unusual in that it has positional constraints different from brominated hydrocarbons, and attractive and repulsive interactions much different from the simpler phospholipids that have been treated in current theories. For these reasons, and because of the unusually broad transition observed, BrDPL and the individual species which comprise it appear to be worthy candidates for further experiment and for theoretical analysis.

BIBLIOGRAPHY

1. Quinn, P.J. (1976) The Molecular Biology of Cell Membranes, University Park Press, Baltimore.

2. Ansell, G. B., Hawthorne, J.N. and Dawson, R.M.C., eds. (1973) Form and Function of Phospholipids, Elsevier Scientific Publishing Company, New York.

3. Danielli, J.F. and Davson, H. (1935) J. Cell. Comp. Physiol. 5, 495-508.

4. Robertson, J.D. (1959) Biochem. Soc. Symposia 16, 3-43.

5. Singer, S.J. and Nicolson, G.L. (1972) Science 175, 720-731.

6. Edidin, M. (1974) Ann. Rev. Biophys. Bioeng. 3, 179-201.

7. Chapman, D., Williams, R.M. and Ladbrooke, B.D. (1967) Chem. Phys. Lipids 1, 445-475.

8. Ladbrooke, B.D. and Chapman, D. (1969) Chem. Phys. Lipids 3, 304-367.

9. Ladbrooke, B.D., Williams, R.M. and Chapman, D. (1968) Biochim. Biophys. Acta 150, 333-340.

10. Reinert, J.C. and Steim, J.M. (1970) Science 168, 1580-1582.

11. Shipley, G.G. (1973) in Biological Membranes (Chapman, D. and Wallach, D.F.H., eds.) 2, 1-89, Academic Press, New York.

12. Worthington, C.R. (1974) J. Biol. Phys. 2, 1-25.

13. Levine, Y.K. (1972) Prog. Biophys. Mol. Biol. 24, 1-74.

14. Hargreaves, A. (1957) Acta Cryst. 10, 196-198.

15. Sherwood, D. (1976) Crystals, X-Rays and Proteins, John Wiley & Sons, New York.

16. Reinert, J.C., Lowry, R.R. and Wickman, H.H. (1978) Lipids 13, 85-87.

17. McElhaney, R.M. and Tourtellotte, M.E. (1969) Science 164, 433-434.

18. Andrews, S.B., Faller, J.W., Barrnett, R.J. and Mizuhira, V. (1978) Biochim. Biophys. Acta 506, 1-17.

19. McIntosh, T.J., Waldbillig, R.C. and Robertson, J.D. (1976) Biochim. Biophys. Acta 448, 15-33.

20. Waldbillig, R.C., Robertson, J.D. and McIntosh, T.J. (1976) Biochim. Biophys. Acta 448, 1-14.

21. Franks, N.P. (1976) J. Mol. Biol. 100, 345-358.

22. Levine, Y.K. and Wilkins, M.H.F. (1971) Nature NB 230, 69-72.

23. Stamatoff, J.B., Krimm, S. and Harvie, N. (1975) Proc. Nat. Acad. Sci. USA 72, 531-534.

24. Blaurock, A.E. (1971) J. Mol. Biol. 56, 35.

25. Worthington, C.R. and King, G.I. (1971) Nature 234, 143.

26. Stamatoff, J.B. and Krimm, S. (1976) Biophys. J. 16, 503-516.

27. Worthington, C.R., King, G.I. and McIntosh, T.J. (1973) Biophys. J. 13, 480-494.

28. Worthington, C.R. and Gras, W.J. (1972) Biophys. Soc. Annu. Meet. Abstr. 12, 255.

29. Worthington, C.R. and McIntosh, T.J. (1973) Nature-Biology 245, 97-99.

30. Borkowski, C.J. and Kopp, M.K. (1968) Rev. Sci. Instrum. 39, 1515-1522.

31. Robinson, A. (1978) Science 199, 39-42.

32. DuPont, Y., Gabriel, A., Chabre, M., Gulik-Krzywicki, T. and Schechter, E. (1972) Nature 238, 331-333.

33. Schelten, J. and Hendricks, R.W. (1975) J. Appl. Cryst. 8, 421-429.

34. Cork, C., Hamlin, R., Vernon, W., Xuong, N.H. and Perez-Mendez, V. (1975) Acta Cryst. A31, 702-703.

35. Rutherford, E. and Geiger, H. (1908) Proc. Roy. Soc. A81, 141.

36. Charpak, G. (1970) Ann. Rev. Nucl. Sci. 20, 195-253.

37. Glassel, P. (1977) Nucl. Instr. and Meth. 140, 61-70.

38. Frieze, Q., Dhawan, S., Disco, A.A., Fajardo, L., Majka, R., Marx, J.N., Nemethy, P., Sandweiss, J. and Slaughter, A. (1976) Nucl. Instr. and Meth. 136, 93-97.

39. Baksay, L., Boh,, A., Foeth, H., Staude, A., Lockman, W., Meyer, T., Rander, J., Schlein, P., Webb, R., Bozzo, M., Ellis, R., Naroska, B., Rubbia, C. and Strolin, P. (1976) Nucl. Instr. and Meth. 133, 219-229.

40. Dwurazny, A., Waligorski, M., Jelen, K. and Ostrowski, K.W. (1976) Nucl. Instr. and Meth. 135, 197-202.

41. Cheng, D.C., Kozanecki, W.A., Piccioni, R.L., Rubbia, C., Sulak, L.R., Weedon, H.J. and Whittaker, J. (1974) Nucl. Instr. and Meth. 117, 157-169.

42. Rand, R.E., Hughes, E.B., Kose, R., Martin, T.W., MacGregor, W.I. and Schilling, R.F. (1974) Nucl. Instr. and Meth. 118, 189-202.

43. Bouclier, R., Charpak, G., Chesi, E., Dumps, L., Fischer, H.G., Hilke, H.J., Innocenti, P.G., Maurin, G., Minten, A., Naumann, L., Piuz, F., Santiard, J.C. and Ullaland, O. (1974) Nucl. Instr. and Meth. 115, 235-244.

44. Charpak, G. (1974) IEEE Trans. NS-21, 38-44.

45. Pollvogt, U. and Kurz, R.J. (1974) IEEE Trans. NS-21, 70-74.

46. Heintze, J. and Walenta, A.H. (1973) Nucl. Instr. and Meth. 111, 461-465.

47. Malowski, B. and Sadoulet, B. (1973) Nucl. Instr. and Meth. 111, 561-565.

48. Buchanan, J., Coulson, L., Gabitzsch, N., Hungerford, E.V., Mutchler, G.S., Persson, R., Scott, M.L., Windish, J. and Phillips, G.C. (1972) Nucl. Instr. and Meth. 99, 159-172.

49. Parker, S., Jones, R., Kadyk, J., Stevenson, M.L., Katsura, T., Peterson, V.Z. and Yount, D. (1971) Nucl. Instr. and Meth. 97, 181-185.

50. Bouclier, R., Charpak, G., Dimcovski, Z., Fischer, G., Sauli, F., Coignet, G. and Flugge, G. (1970) Nucl. Instr. and Meth. 88, 149-161.

51. Borkowski, C.J. and Kopp, M.K. (1977) IEEE Trans. NS-24, 287-292.

52. Breskin, A., Charpak, G. and Sauli, F. (1976) Nucl. Instr. and Meth. 136, 497-503.

53. Borkowski, C.J., Kopp, M.K. and Harter, J.A. (1975) IEEE Trans. NS-22, 896-900.

54. Borkowski, C.J. and Kopp, M.K. (1975) Rev. Sci. Instrum. 46, 951-962.

55. Stumpel, J.W., Sanford, P.W. and Goddard, H.F. (1973) J. Phys. E: Sci. Instrum. 6, 397-400.

56. Borkowski, C.J. and Kopp, M.K. (1971) IEEE Trans. NS-17, 340-349.

57. Harvey, B.G., Mahoney, J., Puhlhofer, F.G., Goulding, F.S., Landis, D.A., Faivre, J.C., Kovar, D.G., Zisman, M.S., Meriwether, J.R., Cosper, S.W. and Hendrie, D.L. (1972) Nucl. Instr. and Meth. 104, 21-32.

58. Gerber, M.S., Miller, D.W., Schlosser, P.A., Steidley, J.W. and Deuchtman, A.H. (1977) IEEE Trans. NS-24, 182-187.

59. Alberi, J., Fischer, J., Radeka, V., ROGERS, L.C. and Schoenborn, B. (1975) Nucl. Instr. and Meth. 127, 507-523.

60. Christie, P., Evans, K.D., Griffiths, J., Mathieson, E. and Murphy, P. (1975) Nucl. Instr. and Meth. 130, 279-284.

61. Homeyer, H., Mahoney, J. and Harvey, B.G. (1974) Nucl. Instr. and Meth. 118, 311-312.

62. Dolce, S.R. (1974) Rev. Sci. Instrum. 45, 499-505.

63. Hough, J. and Drever, R.W.P. (1972) Nucl. Instr. and Meth. 103, 365-372.

64. Miller, G.L., Williams, N., Senator, A., Stensgaard, R. and Fischer, J. (1971) Nucl. Instr. and Meth. 91, 389-396.

65. Atac, M., Bosshard, R., Erhon, S. and Schlein, P. (1977) IEEE Trans. NS-24, 195-199.

66. Sitar, B., Stubbs, R.J. and Beare, J.M. (1976) Nucl. Instr. and Meth. 134, 267-270.

67. Birk, M., Breskin, A. and Trautner, N. (1976) Nucl. Instr. and Meth. 137, 393-395.

68. Lacy, J.L. and Lindsey, R.S. (1974) Nucl. Instr. and Meth. 119, 483-498.

69. Lim, C.B., Chu, D., Kaufman, L., Perez-Mendez, V. and Sperinde, J. (1974) IEEE Trans. NS-21.

70. Cork, C., Fehr, D., Hamlin, R., Vernon, W., Xuong, N.H. and Perez-Mendez, V. (1974) J. Appl. Cryst. 7, 319-323.

71. Lee, D.M., Sobottka, S.E. and Thiessen, H.A. (1974) Nucl. Instr. and Meth. 120, 153-156.

72. Perez-Mendez, V. and Parker, S.I. (1974) IEEE Trans. NS-21 45-50.

73. Cork, C., Fehr, D., Hamlin, R., Vernon, W., Xuong, N.H. and Perez-Mendez, V. (1974) J. Appl. Cryst. 7, 319-323.

74. Kaplan, S.N., Kaufman, L., Perez-Mendez, V. and Valentine, K. (1973) Nucl. Instr. and Meth. 106, 397-406.

75. Allemand, R. and Thomas, G. (1976) Nucl. Instr. and Meth. 137, 141-149.

76. Procedings of the Workshop on X-Ray Instrumentation for Synchrotron Radiation Research (1978). Stanford Synchrotron Radiation Laboratory.

77. Elad, E. and Sareen, R. (1974) IEEE Trans. NS-21, 75-84.

78. Ostgaard Olsen, J. (1977) Nucl. Instr. and Meth. 140, 29-35.

79. Kellogg, E., Henry, P., Murray, S., VanSpeybroeck, L. and Bjorkholm, P. (1976) Rev. Sci. Instrum. 47, 282-290.

80. Wijnaendts von Resandt, R.W., den Harink, H.C. and Los, J. (1976) J. Phys. E: Sci. Instrum. 9, 503-509.

81. Timothy, J.G. and Bybee, R.L. (1975) Rev. Sci. Instrum. 46, 1615-1623.

82. Lawrence, G.M. and Stone, E.J. (1975) Rev. Sci. Instru. 46, 432-435.

83. Price, W.J. (1958) Nuclear Radiation Detection, McGraw-Hill, New York.

84. Stewart, J.L. (1958) Circuit Analysis of Transmission Lines, John Wiley and Sons, N.Y.

85. Holbrook, J.G. (1966) Laplace Transforms for Electronic Engineers, Pergamon Press, N.Y.

86. White, R.E. and Naylor, H. (1976) Nucl. Instr. and Meth. 135, 403-404.

87. Halliday, D. and Resnick, R. (1963) Physics for Students of Science and Engineering, Wiley, New York.

88. Ouseph, P.J. (1975) Introduction to Nuclear Radiation Detectors, Plenum Press, New York.

89. Gray, D.E., ed., (1975) American Institute of Physics Handbook, 3rd edition, McGraw-Hill, New York.

90. Azaroff, L.V. (1968) Elements of X-Ray Crystallography, McGraw-Hill, New York.

91. Hauptman, H.A. (1972) Crystal Structure Determination, Plenum Press, New York.

92. Wilson, A.J.C. (1942) Nature 150, 151-153.

93. Buerger, M.J. (1959) Vector Space, John Wiley and Sons, Inc., New York.

94. Lesslauer, W. and Blasie, J.K. (1972) Biophys. J. 12, 175-190.

95. Hosemann, R. and Bagchi, S.N. (1962) Direct Analysis of Diffraction by Matter, North-Holland Publishing Company, Amsterdam.

96. Ramachandran, G.N. and Srinivasan, R. (1970) Fourier Methods in Crystallography, Wiley-Interscience, New York.

97. Ramaseshan, S. and Abrahams, S.C., eds. (1975) Anomalous Scattering, Munksgaard, Copenhagen.

98. Powers, L. and Clark, N.A. (1975) Proc. Nat. Acad. Sci. USA 72, 840-843.

99. Chapman, D., Williams, R.M. and Ladbrooke, B.D. (1967) Chem. Phys. Lipids 1, 445-475.

100. Stamatoff, J.B. Personal communication.

101. Nagle, J.F. and Wilkinson, D.A. (submitted 1977) Biochim. Biophys. Acta.

102. Cotton, F.A. and Wilkinson, G. (1972) Advanced Organic Chemistry, Interscience, N.Y.

103. Seelig, J. and Niederberger, W. (1974) Biochemistry 13, 1585-1588.

104. Templeton, D.H. and Philips, J.C. (1978) Science 201, 257-259.

105. Nagle, J.F. (1973) J. Chem. Phys. 58, 252-264.

106. Chapman, D., Byrne, P. and Shipley, G.G. (1966) Proc. Roy. Soc. A290, 115-142.

107. Caille, A., Rapini, A., Zuckerman, M., Cros, A. and Doniach, S. (1978) Can. J. Phys. 56, 348-357.

108. Kanehisa, M. and Tsong, T. (1978) J. Am. Chem. Soc. 100:2, 424-431.

APPENDICES

APPENDIX A

Validation of Program PHASE

To determine that the program PHASE performed properly, artificial F data, for which the phase factors were known, were fed to it. The output from PHASE was then compared with the known phases. The artificial data were obtained from program PREDICT, which calculated the sampled Fourier transform of a sum of Gaussian functions described by input parameters.

Table 9 gives the input and output for the two isomorphous sets of PREDICTed data used in this test. Table 10 contains the corresponding result from PHASE for five orders. The spacing used in PHASE (60.1, arbitrary units) was different from the spacing used in PREDICT (60.0), in order to see the effect of small errors in this value.

A range of trial values for halfwidth and position were used for the isomorphous substituent. The correct values were associated with the lowest deviation and with the correct set of phases.

Figure 33 shows the Fourier syntheses of the F data using the correct phases. This figure shows the effect of series truncation on the appearance of a correctly phased electron-density profile.

Table 9. Isomorphous data from PREDICT.

PERIOD (SPACING) = 60.0

SET 1			SET 2		
Gaussians			Gaussians		
Height	Halfwidth	Position	Height	Halfwidth	Position
5.0	3.0	3.0	5.0	3.0	3.0
-2.0	1.0	30.0	-2.0	1.0	30.0
			0.25	2.0	17.0

h	F	h	F
0	(4.62)	0	(4.79)
1	5.59	1	5.56
2	3.04	2	2.88
3	2.96	3	3.04
4	0.26	4	0.36
5	0.64	5	0.54
6	-1.07	6	-1.10
7	0.04	7	0.12
8	-0.99	8	-0.99
9	0.23	9	0.18
10	-0.63	10	-0.61
11	0.37	11	0.39
12	-0.43	12	-0.44
13	0.35	13	0.35
14	-0.33	14	-0.32
15	0.29	15	0.29
16	-0.26	16	-0.26
17	0.23	17	0.23
18	-0.20	18	-0.20
19	0.17	19	0.17
20	-0.15	20	-0.15

Table 10. PHASE results with artificial "data" from PREDICT.

SAMPLE A TESTA. 2 GAUSSIANS (P,W,T)=(5,3,3),(-2,1.30) D=60.0 ++++++-
SAMPLE B TESTB. SAME WITH SUBSTITUENT (1,2,17) ++++++-

REFLECTIONS 5
D-SPACING 60.100
MODEL GAUSSIAN

INPUT DATA--AMPLITUDES

A	5.5900	3.0400	2.9600	.2600	.6400
B	5.4500	2.4300	3.3200	.6300	.2300

BEST RESULTS

	WIDTH	POSITION	DEVIATION	A 1 2 3 4 5	B 1 2 3 4 5
1	1.5000	15.0000	1.1128	+ - - - +	+ + - + +
2	1.5000	15.2500	.4635	+ - - - +	+ - - - +
3	1.5000	15.5000	.3231	+ - - + -	+ - - - -
4	1.5000	15.7500	.1320	+ - - + -	+ - - - -
5	1.5000	16.0000	.0578	+ + + - +	+ + + + +
6	1.5000	16.2500	.1105	+ - - - -	+ - - - -
7	1.5000	16.5000	.0603	+ + + + +	+ + + + +
8	1.5000	16.7500	.0358	+ + + + +	+ + + + +
9	1.5000	17.0000	.0390	+ + + + +	+ + + + +
10	1.5000	17.2500	.0721	+ + + + +	+ + + + +
11	1.5000	17.5000	.1161	+ + + + +	+ + + + +
12	1.5000	17.7500	.1346	+ + - + +	+ + - + +
13	1.5000	18.0000	.1628	+ - - - -	+ - - - +
14	1.5000	18.2500	.1192	+ - - - -	+ - - - +
15	1.5000	18.5000	.2445	+ - + - -	+ - + - +
16	1.5000	18.7500	.5925	+ - + - -	+ - + - -
17	2.0000	15.0000	.7239	+ - - - +	+ - - - +
18	2.0000	15.2500	.4112	+ - - - +	+ - - - +
19	2.0000	15.5000	.3483	+ - - + -	+ - - - -
20	2.0000	15.7500	.1576	+ - - + -	+ - - - -
21	2.0000	16.0000	.0821	+ - - + -	+ - - - -
22	2.0000	16.2500	.0962	+ + + - +	+ + + + +
23	2.0000	16.5000	.0809	+ - - - -	+ - - - -
24	2.0000	16.7500	.0424	+ + + + +	+ + + + +
25	2.0000	17.0000	.0016	+ + + + +	+ + + + +
26	2.0000	17.2500	.0388	+ + + + +	+ + + + +
27	2.0000	17.5000	.0806	+ + + + +	+ + + + +
28	2.0000	17.7500	.1290	+ + + + +	+ + + + +
29	2.0000	18.0000	.1674	+ + - + +	+ + - + +
30	2.0000	18.2500	.1540	+ - - - -	+ - - - +
31	2.0000	18.5000	.2965	+ - + - -	+ - + - +
32	2.0000	18.7500	.6666	+ - + - -	+ - + - -
33	2.5000	15.0000	.4434	+ - - - +	+ - - - +
34	2.5000	15.2500	.4040	+ + - + +	+ + - + +
35	2.5000	15.5000	.3816	+ - - + -	+ - - - -
36	2.5000	15.7500	.1897	+ - - + -	+ - - - -
37	2.5000	16.0000	.1207	+ - - + -	+ - - - -
38	2.5000	16.2500	.1160	+ - - + -	+ - - - -
39	2.5000	16.5000	.1115	+ - - - -	+ - - - -
40	2.5000	16.7500	.0670	+ - - - -	+ - - - -
41	2.5000	17.0000	.0377	+ - - - -	+ - - - -
42	2.5000	17.2500	.0396	+ + + + +	+ + + + +
43	2.5000	17.5000	.0394	+ + + + +	+ + + + +
44	2.5000	17.7500	.0945	+ + + + +	+ + + + +
45	2.5000	18.0000	.1369	+ + - + +	+ + - + +
46	2.5000	18.2500	.1643	+ - + - -	+ - + - -
47	2.5000	18.5000	.2389	+ + + + +	+ + + + -
48	2.5000	18.7500	.3950	+ - - - +	+ - - - +

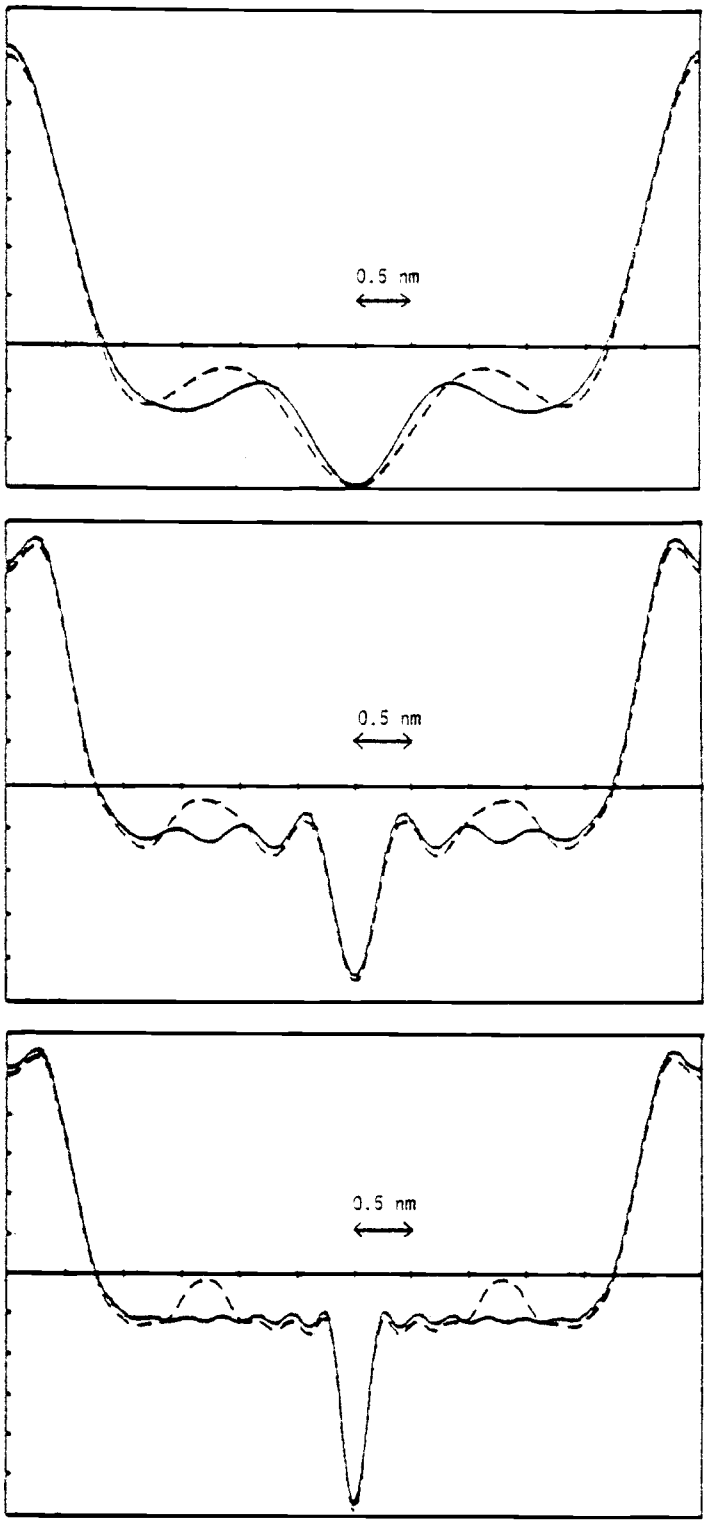

Figure 33. Fourier syntheses of arbitrary Gaussian-sum models.
Top: 5 terms Center: 10 terms Bottom: 19 terms

APPENDIX B

Stepping Motor Schematics

CARD NUMBERING CONVENTION

Ba is pin a of card B
A7 is pin 7 of card A

ON ALL CARDS, 21 = +5 V, 22 = GND

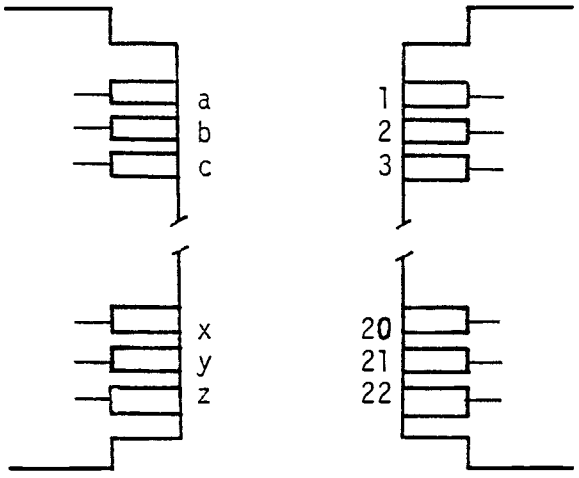

COMPONENT SIDE BACK SIDE

CARDS

A	DISPLAY
B	UP/DOWN COUNTER *
C	COMPARATOR1
D	COMPARATOR2
E	CLOCK
F	RUN/STOP/JOG
G	DISTRIBUTOR/REVERSE

* Kindly provided by
Dr. E.D. Salin

Figure 34. Circuit cards for stepping-motor control.

JUMPERS IN CHASIS
FOR CARD-EDGE
CONNECTOR SOCKETS

ALL CARDS: 21 = +5 V, 22 = GND

CARDS A, B, C, D (Binary Coded Data)

A1 - Ba - Ca - Da
A2 - Bb - Cb - Db
ETC THROUGH
A20 - Bx - Cx - Dx

20 bits = 5 digits, 4 bits each

CARD A DISPLAY

NO ADDITIONAL JUMPERS

CARD B COUNTER

B21	- B1	+5 V
B5	- G3	count down
B6	- G2	count up

CARDS C, D COMPARATORS

Cz	- Dy	EQ1
Dz	- F8	EQ1+2

CARD E TIMER

E5	- F12	reset clock on STP
E20	- E19	trimpot for frequency can be inserted here

CARD F RUN/STOP/JOG

F12	- E5	
F11	- G7	555 monostable
F8	- Dz	EQ1+2

CARD G DISTRIBUTOR

G14	- F7	reverse
G7	- F11	555 monostable

Figure 35. Chasis jumpers.

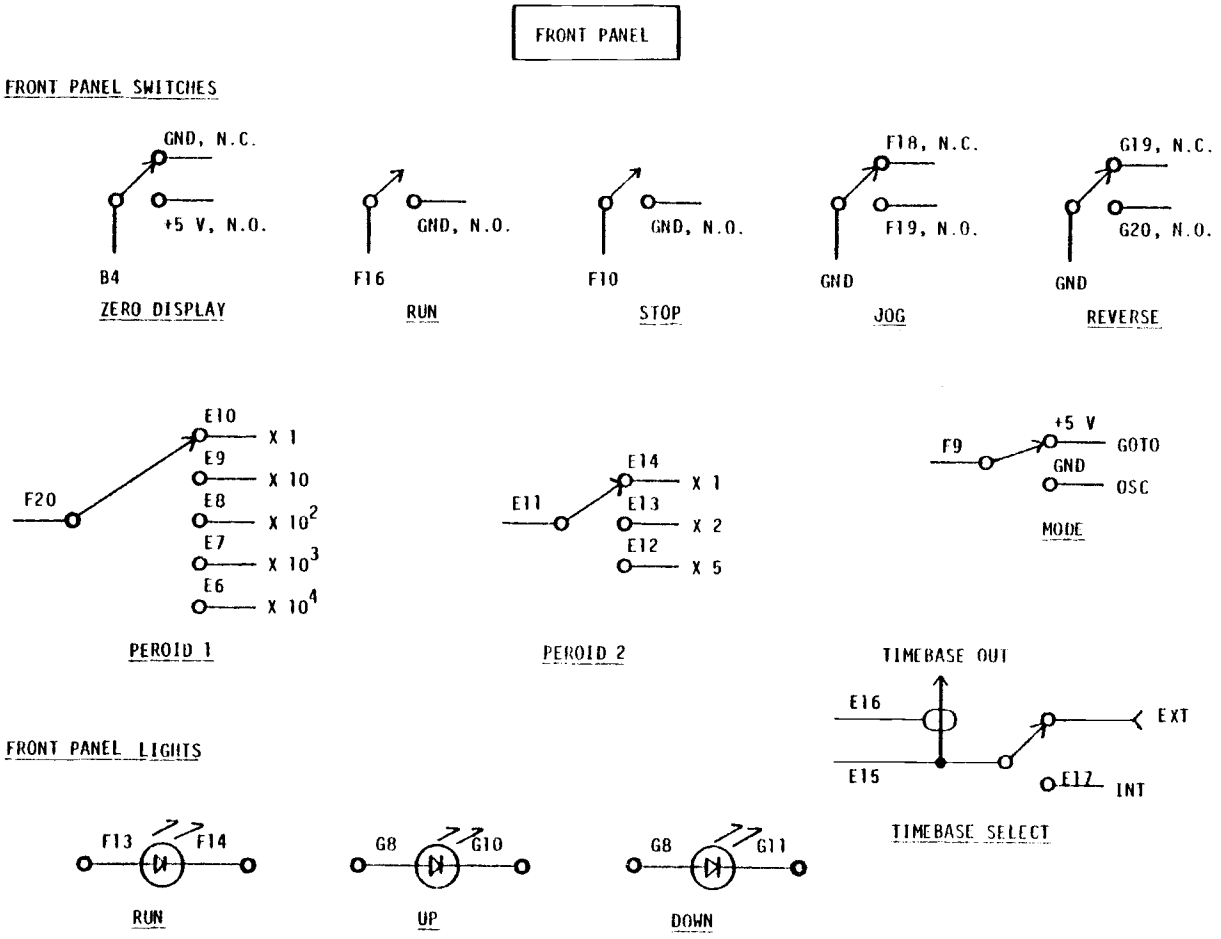

Figure 36. Front panel connections.

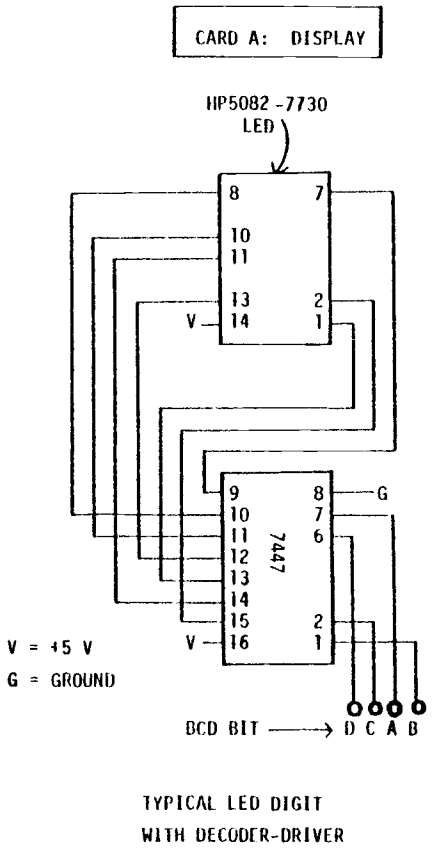

TYPICAL LED DIGIT
WITH DECODER-DRIVER

CARD PINS FOR
BINARY CODED DATA (BCD)

DIGIT	BIT	DISPLAY CARD A PIN	COUNTER CARD B PIN	COMPARATORS CARDS C, D * PIN	†
1	D	1	a	1	a
	C	2	b	2	b
(LSD)	A	3	c	3	c
	B	4	d	4	d
2	D	5	e	5	e
	C	6	f	6	f
	A	7	h	7	h
	B	8	j	8	j
3	D	9	k	9	k
	C	10	l	10	l
	A	11	m	11	m
	B	12	n	12	n
4	D	13	p	13	p
	C	14	r	14	r
	A	15	s	15	s
	B	16	t	16	t
5	D	17	u	17	u
	C	18	v	18	v
(MSD)	A	19	w	19	w
	B	20	x	20	x

* FROM SETPOINT SWITCH
† FROM COUNTER

DECIMAL	BINARY
0	0000
1	0001
2	0010
3	0011
4	0100
5	0101
6	0110
7	0111
8	1000
9	1001

BCD BIT
DCBA

Figure 37. Display circuit and other BCD connections.

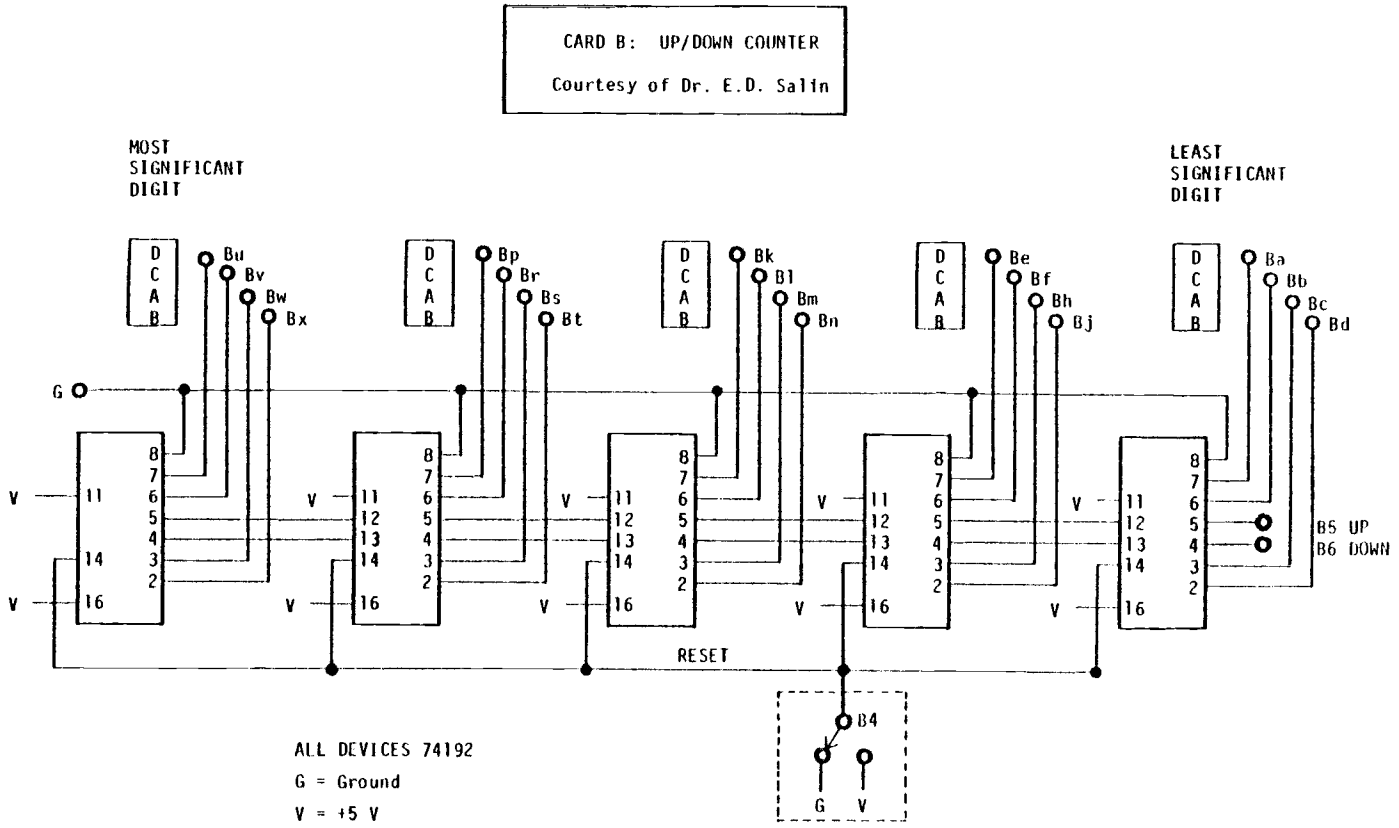

Figure 38. Up/down-counter circuit.

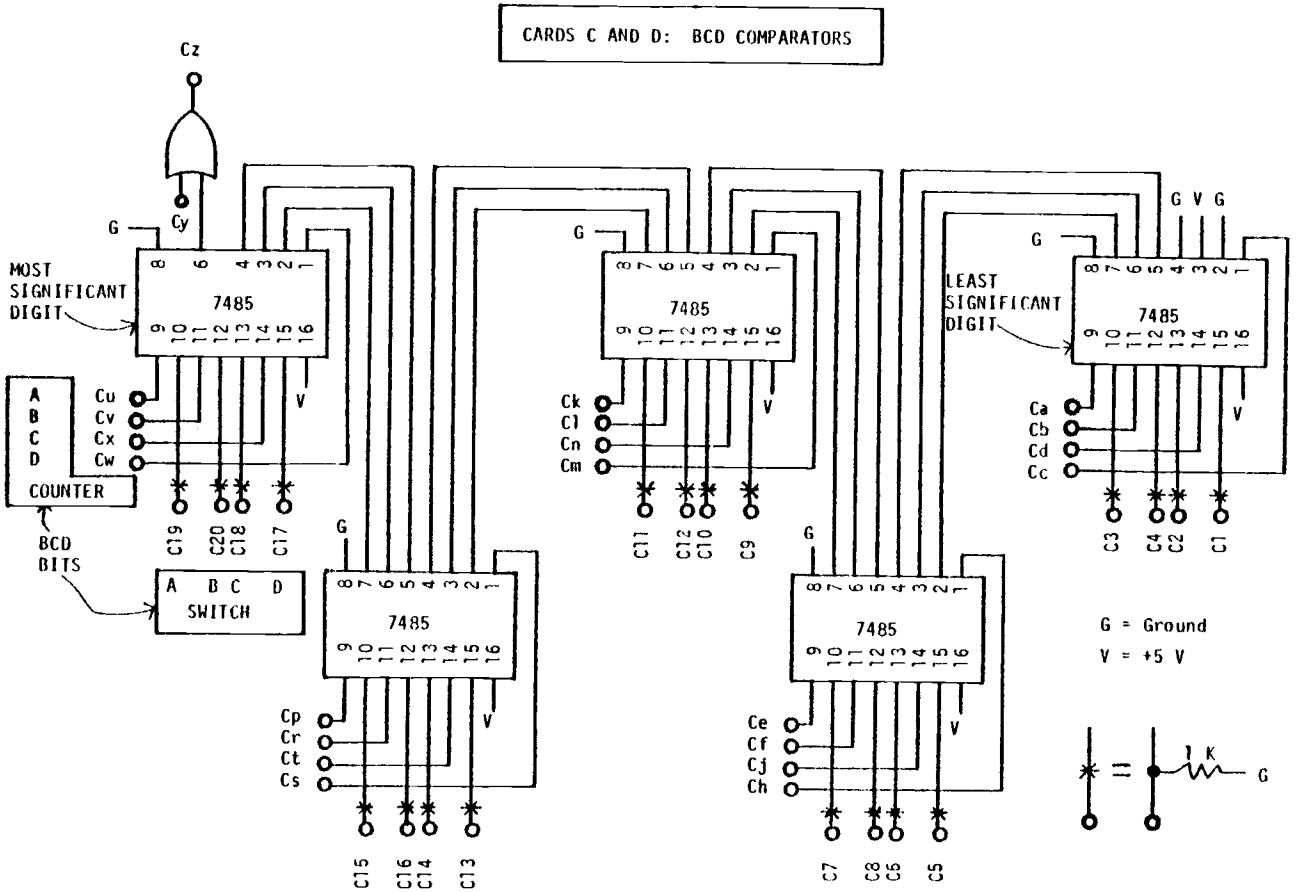

Figure 39. BCD comparator circuit.

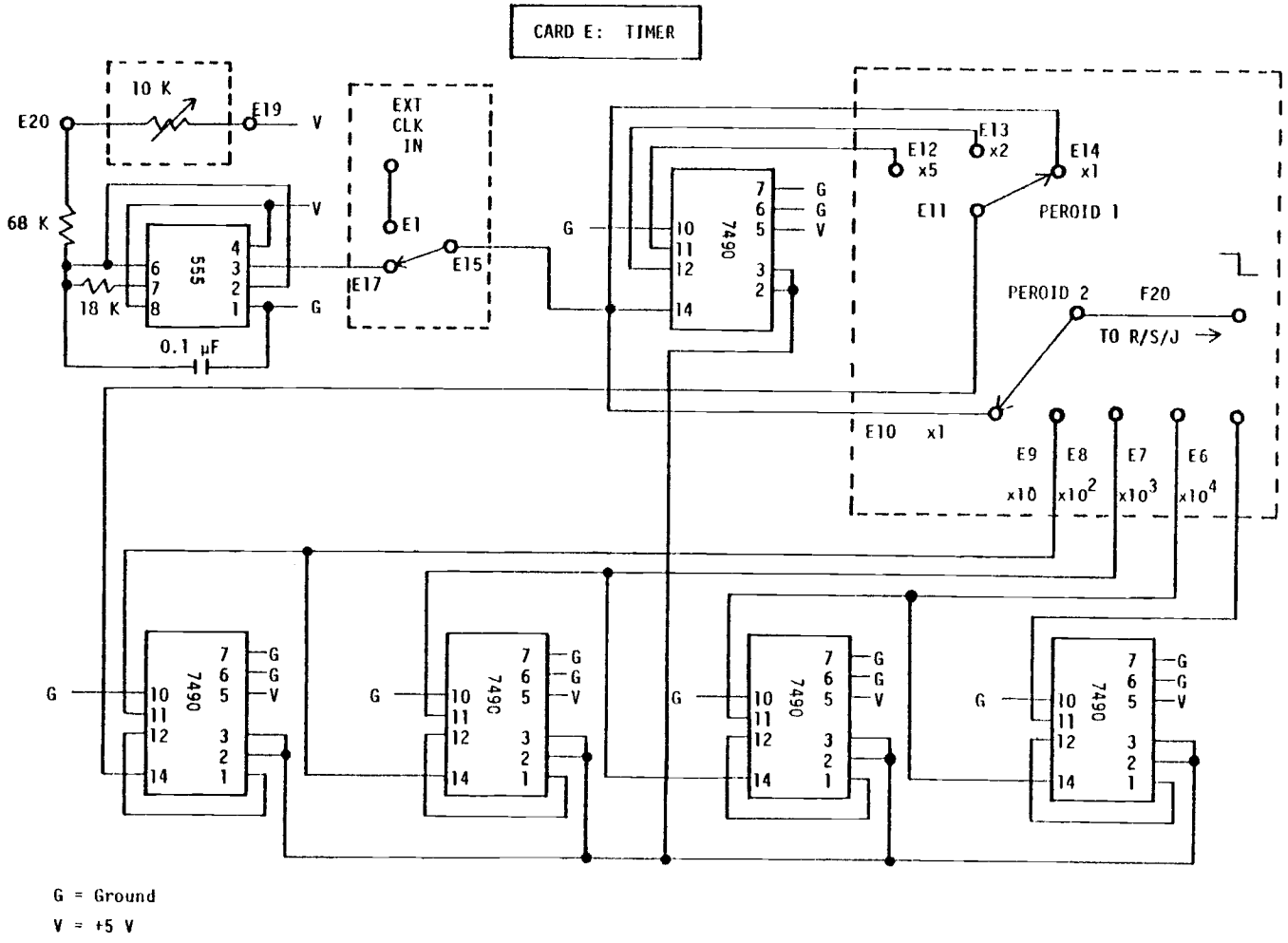

Figure 40. Timer circuit.

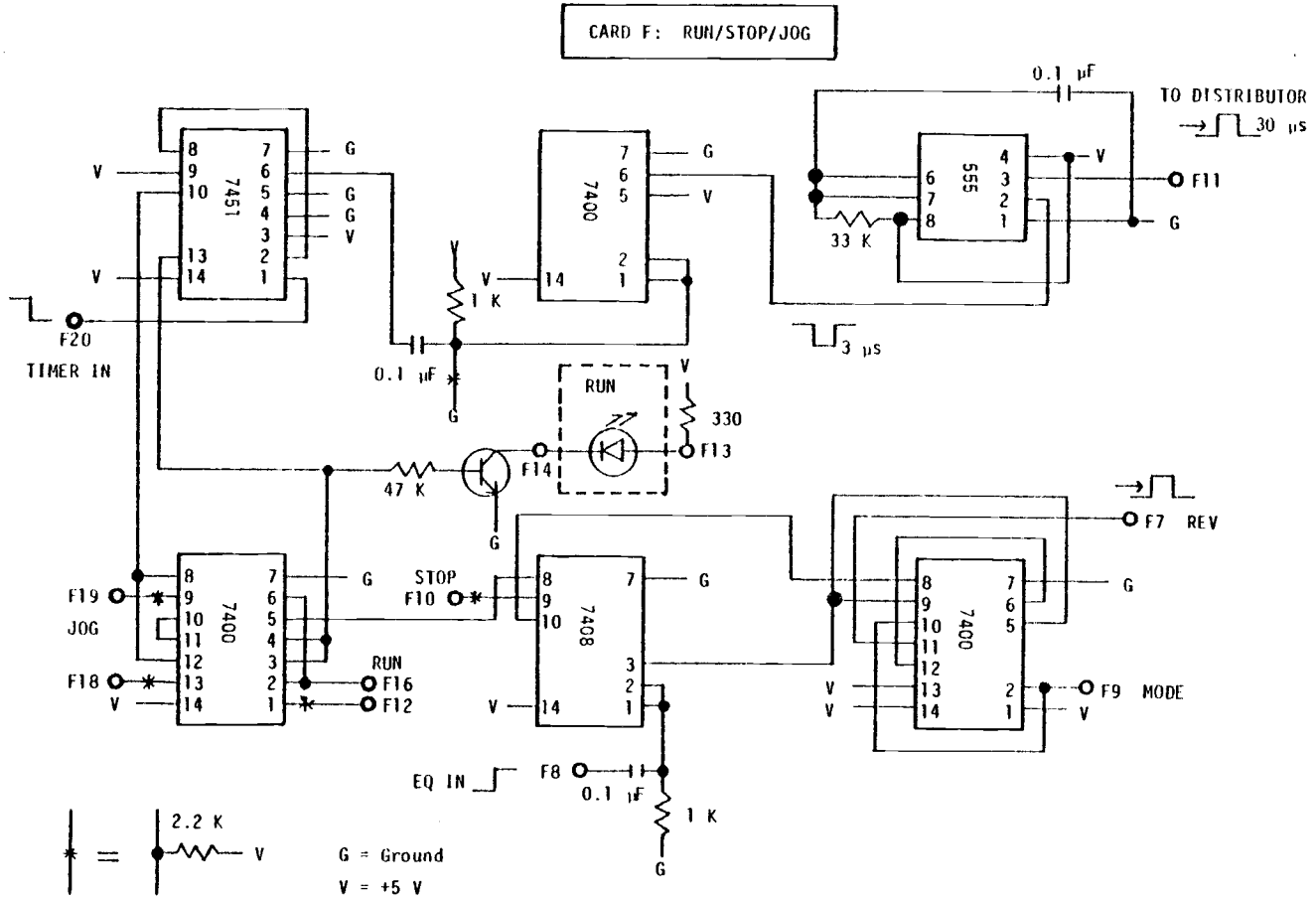

Figure 41. Run/stop/jog circuit.

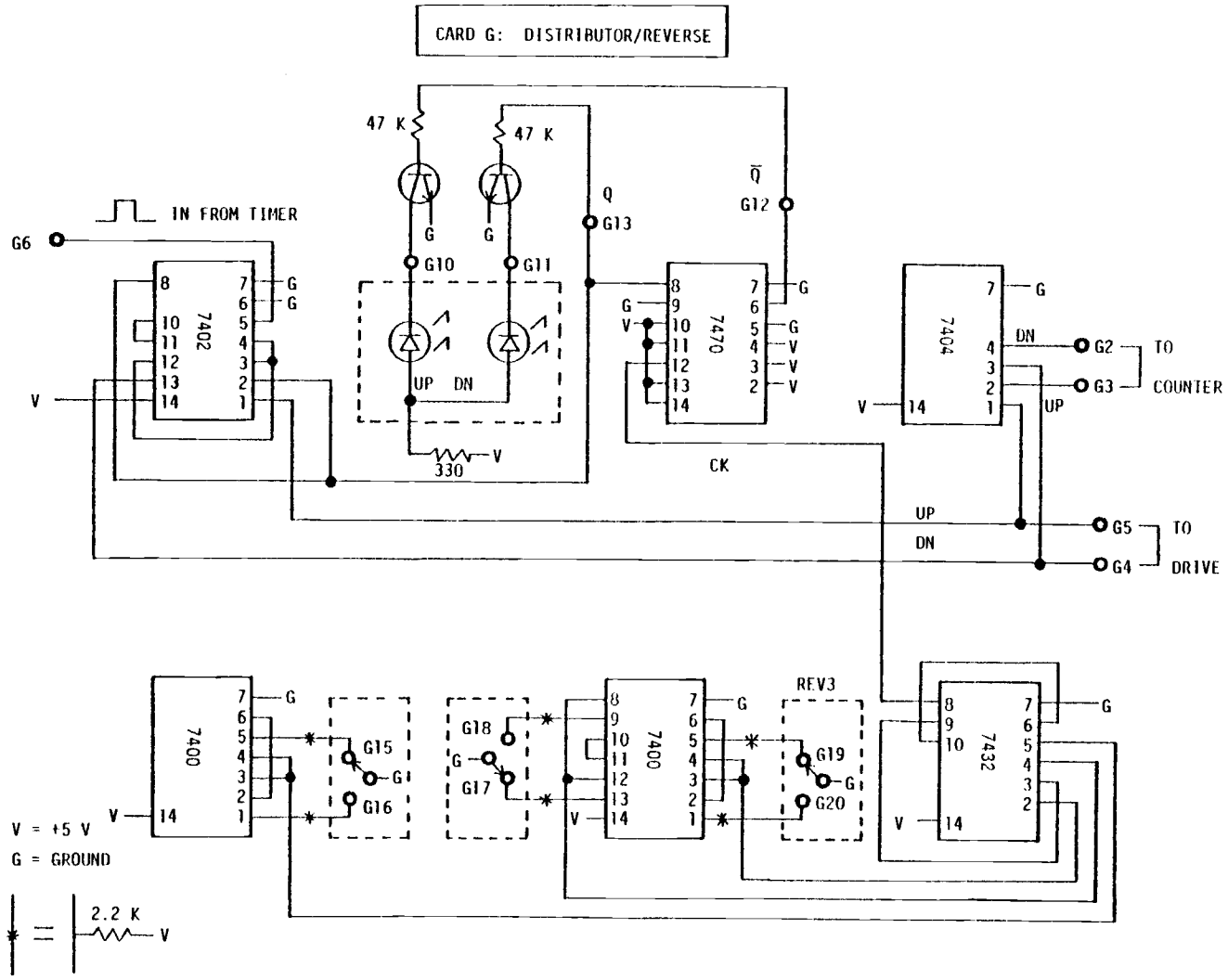

Figure 42. Distributor/reverse circuit.

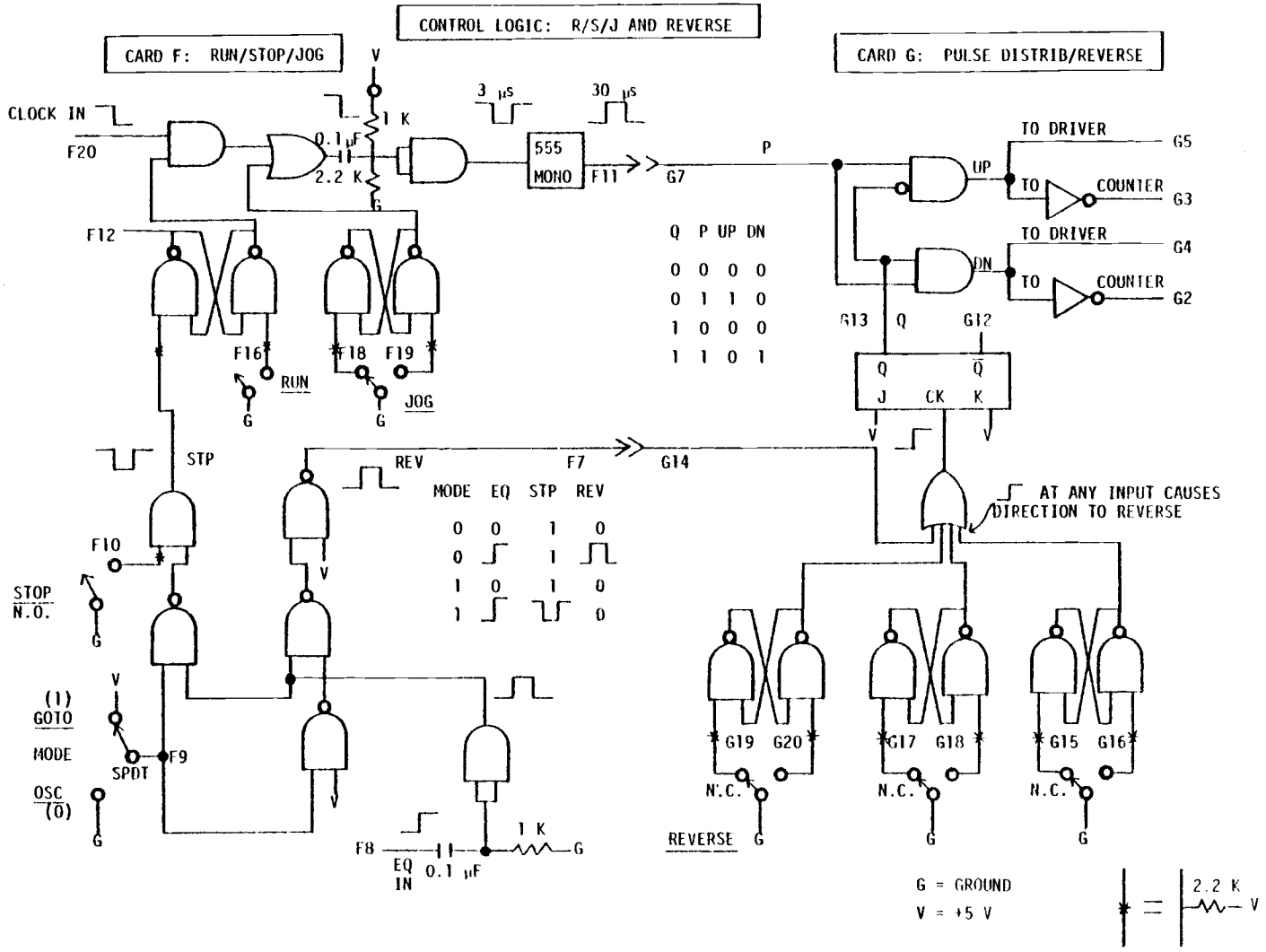

Figure 43. Control logic for stepping-motor drive.

MOTOR CONNECTION - BACK PANEL

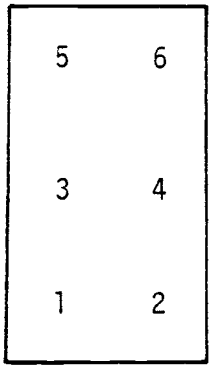

SOCKET
(EXTERNAL)

PHASE	PIN	PLUG	MOTOR
ϕ1	5	Red	Red
ϕ2	6	Green	Green
ϕ3	3	Red/white	Orange
ϕ4	4	Green/white	Blue
ϕ5	1	White	White
ϕ6	2	Black	Black

Figure 44. Motor connection.

APPENDIX C

Computer Programs

```
      PROGRAM PHASE (INPUT=/150, OUTPUT=/150)
C
C      R.LYTZ   14 AUG 77   CSU   CCC CYBER
C
C
C     ISOMORPHOUS REPLACEMENT ALGORITHM
C     FOR DIFFRACTION FROM MULTILAYERS.
C     OUTPUT GIVES CALCULATED PHASES.
C
C     SUBROUTINES REQUIRED
C
C      STR      FOURIER TRANSFORM OF RECTANGLE
C      GTR      FOURIER TRANSFORM OF GAUSSIAN
C      FIT      LINEAR CURVEFIT.  COMMON /CFIT/
C      PACK     BIT MANIPULATION FOR PHASE STORAGE
C               ALTERNATE ENTRY UNPACK
C      SYNCOS   COSINE FOURIER SYNTHESIS
C      USPLH    IMSL LP PLOT
C
C     DATA DECK
C
C      NR, MOD,IOUT   (NR=0 STOPS EXECUTION)
C      D,W1,WINC,NW,T1,TINC,NT
C      HEADA   (8A10)
C      FA(J),J=1,NR
C      HEADB   (8A10)
C      FB(J),J=1,NR
C     ETC
C
C     PROGRAM VARIABLES
C
C     IOUT          OUTPUT FORMAT
C                     0  SUMMARY ONLY
C                     1  STACK FOR EACH (T,W)
C                     2  STACK AND LP PLOTS FOR EACH (T,W)
C     HEADA         INPUT DATA IDENTIFICATION
C     HEADB
C     D             D SPACING
C     NR            NUMBER OF REFLECTIONS
C     MOD           =0 RECTANGULAR MODEL
C                     OTHERWISE GAUSSIAN MODEL
C     W             HALF-WIDTH OF SUBSTITUENT
C     T             POSITION OF SUBSTITUENT IN CELL
C     T1,W1         FIRST VALUES FOR T,W
C     TINC,WINC     INCREMENTS FOR T,W
C     NT,NW         NUMBER OF VALUES FOR T,W
C     FA,FB         STRUCTURE FACTOR MODULI--INPUT DATA
C     PA,PB         PHASE ARRAYS
C     FBC           CALCULATED VALUE OF FB
C     HA,HB         HARGREAVES PLOT VALUES, WITHOUT PHASES
C     HPA,HPB       HARGREAVES PLOT VALUES, WITH PHASES
C     J,JA,JB       REFLECTION INDEX
C     DSTK(I)       DEVIATION STACK
C     PHSTK(I)      PHASE STACK
C                     I=1,...,NS BEST RESULTS
C                     I=NS1=NS+1 WORST RESULT
C     DEV           MEAN RELATIVE DEVIATION BETWEEN FB AND FBC
C     SLOPE,YINT    VALUES FROM HARGREAVES PLOT
C
C     NAMES ENDING IN Z ARE FOR OVERALL SUMMARY TABLE:
C                   WZ,TZ,PHZ,DEVZ
C
      COMMON  /CFIT/ HPA,HPB,NR,SLOPE,YINT
```

```
      DIMENSION    WZ(200),TZ(200),PHZ(200),DEVZ(200)
      DIMENSION    FA(10), FB(10), PA(10), PB(10)
      DIMENSION    SCAL(10)
      DIMENSION    TR(10)
      DIMENSION    HA(10), HB(10), HPA(10), HPB(10)
      DIMENSION    OSTK(21), PHSTK(21)
      DIMENSION    HEADA(8), HEADB(8)
      INTEGER      SIGNA(10),SIGNB(10),PLUS,MINUS,ZERO
C        PLOT ARRAYS
      DIMENSION    A(10,2), B(10,2)
      DIMENSION    PL(160), IMAGE(5151)
      DIMENSION    X(101), Y(101,2)
C
C
C
      EQUIVALENCE (PA1,PA(1)), (PA2,PA(2)), (PA3,PA(3)), (PA4,PA(4))
      EQUIVALENCE (PA5,PA(5)), (PA6,PA(6)), (PA7,PA(7)), (PA8,PA(8))
      EQUIVALENCE (PA9,PA(9)), (PA10,PA(10))
      EQUIVALENCE (PB1,PB(1)), (PB2,PB(2)), (PB3,PB(3)), (PB4,PB(4))
      EQUIVALENCE (PB5,PB(5)), (PB6,PB(6)), (PB7,PB(7)), (PB8,PB(8))
      EQUIVALENCE (PB9,PB(9)), (PB10,PB(10))
      DATA         PL/160*1H   /
      DATA         PLUS/1H+/, MINUS/1H-/, ZERO/1H0/
      DATA         C1/1.47566/
C                  C1=SQRT((PI*LN(2))
   10 FORMAT(1H1)
   11 FORMAT(8A10)
   12 FORMAT(1H0,T5,*SAMPLE A*,T20,8A10)
   14 FORMAT(T5,*SAMPLE B*,T20,8A10)
   16 FORMAT(1H0,T5,*REFLECTIONS*,T20,I3)
   18 FORMAT(T5,*D-SPACING*,T20,F6.3)
   20 FORMAT(T5,*WIDTH*,T20,F6.3)
   21 FORMAT (T5,*MODEL*,T20,*RECTANGULAR*)
   22 FORMAT(T5,*SHIFT*,T20,F6.3)
   23 FORMAT (T5,*MODEL*,T20,*GAUSSIAN*)
   24 FORMAT(1H0,T5,*INPUT DATA--AMPLITUDES*)
   25 FORMAT(1H0,T5,*RELATIVE STRUCTURE FACTORS FOR SUBSTITUENT*)
   26 FORMAT(1H0,T5,*RAW HARGREAVES COEFFICIENTS*)
   28 FORMAT(T5,*A*,T10,10F10.4)
   30 FORMAT(T5,*B*,T10,10F10.4)
   32 FORMAT(1H0,T5,*BEST RESULTS*)
   34 FORMAT(1H0,T5,*WORST RESULTS*)
   36 FORMAT(3X,*INDEX*,6X,*DEV  A*,=I2,*  B*,=I2,
     *    5X,*SLOPE INTERCEPT      PEAK*)
   38 FORMAT(1X,I7,F9.3,3X,=(1X,A1),3X,=(1X,A1),4F10.4)
   40 FORMAT(15X,*WIDTH  POSITION DEVIATION*,
     .    *   A*,=I2,*   B*,=I2)
   45 FORMAT(5X,I5,3F10.4,4X,=(1X,A1),4X,=(1X,A1))
   62 FORMAT(1H0,T10,*BEST FOURIER*)
   64 FORMAT(1H0,T10,*SECOND BEST FOURIER*)
C
C        INPUT DATA.
C
      CALL PACK(PA,PB,0,WORD)
  100 CONTINUE
      IWT=0
      READ*,NR,MOD,IOUT,SCALE
      IF (NR.EQ.0) STOP
      READ*,D,W1,WINC,NW,T1,TINC,NT
      READ 11,HEADA
      READ*,(FA(J),J=1,NR)
      READ 11,HEADB
      READ*,(FB(J),J=1,NR)
```

```
      DO 110 J=1,NR
      SCAL(J)=FB(J)
      IF (FB(J).EQ.C.0) SCAL(J)=SCALE
  110 CONTINUE
C
C          LOOP ON W
C
      W=W1-WINC
      DO 705 NWW=1,NW
      W=W+WINC
C
C      LOOP ON T
C
      T=T1-TINC
      DO 700 NTT=1,NT
      IWT=IWT+1
      T=T+TINC
C
C        FIND RELATIVE STRUCTURE
C        FACTOR FOR SUBSTITUENT
C
      P=1.0
      IF (MOD.EQ.0) GO TO 135
      DO 130 J=1,NR
      S=FLOAT(J)/D
  130 TR(J)=GTR(S,P,W,T)
      GO TO 140
  135 CONTINUE
      DO 137 J=1,NR
      S=FLOAT(J)/D
  137 TR(J)=STR(S,P,W,T)
  140 CONTINUE
C
C        GENERATE RAW HARGREAVES NUMBERS
C
      DO 150 J=1,NR
      TRJ=TR(J)
      IF(TRJ.NE.0.0) GO TO 145
      WRITE*, D,W,T,J
      STOP ≠TRJ=0 IN DO 150 OF PHASE≠
  145 HA(J)=FA(J)/TRJ
  150 HB(J)=FB(J)/TRJ
C
C        INITIALIZE PHASE PERMUTATION SECTION
C
      NS=20
      IF (IOUT.EQ.0) NS=1
      NS1=NS+1
      KA=0
      KB=0
      BOEV=1.0E6
      WOEV=OSTK(NS1)=0.0
      DO 155 J=1,NS
  155 OSTK(J)=1.0E6
      DO 160 J=1,NR
      PA(J)=-1.0
      PB(J)=-1.0
  160 CONTINUE
      PA(1)=+1.0
      PB(1)=+1.0
      NR1=NR-1
C
C        BEGIN PHASE PERMUTATION LOOPS.
```

```
C        DO 350 PERMUTES PA, DO 300
C        PERMUTES PB.
C
      NA2=NA3=NA4=NA5=NA6=NA7=NA8=NA9=NA10=1
      GO TO (202,203,204,205,206,207,208,209,210) NR1
  210 IF(FA(10).NE.0.0) NA10=2
  209 IF(FA(9).NE.0.0) NA9=2
  208 IF(FA(8).NE.0.0) NA8=2
  207 IF(FA(7).NE.0.0) NA7=2
  206 IF(FA(6).NE.0.0) NA6=2
  205 IF(FA(5).NE.0.0) NA5=2
  204 IF(FA(4).NE.0.0) NA4=2
  203 IF(FA(3).NE.0.0) NA3=2
  202 IF(FA(2).NE.0.0) NA2=2
      DO 350 JA10=1,NA10      $PA10=-PA10
      DO 350 JA9=1,NA9        $PA9=-PA9
      DO 350 JA8=1,NA8        $PA8=-PA8
      DO 350 JA7=1,NA7        $PA7=-PA7
      DO 350 JA6=1,NA6        $PA6=-PA6
      DO 350 JA5=1,NA5        $PA5=-PA5
      DO 350 JA4=1,NA4        $PA4=-PA4
      DO 350 JA3=1,NA3        $PA3=-PA3
      DO 350 JA2=1,NA2        $PA2=-PA2
      KA=KA+1
      DO 230 J=1,NR
      HPA(J)=HA(J)*PA(J)
  230 CONTINUE
      NB2=NB3=NB4=NB5=NB6=NB7=NB8=NB9=NB10=1
      GO TO (252,253,254,255,256,257,258,259,260) NR1
  260 IF (FB(10).NE.0.0) NB10=2
  259 IF (FB(9).NE.0.0) NB9=2
  258 IF (FB(8).NE.0.0) NB8=2
  257 IF (FB(7).NE.0.0) NB7=2
  256 IF (FB(6).NE.0.0) NB6=2
  255 IF (FB(5).NE.0.0) NB5=2
  254 IF (FB(4).NE.0.0) NB4=2
  253 IF (FB(3).NE.0.0) NB3=2
  252 IF (FB(2).NE.0.0) NB2=2
      DO 300 JB10=1,NB10      $PB10=-PB10
      DO 300 JB9=1,NB9        $PB9=-PB9
      DO 300 JB8=1,NB8        $PB8=-PB8
      DO 300 JB7=1,NB7        $PB7=-PB7
      DO 300 JB6=1,NB6        $PB6=-PB6
      DO 300 JB5=1,NB5        $PB5=-PB5
      DO 300 JB4=1,NB4        $PB4=-PB4
      DO 300 JB3=1,NB3        $PB3=-PB3
      DO 300 JB2=1,NB2        $PB2=-PB2
      KB=KB+1
      DO 280 J=1,NR
      HPB(J)=HB(J)*PB(J)
  280 CONTINUE
C
C        GENERATE HARGREAVES PLOT FOR
C        CURRENT PHASE TRIAL PA AND PB.
C
      CALL FIT
C
C        USE CALCULATED SLOPE AND INTERCEPT OF
C        HARGEAVES PLOT TO FIND PREDICTED VALUES FBC(J)
C        TO COMPARE WITH INPUT VALUES FB(J).
C        DEV (=MEAN RELATIVE ERROR BETWEEN FB(J) AND FBC(J)  )
C        WILL BE TAKEN AS GOODNESS OF FIT FOR
C        CURRENT PHASE TRIAL PA AND PB.
```

```
C
      DEV=0.0
      DO 282 J=1,NR
      HPBC=YINT+SLOPE*HPA(J)
      FBC=PB(J)*HPBC*TR(J)
  282 DEV=DEV + ABS((FBC-FB(J))/SCAL(J))
      DEV=DEV/NR
C
C        IF DEV QUALIFIES FOR BEST STACK OR IS WORST
C        VALUE YET, ENCODE PHASES.
C
      IF (DEV.GE.BDEV.AND.DEV.LE.WDEV) GO TO 295
      CALL PACK(PA,PB,NR,WORD)
      IF (DEV.GE.BDEV) GO TO 292
      DSTK(NS)=DEV
      PHSTK(NS)=WORD
C
C        DO SORT
C
      DO 285 L=2,NS
      L1=NS-L+1
      L2=L1+1
      IF (DSTK(L2).GE.DSTK(L1))  GO TO 290
      TEMP=DSTK(L2)
      DSTK(L2)=DSTK(L1)
      DSTK(L1)=TEMP
      TEMP=PHSTK(L2)
      PHSTK(L2)=PHSTK(L1)
      PHSTK(L1)=TEMP
  285 CONTINUE
  290 BDEV=DSTK(NS)
  292 CONTINUE
      IF (DEV.LE.WDEV) GO TO 295
      WDEV=DSTK(NS1)=DEV
      PHSTK(NS1)=WORD
  295 CONTINUE
  300 CONTINUE
  350 CONTINUE
C
C     PERMUTATIONS AND DATA EVALUATION COMPLETE
C
C        PUT BEST RESULTS IN SUMMARY TABLE
C
      WZ(IWT)=W
      TZ(IWT)=T
      DEVZ(IWT)=DSTK(1)
      PHZ(IWT)=PHSTK(1)
      IF (IOUT.EQ.0) GO TO 700
C
C        OUTPUT RESULTS
C
      WRITE 10
      WRITE 12,HEADA
      WRITE 14,HEADB
      WRITE 16,NR
      WRITE 18,D
      WRITE 20,W
      WRITE 22,T
      IF (MOD.EQ.0) WRITE 21
      IF (MOD.NE.0) WRITE 23
      WRITE 24
      WRITE 28,(FA(J),J=1,NR)
      WRITE 30,(FB(J),J=1,NR)
```

```
      WRITE 25
      WRITE 28, (TR(J),J=1,NR)
      WRITE 26
      WRITE 28, (HA(J),J=1,NR)
      WRITE 30, (HB(J),J=1,NR)
      WRITE 32
      WRITE 36, NR,(J,J=1,NR), NR,(J,J=1,NR)
      DO 450 I=1,NS1
      CALL UNPACK(PA,PB,NR,PHSTK(I))
      II=I
      DO 370 J=1,NR
      IF (FA(J).EQ.0.0) PA(J)=0.0
      IF (FB(J).EQ.0.0) PB(J)=0.0
      HPA(J)=HA(J)*PA(J)
      HPB(J)=HB(J)*PB(J)
  370 SIGNA(J)=SIGNB(J)=ZERO
      IF (I.GT.2) GO TO 375
C
C        A AND B WILL CONTAIN STRUCTURE FACTORS OF
C        BEST 2 COMBINATIONS FOR PLOTTING
C
      DO 372 J=1,NR
      A(J,I)=FA(J) * PA(J)
  372 B(J,I)=FB(J) * PB(J)
  375 CONTINUE
      DO 380 J=1,NR
      IF(PA(J).LT.0.0) SIGNA(J) = MINUS
      IF(PB(J).LT.0.0) SIGNB(J) = MINUS
      IF(PA(J).GT.0.0) SIGNA(J) = PLUS
      IF(PB(J).GT.0.0) SIGNB(J) = PLUS
  380 CONTINUE
      CALL FIT
C
      P=YINT/W/C1
      IF (I.NE.NS1) GO TO 390
      WRITE 34
      II=KB
  390 CONTINUE
      WRITE 38,II,DSTK(I),NR, (SIGNA(J),J=1,NR), NR,
     *    (SIGNB(J),J=1,NR), SLOPE, YINT, P
  450 CONTINUE
      IF (IDUT.EQ.1) GO TO 600
C
C        DO PLOT OF TWO BEST RESULTS
C
      INC=1
      N=IA=101
      M=2
      XHI=0
      XLO=0.0
      XINC=(XHI-XLO)/(N-1)
      XJ=XLO
      DO 550 J=1,N
      X(J)=XJ
  550 XJ=XJ+XINC
C
C        SYNTHESIZE DENSITY PROFILE
C
      DO 580 I=1,2
      XJ=XLO
      DO 570 J=1,N
      Y(J,1)=SYNCOS(XJ,A(1,I),NR,0)
      Y(J,2)=SYNCOS(XJ,B(1,I),NR,0)
```

```
  570 XJ=XJ+XINC
      CALL USPLH(X,Y,N,M,INC,IA,PL,IMAGE,IER)
      IF (I.EQ.1) WRITE 62
      IF (I.EQ.2) WRITE 64
  580 CONTINUE
  600 CONTINUE
  700 CONTINUE
  705 CONTINUE
  750 CONTINUE
C
C     FOR EACH (W,T) COMBINATION, UNPACK PHASES FROM PHZ,
C     AND OUTPUT SUMMARY.  FIRST,WRITE HEADER.
C
      WRITE 10
      WRITE 12, HEADA
      WRITE 14, HEADB
      WRITE 16, NR
      WRITE 18, D
      IF (MOD.EQ.0) WRITE 21
      IF (MOD.NE.0) WRITE 23
      WRITE 24
      WRITE 28, (FA(J),J=1,NR)
      WRITE 30, (FB(J),J=1,NR)
      WRITE 32
      WRITE 40, NR,(J,J=1,NR), NR,(J,J=1,NR)
      DO 780 I=1,IWT
      CALL UNPACK(PA,PB,NR,PHZ(I))
      DO 770 J=1,NR
      SIGNA(J)=SIGNB(J)=MINUS
      IF (PA(J).GT.0.0) SIGNA(J) = PLUS
      IF (PB(J).GT.0.0) SIGNB(J) = PLUS
      IF (FA(J).EQ.0.0) SIGNA(J) = ZERO
      IF (FB(J).EQ.0.0) SIGNB(J) = ZERO
  770 CONTINUE
      WRITE 45, I,WZ(I),TZ(I),DEVZ(I),
     .  NR,(SIGNA(J),J=1,NR), NR,(SIGNB(J),J=1,NR)
  780 CONTINUE
      GO TO 100
      END
      FUNCTION GTR(S,P,H,T)
C     NO PARAMETERS ALTERED.
C     GTR IS THE FOURIER TRANSFORM OF A DIRECT-SPACE,
C     ORIGIN-REFLECTED GAUSSIAN OF HEIGHT=P, HALF WIDTH
C     AT HALF MAXIMUM=H, AND DISTANCE FROM ORIGIN TO CENTROID=T
C     GTR IS EVALUATED AT POINTS IN RECIPROCAL SPACE.
C     DIRECT SPACE FUNCTION=
C     G(X)=P*EXP(-LN(2)*((X-T)/H)**2)
C     REFLECTED THROUGH X=0
C     A=(SQRT(PI/LN(2)))
C     B=-(PI**2/LN(2))
C     C=2*PI
      DATA  A/2.128934/
      DATA  B/-14.23863/
      DATA  C/6.283185/
      GTR=A*P*H*EXP(B*(S*H)**2)*COS(C*S*T)
      RETURN
      END
      FUNCTION STR(S,P,H,T)
C     NO PARAMETERS ALTERED.
C     STR IS FOURIER TRANSFORM OF DIRECT SPACE, ORIGIN-REFLECTED
C     SQUARE WAVE OF HEIGHT=P, HALFWIDTH=H, AND DISTANCE FROM
C     CENTROID TO ORIGIN=T.  STR IS EVALUATED
C     AT POINTS IN RECIPROCAL SPACE
```

```
C      A=1/PI   B=2*PI
       DATA  A/0.3183099/
       DATA  B/6.283185/
       IF (S .EQ. 0.) GO TO 10
       STR=(P*A/S)*SIN(B*S*H)*COS(B*S*T)
       RETURN
   10  STR=2.*P*H
       RETURN
       END
       SUBROUTINE PACK(PA,PB,NR,WORD)
       DIMENSION PA(1),PB(1)
       INTEGER BITA(20),BITB(20)
       IF (NR.GT.0) GO TO 20
       DO 10 J=1,10
       BITA(J) = 2**(J-1)
       BITB(J)=2**(20+J)
   10  CONTINUE
   20  WORD=0B
       DO 30 J=1,NR
       IF(PA(J).GE.0.0) WORD=WORD.OR.BITA(J)
   30  IF(PB(J).GE.0.0) WORD=WORD.OR.BITB(J)
       RETURN
       ENTRY UNPACK
       DO 40 J=1,NR
   40  PA(J)=PB(J)=-1.0
       DO 50 J=1,NR
       IF ((WORD.AND.BITA(J)).NE.0B) PA(J)=1.0
   50  IF ((WORD.AND.BITB(J)).NE.0B) PB(J)=1.0
       RETURN
       END
       FUNCTION SYNCOS(X,C,N,PER)
C      NO PARAMETERS ALTERED.
C      FOURIER COSINE SERIES WITH COEFFICIENTS C(J),J=1,2,...,N
C      ON PERIOD=PER EVALUATED AT X.
C      C(1) GIVES FUNDAMENTAL.
       DIMENSION C(1)
       DATA  PI/3.1415926/
       IF (PER .EQ. 0.0) STOP *PER=0.0 IN FUNCTION SYNCOS*
       C1=2.0/PER
       C2=C1*PI
       SYNCOS=0.0
       DO 20 J=1,N
       H=FLOAT(J)
       SYNCOS=SYNCOS+ C(J)*COS(C2*X*H)
   20  CONTINUE
       SYNCOS=SYNCOS*C1
       RETURN
       END
       SUBROUTINE FIT
       COMMON   /CFIT/ XX,YY,N,SLOPE,YINT
C
C         XX,YY,N NOT ALTERED
C
C         R. LYTZ 7AUG77   OSU.
C         FIT1 CALCULATES SLOPE, Y-INTERCEPT, AND
C         STANDARD DEVIATION FOR LEAST SQUARES FIT
C         TO  YY(I)=YINT + SLOPE*XX(I), I=1,2,...,N.
C
       DIMENSION   XX(10),YY(10)
       FN=FLOAT(N)
       SX=SX2=SY=SY2=SXY=0.0
       DO 10 I=1,N
       X=XX(I)
```

```
      Y=YY(I)
      SX=SX+X
      SX2=SX2+X*X
      SY=SY+Y
      SY2=SY2+Y*Y
      SXY=SXY+X*Y
   10 CONTINUE
      YAVG=SY/FN
      SXQ=SX*SX
      DENOM=FN*SX2-SXQ
      IF(DENOM.EQ.0.0) STOP * DIVIDE BY ZERO IN FIT1 *
      SLOPE=(FN*SXY-SX*SY)/DENOM
      YINT=(SX2*SY-SX*SXY)/DENOM
      RETURN
      END
```

```
      PROGRAM POSIT(INPUT=/15),OUTPUT=/150,PUNCH)
C
C      R LYTZ  23 OCT 77  OREGON STATE UNIVERSITY  CDC CYBER.
C     PROGRAM DOES 3RD DEGREE CURVEFIT RELATING
C     POSITION TO CHANNEL FOR POSITION-SENSITIVE DETECTOR.
C      PUNCH OUTPUT FOR INPUT TO DIFRAX.
C
C     CALLS SUBROUTINES FIT3 AND EVAL3
C      REQUIRES IMSL LIBRARY
C     INPUT DATA DECK -- *INDICATES FREEFORM INPUT
C
C        NIN *  (NIN= 0 ENDS EXECUTION)
C        HEAD (7A10)
C        CIN(1) *
C        CIN(2) *
C        ...
C        CIN(NIN)
C        NIN * FOR NEXT SET
C        ETC
C
C
C        VARIABLES
C        NIN          NUMBER OF CALIBRATION POINTS
C        HEAD         DATA SET IDENTIFICATION
C        CIN          INPUT CHANNEL
C        XC           FIRST POSITION (MM)
C        XINC         POSITION INCREMENT (MM)
C        X.XX         CALCULATED POSITION
C        C            CALCULATED CHANNEL
C        A(I)         CURVEFIT COEFFICIENTS FOR X=X(C)
C        B(I)         CURVEFIT COEFFICIENTS FOR C=C(X)
C
      DIMENSION    HEAD(7)
      DIMENSION    CIN(50), XIN(50)
      DIMENSION    XX(500)
      DIMENSION    A(4),B(4)
   10 FORMAT (7A10)
   15 FORMAT (1H0,T10,*PROGRAM POSITION--3RD DEGREE CURVEFIT*,
     2   *FOR DETECTOR POSITION CALIBRATION*)
   20 FORMAT (T10,7A10, /,T10,*CALIBRATION POINTS=*, I3)
   35 FORMAT (1H0,T10,*CURVEFIT COEFFICIENTS*)
   40 FORMAT (1H0,T10,*X=X(C)=SUM(I=1,4) OF A(I) * C ** (I-1)*)
   45 FORMAT (T10,*A(*, I1, *)=*, 1P,E12.5)
   50 FORMAT (T10,*DEV =*, 1P,E12.5)
   55 FORMAT (1H0,T10,*C=C(X)=SUM(I=1,4) OF B(I) * X ** (I-1)* )
   60 FORMAT (T10, *B(*, I1, *)=*, 1P,E12.5)
   65 FORMAT (1H0, T13,
     1  *    ACTUAL       CALC       DIFF*,
     2  *    ACTUAL       CALC       DIFF* /, T13,
     3  *  POSITION   POSITION   POSITION*,
     4  *   CHANNEL    CHANNEL    CHANNEL*  )
   70 FORMAT (    T10,I3,6F10.3 )
   75 FORMAT (1H1)
   76 FORMAT (1H0)
   80 FORMAT (10(3X,I3,F7.2) )
   82 FORMAT (A10,A5,* CTP *, 4E15.8)
   84 FORMAT (A10,A5,* PTC *, 4E15.8)
  100 READ *, NIN
      IF (NIN.EQ. 0) STOP
      READ 10, HEAD
      WRITE 75
      WRITE 76
      WRITE 76
```

```
      WRITE 15
      WRITE 20, HEAD, NIN
      READ *, X0, XINC
C
C        FILL XIN ARRAY
C
      X=X0
      DO 120 I=1,NIN
      XIN(I)=X
      READ *,  CIN(I)
      X=X + XINC
  120 CONTINUE
C
C        CALCULATE A FOR X=X(C)
C
      CALL FIT3(CIN,XIN,NIN,A,ADEV)
      PUNCH 82, HEAD(1), HEAD(2), A
C
C        CALCULATE B FOR C=C(X)
C
      CALL FIT3(XIN,CIN,NIN,B,BDEV)
      PUNCH 84, HEAD(1), HEAD(2), B
      WRITE 35
      WRITE 40
      DO 130 I=1,4
      WRITE 45, I,A(I)
  130 CONTINUE
      WRITE 50,  ADEV
      WRITE 55
      DO 140 I=1,4
      WRITE 60,  I,B(I)
  140 CONTINUE
      WRITE 50,  BDEV
      WRITE 65
C
C        COMPARE FITTED VALUES TO INPUT VALUES
C
      DO 200 I=1,NIN
      CI=CIN(I)
       XI=XIN(I)
      X=EVAL3(CI,A)
      ADEV = XI - X
      C=EVAL3(XI,B)
      BDEV = CI - C
      WRITE 70,  I,XI,X,ADEV,CI,C,BDEV
  200 CONTINUE
C
C        WRITE OUT 500 CHANNEL INTERPOLATION
C
      DO 300 J=1,500
      C=FLOAT(J)
      XX(J)=EVAL3(C,A)
  300 CONTINUE
      WRITE 75
      WRITE 76
      WRITE 20,  HEAD, NIN
      WRITE 76
      WRITE 80,  (J,XX(J), J=1,500)
      GO TO 100
      END
      SUBROUTINE FIT3(P,Q,N,A,SDEV)
C     Q=A0 + A1*P + A2*P**2 + A3*P**3
      DIMENSION P(1), Q(1)
```

```
      DIMENSION T(4,4), A(4), B(4)
      DIMENSION TINV(4,4), WK(4,4)
      SX1=SX2=SX3=SX4=SX5=SX6=0.0
      SY=SXY=SX2Y=SX3Y=0.0
C
C     XX WILL CONTAIN P TO THE APPROPRIATE POWER.
C
      DO 300 I=1,N
      X=P(I)
      Y=Q(I)
C
C     ACCUMULATE X**0 TERMS
      XX=1.0
      XY=Y
      SY=SY+XY
C
C     ACCUMULATE X**1 TERMS.
      XX=XX*X
      XY=XY*X
      SX1=SX1+XX
      SXY=SXY+XY
C
C     ACCUMULATE X**2 TERMS
      XX=XX*X
      XY=XY*X
      SX2=SX2+XX
      SX2Y=SX2Y+XY
C
C     ACCUMULATE X**3 TERMS
      XX=XX*X
      XY=XY*X
      SX3=SX3+XX
      SX3Y=SX3Y+XY
C
C     ACCUMULATE X**4 TERMS.
      XX=XX*X
      SX4=SX4+XX
C
C     ACCUMULATE X**5 TERMS.
      XX=XX*X
      SX5=SX5+XX
C
C     ACCUMULATE X**6 TERMS.
      XX=XX*X
      SX6=SX6+XX
  300 CONTINUE
      FN=FLOAT(N)
C
C     STUFF X**N SUMS INTO T, THE COEFFICIENT MATRIX.
C
      T(1,1)=FN
      T(1,2)=SX1
      T(2,1)=SX1
      T(1,3)=SX2
      T(2,2)=SX2
      T(3,1)=SX2
      T(1,4)=SX3
      T(2,3)=SX3
      T(3,2)=SX3
      T(4,1)=SX3
      T(2,4)=SX4
      T(3,3)=SX4
      T(4,2)=SX4
```

```
      T(3,4)=SX5
      T(4,3)=SX5
      T(4,4)=SX6
      DO 400 I=1,4
  400 CONTINUE
C
C     STUFF Y*X**N SUMS INTO B VECTOR
C
      B(1)=SY
      B(2)=SXY
      B(3)=SX2Y
      B(4)=SX3Y
      IDGT=5
      CALL LINV1F(T,4,4,TINV,IDGT,WK,IER)
C
C     NEXT CALC POLYNOMIAL COEFFS A(I).  A=INV(T)*B.
C
      A(1)=A(2)=A(3)=A(4)=0.0
      DO 600 J=1,4
      DO 600 K=1,4
      A(J)=A(J) + TINV(J,K)*B(K)
  600 CONTINUE
      DO 700 I=1,4
      J=I-1
  700 CONTINUE
      A0=A(1)
      A1=A(2)
      A2=A(3)
      A3=A(4)
      SDEV=0.0
      DO 800 J=1,N
      PJ=P(J)
      QJ=Q(J)
      QCALC = A0 + A1*PJ + A2*PJ*PJ + A3*PJ*PJ*PJ
      DEV = QJ-QCALC
      DEV=DEV*DEV
      SDEV=SDEV+DEV
  800 CONTINUE
      SDEV=SQRT(SDEV/(FN-1.0))
      RETURN
      END
      FUNCTION EVAL3(Z,C)
C
C        R LYTZ 23 OCT 77  OREGON STATE UNIVERSITY
C
C        ARGUMENTS NOT CHANGED
C        RETURNS SUM(I=1,4) OF C(I) * Z ** (I-1)
C
      DIMENSION C(4)
      EVAL3 = (( C(4)*Z + C(3))*Z + C(2))*Z + C(1)
      RETURN
      END
```

```
      PROGRAM DIFRAX (INPUT,OUTPUT,PUNCH,TAPE30)
C
C      R LYTZ   25 JAN 78   OSU   CDC CYBER
C
C
C        DATA DECK
C
C          LCTP,CTP   (2A10,4E15.8)
C          LPTC,PTC   (2A10,4E15.8)
C          SPFIL      (8A10) --IF BLANK, EXECUTION STOPS
C          CORFIL      (8A10) --IF BLANK, CORRECTED SPECTRUM NOT SENT TO CARDS
C          SPFIL
C          ...ETC
C
C
C      LCTP,CTP POSITION-CHANNEL CURVE FIT
C      LPTC,PTC COEFFICIENTS, AS DUMPED DIRECTLY ONTO
C              CARDS BY PROGRAM POSI .
C
C      SPFIL    NAME OF MASS STORAGE FILE WHICH CONTAINS THE
C              SPECTRUM TO BE EVALUATED.  SPFIL MUST CONTAIN:
C              LSP         LABEL
C              NP          NUMBER OF PEAKS
C              IWID        DISTANCE IN CHANNELS BETWEEN PEAKS
C              ISTART      FIRST CHANNEL TO APPEAR IN CORRECTED SPECTRUM
C              WL          WAVELENGTH
C              SD          SAMPLE-DETECTOR DISTANCE
C              BEAM        CENTROID CHANNEL OF BEAM POSITION
C              WT          NORMALIZING FACTOR FOR F**2
C              MAX(I)      CHANNEL POSITIONS OF PEAK CENTROIDS
C              SP(J)       CHANNEL DATA
C
C
      DIMENSION SPCC(500)
      DIMENSION SP(500),SPC(500),BK1(500),BK2(500)
      DIMENSION MAX(20),MIN(20),L(20), M(20)
      DIMENSION LSP(8),LCTP(2),LPTC(2),LBCR(2)
      DIMENSION CTP(4),PTC(4),BCR(4)
      DIMENSION CHAN(100),COUNT(100)
      DIMENSION A(10)
      DIMENSION X(20),Y(20),E(20)
      EQUIVALENCE (BK2,SPC)
      DATA A  (DEG=57.2958)
    5 FORMAT (6A10,////)
    6 FORMAT ((7X,5(1X,F10.0)))
   10 FORMAT (8A10)
   12 FORMAT (3I5)
   13 FORMAT (5F10.5)
   14 FORMAT (16I5)
   16 FORMAT (10F7.0)
   18 FORMAT (2A10,4E15.8)
   24 FORMAT (1H1,//)
   26 FORMAT (2X,10F6.0,2X,10F6.0)
   28 FORMAT (1H0,//)
   40 FORMAT (T10,*SPECTRUM*,T25,8A10)
   42 FORMAT (T10,*BACKGROUND*,T25,8A10)
   44 FORMAT (T10,*CHAN TO POS*,T25,2A10,4E12.5)
   46 FORMAT (T10,*POS TO CHAN*,T25,2A10,4E12.5)
   50 FORMAT (T10,*WAVELENGTH *,F8.3)
   52 FORMAT (T10,*SAMPLE-DET *  ,F8.3)
   54 FORMAT (T10,*PEAKWIDTH*,I7)
   60 FORMAT (1H0,T20,*ORIGINAL SPECTRUM*,//)
   62 FORMAT (1H0,T20,*CALCULATED BACKGROUND*,//)
```

```
   64 FORMAT (1H0,T20,*CORRECTED SPECTRUM*,//)
   66 FORMAT (1H0,T20,*INTERMEDIATE CALCULATIONS*,//)
   79 FORMAT (T17,*...CENTROID....*,33X,*INTEGRATION*,/,
     2  T11,*N*,5X,*INPUT*,5X,*CALCD*,9X,*X*,2X,
     3  *INTEGRAL*,5X,*ERROR*,6X,*CHANNELS*)
   80 FORMAT (T10,I2,I10,4F10.2,2I7)
   89 FORMAT (T11,*N*,5X,*THETA*,9X,*D*,8X,*F2*,
     2  5X,*E(F2)*,9X,*F*,6X,*E(F)* )
   90 FORMAT (T10,I2,6F10.2)
      NCH=500
      READ 18, LCTP,CTP
      READ 19, LPTC,PTC
  200 CONTINUE
      READ 10, SPFIL
      IF (SPFIL .EQ. 10H            ) STOP
      CALL UGET (6LTAPE30,SPFIL)
      ICOR=0
      READ 10,CORFIL
      IF(CORFIL.EQ.10H              ) GO TO 220
C      CORRECTED SPECTRUM WILL BE DUMPED TO CARDS
      ICOR=1
  220 CONTINUE
C
C      READ DATA FROM SPECTRUM FILE
C
      READ(30,10) LSP
      READ (30,12) NP,IWID,ISTART
      READ (30,13)  WL,SD,BEAM,WT
      IF (WT.EQ.0.0) WT=100.0
      READ(30,14) (MAX(I),I=1,NP)
      READ(30,16) (SP(J),J=1,NCH)
C
C      WRITE HEADINGS
C
       WRITE 24
      WRITE 40, LSP
      WRITE 44, LCTP, CTP
      WRITE 46, LPTC,PTC
      WRITE 50, WL
      WRITE 52, SD
      WRITE 28
      DO 280 J=1,NCH
  280 BK1(J)=BK2(J)=0.0
C
C     CALCULATE CHANNEL MARKERS.
C
      IWID2=IWID/2
      NP1=NP+1
      DO 300 I=2,NP
  300 MIN(I)=(MAX(I)+MAX(I-1))/2
      MIN1=MIN(1)=ISTART
      MIN(NP1)=2*MIN(NP) - MIN(NP-1)
      DO 310 I=1,NP
      L(I)=MAX(I) - IWID2
  310 M(I)=MAX(I)+IWID2
      WRITE 66
      WRITE*, MAX
      WRITE*, MIN
      WRITE*, L
      WRITE*,M
C
C
C
```

```
C       FIND AVERAGE BETWEEN PEAKS 3 AND 4
C
        J1=M(3)
        J2=L(4)
        JJ=J2-J1
        AVG34=0.0
        DO 315 J=J1,J2
  315   AVG34=AVG34 + SP(J)
        AVG34 = AVG34 / FLOAT(JJ)
        WRITE *, AVG34
        WRITE 28
C
C       PUT FIT DATA BELOW PEAK 4 INTO BK2
C       AND SUBTRACT AVG34
C
        JJ=0
        DO 330 I=1,4
        J1=MIN(I)
        J2=L(I)
        IF (I.GT.2) J1=M(I-1)
        DO 320 J=J1,J2
        JJ=JJ+1
        BK1(JJ)=J
  320   BK2(JJ)=SP(J)-AVG34
  330   CONTINUE
C
C       SEND DATA TO CURVEFIT.  A IS COEFF ARRAY.
C       K IS NUMBER OF TERMS.  P IS NONLINEARITY PARAM.
C
        K=4
        MIN1=MIN(1)
        P=SP(MIN1) - SP(MIN1 + 1)
        P= P/SP(MIN1)/FLOAT(K)
        CALL EXPFIT(BK1,BK2,JJ,P,K,A)
        WRITE *,A
        WRITE 28
C
C       EVALUATE FITTING FUNCTION AND ADD AVG34
C
        DO 340 J=1,NCH
  340   BK1(J)=SPC(J)=0.0
        J1=MIN(1)
        J2=MIN(NP1)
        DO 350 J=J1,J2
        CH=J
        BK=BK1(J)=EVALEX(CH,K,P,A) + AVG34
  350   SPC(J)=SP(J)-BK
C
C       DO PIECEWISE LINEAR FIT BETWEEN PEAKS
C       TO REMOVE RESIDUAL BACKGROUND
C
        DO 400 I=1,NP
        J1=MIN(I)
        J2=L(I)
        J3=M(I)
        J4=L(I+1)
C
C       THESE IFS COMPENSATE FOR NONUNIFORM PEAK WIDTHS.
C
        IF (I.EQ.2) J1=J1+4
        IF (I.EQ.2) J2=J2+4
        IF (I.GT.2) J1=M(I-1)
        IF (I.EQ.1) J3=MIN(2)
```

```
      IF (I.EQ.NP) J4=MIN(NP1)
C
C       PUT DATA INTO CHAN, COUNT TO BE FIT
C
      JJ=0
      DO 360 J=J1,J2
      JJ=JJ+1
      CHAN(JJ)=J
  360 COUNT(JJ)=SPC(J)
      DO 365 J=J3,J4
      JJ=JJ+1
      CHAN(JJ)=J
  365 COUNT(JJ)=SPC(J)
      CALL FIT1(CHAN,COUNT,JJ,SLOPE,YINT,DEV)
      WRITE *,  I,J1,J2,J3,J4,JJ,SLOPE,YINT,DEV
C
C       MAKE PIECEWISE CORRECTION
C
      J1=MIN(I)
      J2=MIN(I+1)
      IF(I.NE.NP) J2=J2-1
      DO 370 J=J1,J2
      CH=J
      BK=BK1(J)=BK1(J)+SLOPE*CH + YINT
  370 SPCC(J)=SP(J)-BK
  400 CONTINUE
      DO 410 J=1,NCH
  410 SPC(J)=SPCC(J)
      WRITE 24
      WRITE 60
      WRITE 26,(SP(J),J=1,NCH)
      WRITE 24
      WRITE 62
      WRITE 26,(BK1(J),J=1,NCH)
      WRITE 64
      WRITE 26,(SPC(J),J=1,NCH)
      IF (IDOR.EQ.0) GO TO 420
      PUNCH 5,CORFIL
      PUNCH 6,(SPC(J),J=1,NCH)
      B2=J2=MIN(NP1)
  420 CONTINUE
C
C       ANALYZE DATA.  FIND CENTROIDS C, POSITIONS X,
C       INTEGRALS Y, AND RELATIVE ERRORS E.
C
      BEAM=EVAL3(BEAM,CTP)
      TOTAL = 0.0
C
C       WRITE HEADINGS
C
      WRITE 24
      WRITE 40, LSP
      WRITE 42,BKFIL
      WRITE 44, LCTP, CTP
      WRITE 46, LPTC,PTC
      WRITE 50, WL
      WRITE 52, SD
      WRITE 54,  IWID
       WRITE 26
      WRITE 79
      DO 500 I=1,NP
      J1=MIN(I)
      J2=MIN(I+1)
```

```
      CALL CENTSUM(SPC,J1,J2,C,SUM)
      YI=Y(I)=SUM*FLOAT(I)
      TOTAL=TOTAL + YI
      X(I)=EVAL3(C,CTF) - BEAM
      E(I)= 1.0/SQRT(ABS(SUM))
      WRITE 80,  I,MAX(I),C,X(I),SUM,E(I),J1,J2
  500 CONTINUE
       WRITE 28
      TOTAL=TOTAL/WT
C
C      FIND THETA,D,F2,F,AND ERRORS EF2, EF.
C
      WRITE 89
      DO 600 I=1,NP
      THETA=0.5*ATAN(X(I)/SD)
      D=0.5*FLOAT(I)*WL/SIN(THETA)
      THETA=THETA*DEG
      F2=Y(I)/TOTAL
      F=SQRT(ABS(F2))
      EF2=E(I)*F2
      EF=0.5*EF2
      WRITE 90, I,THETA,D,F2,EF2,F,EF
  600 CONTINUE
      CALL FCLOSE(30)
      GO TO 200
      END
      SUBROUTINE FIT1(XX,YY,N,SLOPE,YINT,DEV)
C
C        XX,YY,N NOT ALTERED
C
C        R. LYTZ 7AUG77   OSU.
C        FIT1 CALCULATES SLOPE, Y-INTERCEPT, AND
C        STANDARD DEVIATION FOR LEAST SQUARES FIT
C        TO  YY(I)=YINT + SLOPE*XX(I), I=1,2,...,N.
C
      DIMENSION    XX(1),YY(1)
      FN=FLOAT(N)
      SX=SX2=SY=SY2=SXY=0.0
      DO 10 I=1,N
      X=XX(I)
      Y=YY(I)
      SX=SX+X
      SX2=SX2+X*X
      SY=SY+Y
      SY2=SY2+Y*Y
      SXY=SXY+X*Y
   10 CONTINUE
      SXQ=SX*SX
      DENOM=FN*SX2-SXQ
      IF(DENOM.EQ.0.0) STOP * DIVIDE BY ZERO IN FIT1 *
      SLOPE=(FN*SXY-SX*SY)/DENOM
      YINT=(SX2*SY-SX*SXY)/DENOM
      DEV=0.0
      DO 20 I=1,N
      YCALC=YINT + SLOPE*XX(I)
      YDEV=ABS(YY(I) - YCALC)
      DEV=DEV+YDEV
   20 CONTINUE
      DEV=DEV/FN
      RETURN
      END
      FUNCTION EVALEX(X,M,P,COEF)
      DIMENSION COEF(1)
```

```
      EVALEX=0.0
      DO 10 J=1,M
   10 EVALEX=EVALEX+COEF(J)*EXP(-J*P*X)
      RETURN
      END
      SUBROUTINE CENTSUM(A,J1,J2,CENT,SUM)
      DIMENSION A(1)
      SUM=0.0
      CENT=0.0
      DO 100 J=J1,J2
      AJ=A(J)
      CENT=FLOAT(J) * AJ  +  CENT
      SUM=SUM+AJ
  100 CONTINUE
      CENT=CENT/SUM
      RETURN
      END
      FUNCTION EVAL3(Z,C)
C
C        R LYTZ 23 OCT 77  OREGON STATE UNIVERSITY
C
C        ARGUMENTS NOT CHANGED
C        RETURNS SUM(I=1,4) OF C(I) * Z ** (I-1)
C
      DIMENSION C(4)
      EVAL3 = (( C(4)*Z + C(3))*Z + C(2))*Z + C(1)
      RETURN
      END
```

```
      PROGRAM PREDICT(INPUT,OUTPUT)
C*****************************************************
C
C PROGRAM PREDICT   21 OCT 75 R. LYTZ  OSU CYBER
C
C PROGRAM TO PREDICT DIFFRACTED INTENSITY FROM INFINITE STACK OF
C LAYERS OF SPACING D.  LAYER ELECTRON-DENSITY
C PROFILE IS GIVEN BY SUM OF GAUSSIANS OR SUM OF SQUARE WAVES
C WHOSE PARAMETERS ARE INPUT AS DATA.
C
C G(X)=SUM OF GAUSSIANS
C S(X)=SUM OF SQUARE WAVES
C
C S AND G ARE REFLECTED THROUGH ORDINATE, AND THEIR
C TRANSFORMS ARE THEREFORE REAL.
C
C GTR(S)=FOURIER TRANSFORM OF G(X).
C STR(S)=FOURIER TRANSFORM OF S(X).
C
C INTEGRATED DIFFRACTION INTENSITY IS PROPORTIONAL TO
C SQUARE OF GTR OR STR SAMPLED AT  POINTS
C S=H/D, WHERE H=0,1,2,.. .
C
C INPUT DATA
C
C WL      WAVELENGTH
C ND      NUMBER OF DIFFERENT D SPACINGS TO USE
C N       NUMBER OF PEAKS (GAUSSIAN OR SQUARE) IN LAYER MODEL
C NP      NUMBER OF DIFFRACTION ORDERS TO CALCULATE
C NT      NUMBER OF TERMS IN SYNTHESES
C I       INDEX FOR MODEL PEAK. I=1,2,...,N
C A(I)    HEIGHT OF MODEL PEAK I
C W(I)    HALFWIDTH OF MODEL PEAK I
C T(I)    DISTANCE BETWEEN ORIGIN AND MODEL PEAK I
C CHAR    DATASET IDENTIFICATION
C
C***DATA DECK STRUCTURE
C
C WL
C ND,NT
C D1,D2,D3,...
C N,CHAR            (I3,5A10)  SET 1
C A(1),W(1),T(1)
C A(2),W(2),T(2)
C ...
C N,CHAR            (I3,5A10)  SET 2
C A(1),W(1),T(1)
C A(2),W(2),T(2)
C ...
C ...
C 0                 (N=0 ENDS EXECUTION)
C
C
C*************************************************************
      DIMENSION A(20), W(20), T(20), DD(20), CHAR(5)
      DIMENSION GA(30), GI(30), SA(30), SI(30)
      DIMENSION XPLT(101)
      DIMENSION YPLT(101,10)
      DIMENSION    APLT(175), IMAG4(5151)
      DATA         APLT /175*1H     /
   50 FORMAT(10X,5A10)
   51 FORMAT(10X,*TRANSFORM OF SQUARE MODEL*)
   52 FORMAT(10X,*INTENSITY FROM SQUARE MODEL*)
```

```
 53 FORMAT(10X,*TRANSFORM OF GAUSSIAN MODEL*)
 54 FORMAT(10X,*INTENSITY FROM GAUSSIAN MODEL*)
 55 FORMAT(10X,I2,* AND *,I2,
   2       *-TERM PATTERSON FROM SQUARE MODEL*)
 56 FORMAT(10X,I2,* AND *,I2,
   2       *-TERM PATTERSON FROM GAUSSIAN MODEL*)
 57 FORMAT(10X,I2,* AND *,I2,
   2       *-TERM FOURIER RECONSTRUCTION OF SQUARE MODEL*)
 58 FORMAT(10X,I2,* AND *,I2,
   2       *-TERM FOURIER RECONSTRUCTION OF GAUSSIAN MODEL*)
105 FORMAT (5F10.4 /)
110 FORMAT (I3,5A10)
115 FORMAT (2I5)
120 FORMAT (*1*  ////  5X,5A10)
125 FORMAT (/ 20X *     HEIGHT       HWHM      SHIFT*)
130 FORMAT (*          PEAK* I4,4X,3F10.4)
135 FORMAT (/ *      D=* F8.4 *,  WAVELENGTH=* F8.4 *,*)
140 FORMAT (*0*,32X,*------------GAUSSIAN------------*,
   1    *    -----------SQUARE WAVE-----------*/ ,
   2    *      H  2THETA DEG            S*          ,
   3    *    AMPLITUDE    INTENSITY  NORM INTEN*,
   4    *    AMPLITUDE    INTENSITY  NORM INTEN*  ,
   5    *    SQUA/GAUS*    4X   *H*    )
145 FORMAT (* *  I5, 2F12.4, 1P, 6E12.4,  0P, F12.4, I5 )
    PI=4.*ATAN(1.)
    READ*,WL
    READ*,ND,NT
    READ*,(DD(I),I=1,ND)
    IS=0
200 CONTINUE
    NP=21
    IS=IS+1
    READ 110, N, (CHAR(I),I=1,5)
    IF (N.EQ.0) STOP
    DO 220 I=1,N
220 READ*, A(I), W(I), T(I)
    DO 900 IND=1,ND
    D=DD(IND)
    PRINT 120, (CHAR(I),I=1,5)
    PRINT 125
    DO 240 I=1,N
240 PRINT 130, I,A(I),W(I),T(I)
    PRINT 135, D,WL
    PRINT 140
    G1=S1=0.0
    DO 400 I=1,NP
    HH=IH=I-1
    DO 300 J=1,N
    S=HH/D
    G1=G1+GTR(S,A(J),W(J),T(J))/D
    S1=S1+STR(S,A(J),W(J),T(J))/D
300 CONTINUE
    GA(I)=G1
    SA(I)=S1
    GI(I)=G1*G1
    SI(I)=S1*S1
    G1=S1=0.0
400 CONTINUE
    DO 450 I=2,NP
    G1=G1+GI(I)
    S1=S1+SI(I)
450 CONTINUE
    DO 600 I=1,NP
```

```
      HH=IH=I-1
      S=HH/D
      GN=GI(I)/G1
      SN=SI(I)/S1
      QSG=SN/GN
      TH2R=2.*ASIN(HH*WL/2./J)
      TH2D=TH2R*180./PI
      PRINT 145, IH,Th2D,S,GA(I),GI(I),GN,   SA(I),SI(I),SN,QSG,IH
  600 CONTINUE
      IF (NT.EQ.0) GO TO 200
C
C     DO PLOTS
C
      NP=NP-1
      N1=N+1
      N2=N+2
      NPLT=IA=101
      INC=1
C
C     PLOT TRANSFORMS OF FEATURES, SUM, AND INTENSITY
C     L=1   SQUARE
C     L=2   GAUSSIAN
C
      N2=N+2
      XL=1.0/D
      XH=11.0/D
      XINC=(XH-XL)/(NPLT-1)
      DO 645 L=1,2
      XJ=XL
      DO 640 J=1,NPLT
      XPLT(J)=XJ
      YPLT(J,N1)=0.0
      DO 635 K=1,N
      IF(L .EQ. 1) Y = STR(XJ, A(K), W(K), T(K))
      IF (L .EQ. 2) Y = GTR(XJ, A(K), W(K), T(K))
      YPLT(J,K)=Y
      Y=YPLT(J,N1)=YPLT(J,N1)+Y
      YPLT(J,N2)=Y*Y
  635 CONTINUE
      XJ=XJ+XINC
  640 CONTINUE
      CALL USPLH(XPLT, YPLT, NPLT, N1, INC, IA, APLT, IMAG4, IER)
      WRITE 50, CHAR
      IF (L .EQ. 1) WRITE 51
      IF (L .EQ. 2) WRITE 53
      CALL USPLH(XPLT,YPLT(1,N2),NPLT,1,INC,IA,APLT, IMAG4, IER)
      WRITE 50, CHAR
      IF (L .EQ. 1) WRITE 52
      IF (L .EQ. 2) WRITE 54
  645 CONTINUE
C
C     PLOT PATTERSONS
C
      N=2
      XL=-D
      XH=+D
      XINC=(XH-XL)/(NPLT-1)
      XJ=XL
C
C     PATTERSONS BASED ON SQUARE WAVE MODEL
C
      DO 660 J=1,NPLT
      XPLT(J)=XJ
```

```
      YPLT(J,1) = SYNCOS(XJ, SI(2), NT, 0)
      YPLT(J,2) = SYNCOS(XJ, SI(2), NP, 0)
      XJ=XJ+XINC
  660 CONTINUE
      CALL USPLH(XPLT, YPLT, NPLT, 4, INC, IA, APLT, IMAG+, IER)
      WRITE 50, CHAR
      WRITE 55,NT,NP
C
C     PATTERSONS BASED ON GAUSSIAN MODEL
C
      XJ=XL
      DO 680 J=1,NPLT
      YPLT(J,1) = SYNCOS(XJ, GI(2), NT, 0)
      YPLT(J,2) = SYNCOS(XJ, GI(2), NP, 0)
      XJ=XJ+XINC
  680 CONTINUE
      CALL USPLH(XPLT, YPLT, NPLT, 4, INC, IA, APLT, IMAG+, IER)
      WRITE 50, CHAR
      WRITE 56,NT,NP
C
C     PLOT FOURIERS
C
C     FOURIER BASED ON SQUARE MODEL
C
      XJ=XL
      DO 700 J=1,NPLT
      YPLT(J,1)= SYNCOS(XJ,SA(2),NT,0)
      YPLT(J,2)= SYNCOS(XJ,SA(2),NP,0)
      XJ=XJ+XINC
  700 CONTINUE
      CALL USPLH(XPLT, YPLT, NPLT, 4, INC, IA, APLT, IMAG+, IER)
      WRITE 50, CHAR
      WRITE 57,NT,NP
C
C     FOURIER BASED ON GAUSSIAN MODEL
C
      XJ=XL
      DO 720 J=1,NPLT
      YPLT(J,1)= SYNCOS(XJ,GA(2),NT,0)
      YPLT(J,2)= SYNCOS(XJ,GA(2),NP,0)
      XJ=XJ+XINC
  720 CONTINUE
      CALL USPLH(XPLT, YPLT, NPLT, 4, INC, IA, APLT, IMAG+, IER)
      WRITE 50, CHAR
      WRITE 58,NT,NP
  900 CONTINUE
      GO TO 200
      END
      FUNCTION SYNCOS(X,C,N,PER)
C     NO PARAMETERS ALTERED.
C     FOURIER COSINE SERIES WITH COEFFICIENTS C(J), J=1,2,...,N
C     ON PERIOD=PER EVALUATED AT X.
C     C(1) GIVES FUNDAMENTAL.
      DIMENSION C(1)
      DATA  PI/3.1415926/
      IF (PER .EQ. 0.0) STOP *PER=0.0 IN FUNCTION SYNCOS*
      C1=2.0/PER
      C2=C1*PI
      SYNCOS=0.0
      DO 20 J=1,N
      H=FLOAT(J)
      SYNCOS= SYNCOS+ C(J)*COS(C2*X*H)
   20 CONTINUE
```

```
      SYNCOS=SYNCOS*C1
      RETURN
      END
      FUNCTION GTR(S,P,H,T)
C     NO PARAMETERS ALTERED.
C     GTR IS THE FOURIER TRANSFORM OF A DIRECT-SPACE,
C     ORIGIN-REFLECTED GAUSSIAN OF HEIGHT=P, HALF WIDTH
C     AT HALF MAXIMUM=H, AND DISTANCE FROM ORIGIN TO CENTROID=T
C     GTR IS EVALUATED AT POINTS IN RECIPROCAL SPACE.
C     DIRECT SPACE FUNCTION=
C     G(X)=P*EXP(-LN(2)*((X-T)/H)**2)
C     REFLECTED THROUGH X=0
C     A=(SQRT(PI/LN(2)))
C     B=-(PI**2/LN(2))
C     C=2*PI
      DATA  A/2.128934/
      DATA  B/-14.23883/
      DATA  C/6.283185/
      GTR=A*P*H*EXP(B*(S*H)**2)*COS(C*S*T)
      RETURN
      END
      FUNCTION STR(S,P,H,T)
C     NO PARAMETERS ALTERED.
C     STR IS FOURIER TRANSFORM OF DIRECT SPACE, ORIGIN-REFLECTED
C     SQUARE WAVE OF HEIGHT=P, HALFWIDTH=H, AND DISTANCE FROM
C     CENTROID TO ORIGIN=T.  STR IS EVALUATED
C     AT POINTS IN RECIPROCAL SPACE
C     A=1/PI    B=2*PI
      DATA  A/0.3183099/
      DATA  B/6.283185/
      IF (S .EQ. 0.) GO TO 10
      STR=(P*A/S)*SIN(B*S*H)*COS(B*S*T)
      RETURN
   10 STR=2.*P*H
      RETURN
      END
```

```
      PROGRAM CSPLT1 (INPUT=/150,OUTPUT=/150,TAPE10=0)
C      R LYTZ.   22 APR 78   OSU   CDC CYBER
C
C      EVALUATES AND PLOTS COSINE SERIES.
C      DESIGNED FOR INTERACTIVE USE.
C
C      REQUIRES COMPLOT AND PLIB LIBRARIES.
C
C
      DIMENSION A(20,10), X(500), Y(500)
      DIMENSION PERIOD(10)
      DATA PI2/6.28319/
      W=8.0
      H=8.0
      X1=1.0
      X2=0.5
      Y1=1.0
      Y2=0.5
      NX=10
      NY=10
      X0=0.0
      Y0=0.0
      LX=-1
      LY=-1
      NSX=0
      NSY=0
      ITP=1
      MARK=0
      IPEN=1
      PRINT*, ≠PLOTYPE≠,
      READ*, ICODE
      CALL PLOTYPE (ICODE)
      CALL LAYOUT(W,H,X1,X2,Y1,Y2)
  100 PRINT*, ≠ ≠
      PRINT*, ≠ ≠
  120 PRINT*, ≠NCURVES≠,
      READ*, NCURV
      IF (NCURV .EQ. 0) STOP
      IF (NCURV .GT. 10) GO TO 120
  130 PRINT*, ≠XLO≠,
      READ*, XLO
      PRINT*, ≠XHI≠,
      READ*, XHI
      IF (XHI .LE. XLO) GO TO 130
  150 PRINT*, ≠NPOINTS≠,
      READ*, NPOINTS
      IF (NPOINTS .GT. 500) GO TO 150
      IF (NPOINTS .LE. 20) GO TO 150
      XINC=(XHI-XLO)/FLOAT(NPOINTS)
      XX=XLO-XINC
      DO 200 J=1,NPOINTS
      XX=XX+XINC
      X(J)=XX
  200 CONTINUE
      DO 300 I=1,NCURV
      PRINT*, ≠ ≠
      PRINT*, ≠-CURVE ≠, I, ≠ -≠
  210 PRINT*,≠    NTERMS≠,
      READ*, NT
      IF (NT .GT. 20) GO TO 210
      IF (NT .LE. 0) GO TO 210
      NT1=NT+1
  220 PRINT*, ≠    PERIOD≠,
```

```
      READ*, PER
      IF (PER. LE. 0.0) GO TO 220
      PERIOD(I)=PER
      PRINT*, *    COEFFICIENTS*
      DO 250 M=1,NT1
      MM=M-1
      PRINT*, *        *, MM,
      READ*, A(M,I)
  250 CONTINUE
  300 CONTINUE
C
C      EVALUATE SERIES
C
      DO 400 I=1,NCURV
      PP=PI2/PERIOD(I)
      DO 320 J=1,NPOINTS
      THETA=PP*X(J)
      Y(J)=COSER(NT, A(1,I), A(2,I), THETA)
  320 CONTINUE
      IF (I .GT. 1) GO TO 340
C
C      FOR FIRST DATA SET, AUTOSCALE
C      AND DRAW AXIS
C
      CALL EXTREME(Y, NPOINTS, YLO, YHI)
      CALL LIMITS(XLO,XHI,NX,YLO,YHI,NY)
      CALL AX(XO, YO, LX, LY, NSX, NSY, ITP)
  340 CONTINUE
      CALL GRAPH(X, Y, NPOINTS, MARK, IPEN)
  400 CONTINUE
      CALL PLOTEND
      GO TO 100
      END
```

```
      PROGRAM PDATA (INPUT=/150,OUTPUT=/150,TAPE10=0)
C
C      R. LYTZ   23 APR 78   OSL   CDC CYBER
C
C      INTERACTIVE PROGRAM TO PLOT UP TO 5 SETS OF
C      DATA SUPPLIED AT TERMINAL.
C
      DIMENSION X(50,5), Y(50,5)
      DIMENSION NP (10), MK(10), MD(10)
      DIMENSION LABX(10), LABY(10), LABT(10)
      DATA LABX, LABY, LABT/30*10H           /
      DATA LBLANK/10H          /
   10 FORMAT (10A10)
C
C      SET UP DEFAULTS
C
      INPUT=5LINPUT
      NPMAX=50
      NSMAX=5
      W=11.0
      H=8.5
      CSL=0.4
      NLX=NLY=NLT=0
      XLO=XHI=YLO=YHI=0.0
      NX=NY=10
      LINTX=LINTY=-1
      X0=Y0=0.0
      MMK=17
      MMD=-1
      ITYPE=1
      NSX=NSY=0
      IAX=1
C
C      INPUT DATA
C
  100 CONTINUE
      DO 110 J=1,10
  110 LABX(J)=LABY(J)=LABT(J)=LBLANK
      PRINT*, *-SIZE INFO-*
      PRINT*, *  WIDTH*,
      READ*, W
      PRINT*, *  HEIGHT*,
      READ*, H
      PRINT*, *  LABEL SIZE*,
      READ*, CSL
C
      PRINT*, *-LABEL INFO-*
      PRINT*, *  X-AXIS*
      PRINT*, *    N CHAR*,
      READ*, NLX
      IF(NLX.LE.0) GO TO 160
      PRINT*, *    LABEL* ,
      READ 10, LABX
      IF (EOF(INPUT).NE.0.0) CONTINUE
  160 CONTINUE
      PRINT*, *  Y-AXIS*
      PRINT*, *    N CHAR*,
      READ*, NLY
      IF(NLY.LE.0) GO TO 170
      PRINT*, *    LABEL*,
      READ 10, LABY
      IF (EOF(INPUT).NE.0.0) CONTINUE
  170 CONTINUE
```

```
      PRINT*, ≠  HEADING≠
      PRINT*, ≠    NCHAR≠,
      READ* , NLT
      IF(NLT.LE.0) GO TO 180
      PRINT*, ≠    LABEL≠,
      READ 10, LABT
      IF (EOF(INPUT).NE.0.0) CONTINUE
C
  180 CONTINUE
      PRINT*, ≠-AXIS INFO-≠
  200 PRINT* , ≠  XLO,XHI≠,
      READ*, XLO,XHI
      IF (XLO .GE. XHI) GO TO 200
  210 PRINT*, ≠  YLO,YHI≠,
      READ* , YLO,YHI
      IF (YLO .GE. YHI) GO TO 210
      PRINT*, ≠  NX,NY≠,
      READ*, NX,NY
      PRINT*, ≠  XO,YO≠,
      READ*, XO,YO
      PRINT*, ≠  LINTX,LINTY≠,
      READ*, LINTX,LINTY
C
      NS=0
      PRINT*, ≠-DATA INFO-≠
      DO 300 I=1,NSMAX
      PRINT*, ≠  SET ≠,I
  240 PRINT*, ≠    N POINTS≠,
      READ*, NPOINTS
      IF (NPOINTS .GT. NPMAX) GO TO 240
      IF (NPOINTS .LE. 0) GO TO 320
      NS=NS+1
      NP(I)=NPOINTS
      PRINT*, ≠    MARK≠,
      READ*, MMK
      MK(I)=MMK
      PRINT*, ≠    MODE≠,
      READ*, MMO
      MO(I)=MMO
      DO 260 J=1,NPOINTS
      PRINT*, ≠    ≠, J, ≠  X, Y ≠,
      READ*, X(J,I), Y(J,I)
  260 CONTINUE
  300 CONTINUE
  320 CONTINUE
      PRINT*, ≠PLOTYPE≠,
      READ*, ITYPE
C
C      DO CALLS FOR LAYOUT
C
      CALL PLOTYPE(ITYPE)
      Y1=2.5*CSL + 0.07*H
*H
      Y2=2.5*CSL
      WIDNUM=0.3*(H-Y1-Y2)
      X1=2.0*CSL+WIDNUM
      X2=2.0*CSL
      CALL LAYOUT(W,H,X1,X2,Y1,Y2)
      CALL LIMITS(XLO,XHI,NX,YLO,YHI,NY)
      CALL AX (XO,YO,LINTX,LINTY,NSX,NSY,IAX)
C
C      DO CALLS FOR LABELS
C
```

```
      XLX=0.5*(W+X1-X2-CSL*NLX)
      YLX=CSL
      XLY=2.*CSL
      YLY=0.5*(H+Y1-Y2-CSL*NLY)
      XLT=0.5*(W+X1-X2-CSL*NLT)
      YLT=H-2.0*CSL
      IF (NLX .LE. 0) GO TO 340
      CALL LABEL (XLX,YLX,0.0,CSL,NLX,LABX)
  340 IF (NLY .LE. 0) GO TO 350
      CALL LABEL(XLY,YLY,90.0,CSL,NLY,LABY)
  350 IF (NLT .LE. 0) GO TO 360
      CALL LABEL (XLT,YLT,0.0,CSL,NLT,LABT)
  360 CONTINUE
C
C      PLOT DATA
C
      DO 400 I=1,NS
      CALL MODE(MD(I))
      CALL LINE (X(1,I), Y(1,I), NK(I), NP(I))
  400 CONTINUE
      CALL PLOTEND
      IF (ITYPE.NE.1) ENDFILE 10
      PRINT*, ' MORE',
      READ*, MORE
      IF (MORE.GT. 0) GO TO 100
      STOP
      END
```

```
C
C
C     LIBRARY PLIB
C
C     SUBROUTINES WHICH INTERFACE FORTRAN PROGRAMS
C     WITH CYBER COMPLOT.
C
C
C
      SUBROUTINE LAYOUT(WIDTH,HEIGHT,X1,X2,Y1,Y2)
C
C      R LYTZ   21 JAN 78   OSU   CDC CYBER
C
C      ARGUMENTS NOT ALTERED.
C      FIRST OF GENERAL PLOT SUBS FOR USE WITH COMPLOT.
C      WIDTH,HEIGHT    SIZE(INCHES) OF BOX AROUND GRAPH.
C      X1,X2,Y1,Y2     DISTANCE (INCHES) BETWEEN
C                      AXIS ENDS AND BOX SIDES.
C
C      COMMON /PLC/    CONTENTS:
C      XSC,YSC      ARGUMENTS FOR SIZE
C      XBC,YBC      BIAS ARGUMENTS FOR SCALE
C      XFC,YFC      FACTOR ARGUMENTS FOR SCALE (INCH/USER UNITS)
C      XAC,YAC      LENGTH OF AXES (INCH)
C      X1C,X2C      =X1,X2
C      Y1C,Y2C      Y1,Y2
C      XLC,XHC      AXIS EXTREMES (USER)
C      YLC,YHC      --
C      BBC,BTC      BOX COORDINATES (USER) BOTTOM AND TOP
C      BLC,BRC      SAME, LEFT AND RIGHT
C      XTC,YTC      DISTANCE (USER) BETWEEN LARGE TICS
C
       COMMON/PLC/ XSC,YSC,XBC,YBC,XFC,YFC,
     1 XAC,YAC,X1C,Y1C,X2C,Y2C,XLC,YLC,
     2 XHC,YHC,BBC,BTC,BLC,BRC,XTC,YTC
       XFC=YFC=1.0
       XLC=YLC=-10.0
       XHC=YHC=10.0
       EDGE=1.0
       EDGE2=2.0
       XSC=WIDTH+EDGE2
       YSC=HEIGHT + EDGE2
       XBC=X1+EDGE
       YBC=Y1+EDGE
       XAC=WIDTH-X1-X2
       YAC=HEIGHT-Y1-Y2
       X1C=X1
       X2C=X2
       Y1C=Y1
       Y2C=Y2
       IF (XAC .LT. 0.0) GO TO 200
       IF (YAC .LT. 0.0) GO TO 200
       CALL SIZE(XSC,YSC)
       RETURN
  200  PRINT 205
  205  FORMAT(* ERROR IN LAYOUT*)
       STOP *ERROR IN LAYOUT*
       END
       SUBROUTINE LIMITS(XL,XH,NX,YL,YH,NY)
C
C      R LYTZ   21 JAN 78   OSU   CDC CYBER
C
C      PLOT SUB FOR USE WITH COMPLOT
```

```
C       LAYOUT MUST BE CALLED BEFORE RANGE
C       SEE COMMENTS IN LAYOUT FOR DEFINITION OF COMMON/PLOT/
C       ARGUMENTS NOT ALTERED
C
C       XL,XH     (APPROXIMATE) AXIS EXTREMES
C       YL,YH
C       NX,NY     (APPROXIMATE) NUMBER OF TIC DIVISIONS
C                 ON AXES.  IF .GE. 0, AXIS IS AUTOSCALED.
C                 IF .LT. 0, AXIS NOT AUTOSCALED.
C
      COMMON/PLOT/ XSC,YSC,XBC,YBC,XFC,YFC,
     1 XAC,YAC,X1C,Y1C,X2C,Y2C,XLC,YLC,
     2 XHC,YHC,LBC,BTC,BLC,BRC,XTC,YTC
      IF(XL.GE.XH) STOP *XL.GE.XH  IN RANGE*
      IF(YL.GE.YH) STOP *YL.GE.YH IN RANGE*
      NXX=NX
      NYY=NY
      IF (NXX) 100,110,120
  100 NXX=-NXX
      XLC=XL
      XHC=XH
      XTC=(XH-XL)/NXX
      GO TO 125
  110 NXX=1
  120 CALL RANGE (XL,XH,NXX,XLC,XHC,XTC)
  125 CONTINUE
      IF (NYY) 130,140,150
  130 NYY=-NYY
      YLC=YL
      YHC=YH
      YTC=(YH-YL)/NYY
      GO TO 155
  140 NYY=1
  150 CALL RANGE (YL,YH,NYY,YLC,YHC,YTC)
  155 CONTINUE
C
C      COMPUTE FACTORS  (INCH/USER UNIT)
C
      XFC=XAC/(XHC-XLC)
      YFC=YAC/(YHC-YLC)
      CALL SCALE(XFC,YFC,XBC,YBC,XLC,YLC)
C
C      COMPUTE BOX COORDINATES (USER UNITS)
C
      BLC=XLC-X1C/XFC
      BRC=XHC+X2C/XFC
      BBC=YLC-Y1C/YFC
      BTC=YHC+Y2C/YFC
      CALL WINDOW (BLC,BBC,BRC,BTC)
      RETURN
      END
      SUBROUTINE AX(X0,Y0,LX,LY,NSX,NSY,ITP)
C
C      R LYTZ   21 JAN 78   OSU   CDC CYBER
C
C      NO ARGUMENTS CHANGED.
C      DRAWS BOX AND/OR AXIS.
C      LAYOUT AND RANGE MUST BE CALLED FIRST
C
C      ITP NEGATIVE:  AXIS WITHOUT BOX
C      ITP ZERO    :  BOX ONLY
C      ITP POSITIVE:  AXIS WITH BOX
C
```

```
C       ABS(ITP)=1    STANDARD X AND Y
C                2    STANDARD X, LOG Y
C                3    STANDARD Y, LOG X
C                4    LOG X AND Y
C
C       LX,LY    LABEL INTERVAL
C       X0,Y0    AXIS INTERSECTION
C       NSX,NSY    NUMBER OF SMALL TICS BETWEEN LARGE TICS
C
        COMMON/PLO/ XSC,YSC,XBC,YBC,XFC,YFC,
     1 XAC,YAC,X1C,Y1C,X2C,Y2C,XLC,YLC,
     2 XHC,YHC,BBC,BTC,BLC,BRC,XTC,YTC
        CALL ERASE
        IT=ITP
        IF (IABS(IT).GT.4) IT=1
        IF (IT .LT. 0) GO TO 200
C
C       DRAW BOX
C
        CALL VECTORS
        CALL PLOT(BLC,BBC,0,0)
        CALL PLOT(BLC,BTC,1,0)
        CALL PLOT(BRC,BTC,1,0)
        CALL PLOT(BRC,BBC,1,0)
        CALL PLOT(BLC,BBC,1,0)
        IF (IT .EQ. 0) GO TO 300
C
C       DRAW AXIS
C
  200 IT=IABS(IT)-1
        CS=0.03*YAC
        CALL AXISL(XLC,XHC,X0,YLC,YHC,Y0,XTC,YTC,
     *    NSX,NSY,LX,LY,1.0,1.0,CS,IT)
  300 CONTINUE
        RETURN
        END
        SUBROUTINE EXTREME(Z,N,ZL,ZH)
C
C       R LYTZ   28 JAN 78.   OSL.   CDC CYBER.
C
C       Z,N NOT CHANGED.
C       RETURNS MIN AND MAX VALUES (ZL,ZH)
C       IN ARRAY Z OF N ELEMENTS.
C
        DIMENSION Z(1)
        ZL=1.0E300
        ZH=-ZL
        DO 100 I=1,N
        ZZ=Z(I)
        IF (ZZ .GT. ZH) ZH=ZZ
        IF (ZZ .LT. ZL) ZL=ZZ
  100 CONTINUE
        RETURN
        END
        SUBROUTINE GRAPH(X,Y,N,MARK,I)
        DIMENSION X(1),Y(1)
         COMMON/PLO/ XSC,YSC,XBC,YBC,XFC,YFC,
       1 XAC,YAC,X1C,Y1C,X2C,Y2C,XLC,YLC,
       2 XHC,YHC,BBC,BTC,BLC,BRC,XTC,YTC
        CALL WINDOW(XLC,YLC,XHC,YHC)
        IF (I.EQ.0) GO TO 10
        CALL VECTORS
        GO TO 20
```

```
   10   CALL POINTS
   20   CONTINUE
        CALL PLOT (X(1),Y(1),0,3)
        DO 300 J=1,N
        CALL PLOT(X(J),Y(J),1,MARK)
  300   CONTINUE
        CALL WINDOW(BLC,BBC,BRC,BTC)
        RETURN
        END
        FUNCTION COSER(N,B0,B,THETA)
C
C       R LYTZ.  15APR79.  OSU.  CDC CYBER.
C
C       COSER=B0 + SUM(K=1,N) B(K)*COS(K*THETA)
C
C       USES FAST ITERATIVE METHOD
C
        DIMENSION B(1)
        C=COS(THETA)
        C2=2.0*C
        U=V=0.0
        I=N
        DO 100 J=1,N
        T=C2*U - V + B(I)
        V=U
        U=T
        I=I-1
   100  CONTINUE
        T=C2*U - V + B0
        COSER= T - U*C
        RETURN
        END
        SUBROUTINE LABEL(X,Y,DEG,HEIGHT,NCHAR,LABELS)
C
C       R LYTZ.  20APR78.  OSU.  CDC CYBER.
C       ARGUMENTS NOT ALTERED
C
C       ARGUMENTS SAME AS FOR SYMBOL IN COMPLOT,
C       EXCEPT X,Y ARE IN INCHES FROM LOWER LEFT CORNER OF BOX
C
C       HEIGHT=0.0 DEFAULTS TO HEIGHT=0.02*YAC
C
        DIMENSION LABELS(1)
         COMMON/PLC/ XSC,YSC,XBC,YBC,XFC,YFC,
       1 XAC,YAC,X1C,Y1C,X2C,Y2C,XLC,YLC,
       2 XHC,YHC,BBC,BTC,BLC,BRC,XTC,YTC
         XX=XLC+(X-X1C)/XFC
         YY=YLC+(Y-Y1C)/YFC
         H=HEIGHT
         IF (H.EQ.0.0) H=YAC*0.02
         CALL SYMBOL(XX,YY,DEG,H,NCHAR,LABELS)
         RETURN
         END
         SUBROUTINE MODE(M)
C
C        R LYTZ   23 APR 78   OSU   CDC CYBER
C
C        SETS PLOT MODE.
C        M .LT. 0   POINTS
C        M .EQ. 0   VECTORS
C        M .GT. 0   DASHES
C
         IF(M) 100,200,300
```

```
100 CALL POINTS
    RETURN
200 CALL VECTORS
    RETURN
300 CALL DASHES
    RETURN
    END
```

```
      PROGRAM MCAIK
C*************************************************************
C
C     ROBERT LYTZ
C     OREGON STATE UNIVERSITY OS3 SYSTEM
C     15 DECEMBER 1976
C
C     PROGRAM PLOTS 500 DATA POINTS FROM FILE.
C     TTY EXECUTION, USING CONMODE.
C
C     DATA INPUT---
C     CARD 1          LEGEND  (15A4)
C     CARD 2          IGNORED
C     CARD 3          IGNORED
C     CARD 4-104      500 DATA POINTS  (6X,5(1X,I10))
C
C     HOLLERITH OR COSY DATA ACCEPTED FROM  LUN OR SAVED
C     FILE,  CONTAINING ONE 500-POINT DATA SET.  SAVED FILE
C     INTERNALLY EQUIPPED TO LUN 49.  ALL DATA FILES REWOUND
C     DURING EXECUTION AND BEFORE READING.
C
C     AUTOSCALE IS OPTIONAL DURING EXECUTION.
C
C     SEVERAL PLOTS MAY BE DONE DURING ONE EXECUTION,
C     BUT ONLY IF EACH DATA SET IS ON A SEPARATE FILE.
C
C     COMPLOT SUBPROGRAMS AND CONMODE TTY I/O
C     SUBPROGRAMS ARE USED.  THESE RESIDE ON
C     THE *ARANO LIBRARY.
C
C     ***  TO EXECUTE  ***
C     LOAD,OBJECTDECK.LIB=*ARANO
C     RUN
C*************************************************************
      DIMENSION M1(5),M2(5),M3(5),M4(5),M5(5),M6(5),M7(5)
      DIMENSION IY(500), LABEL(7), LEGEND(15), NAME(3), NUMB(6)
      DIMENSION M8(5),M9(5)
      EQUIVALENCE (LABEL(4),NAME(1))
      DATA  (NUMB=24H100 200 300 400 500 600     )
      DATA (FIL =8H                )
      DATA (LABEL=29H SAVE FOR                      )
      DATA (M2 =*DATA ON SAVED FILE^$*)
      DATA (M3 =*LUN =              $*)
      DATA (M4 =*FILE NAME =        $*)
      DATA (M5 =*AUTOSCALE^         $*)
      DATA (M6 =*ORDINATE MAX =     $*)
      DATA (M7 =*MORE PLOTS^        $*)
      DATA (M8 =*MARK=              $*)
      DATA (M9 =*MODE=              $*)
      CALL TK4010
      CALL PLOTTYPE(1)
100   CONTINUE
      WRITE (61,110)
110   FORMAT(*-*)
C
      MARK=DECINA(M8)
      MODE=DECINA(M9)
      IF (INQUIREA(M2)) GOTO 200
C
C     READ MCA DATA FROM LUN TO IY
C
      LUN = DECINA(M3)
      REWIND LUN
      READ (LUN,120) LEGEND
120   FORMAT (15A4,///)
      READ (LUN,150) (IY(J),J=1,500)
150   FORMAT (6X, 5(1X,I10))
      GOTO 300
200   CONTINUE
C
C     READ MCA DATA FROM SAVED FILE TO IY
C
      KK = INCHARA(FIL,M4)
      CALL UNEQUIP(49)
      CALL EQUIP (49,FIL)
      REWIND 49
      READ (49,120) LEGEND
      READ (49,150) (IY(J),J=1,500)
300   CONTINUE
```

```
      WRITE (61,320) LEGEND
320   FORMAT (5X,15A4)
C
C  AUROSCALE^
C
      IF (INQUIREA(M5)) GOTO 400
C
C  AUTOSCALE NOT SELECTED. READ YHI.
C
      YHI = DECINA(M6)
      CHAR = 0.0
      GOTO 500
400   CONTINUE
C
C  AUTOSCALE SELECTED. CALCULATE YHI.
C
      IYHI = IY(1)
      DO 420 J=2,500
      II = IY(J)
      IF (II . GT. IYHI) IYHI = II
420   CONTINUE
      YHI = IYHI
      YLOG = ALOG10(YHI)
      ILOG = YLOG
      DIG = YLOG - ILOG
      DIG = 10.**DIG
      IG = DIG
      CHAR = 10.**ILOG
      YHI = FLOAT(IG + 1)*CHAR
      WRITE (61,450) IYHI,YHI
450   FORMAT (' HI DATA =',I6, '    AUTOSCALE =', E8.1)
500   CONTINUE
C
C  DETERMINE FACT (= INCHES/GRAPH UNITS)
C  AND PLOT AXIS
C
      CALL PLOTENO
      CALL SIZE (11.5,9.0)
      YFACT = 7.75/YHI
      XFACT = 10./500.
      CALL SCALE (XFACT,YFACT,1.,1.,0.,0.)
      CALL AXIS (0.,500.,0.,0.,YHI,0.,100.,CHAR,4,0)
C
C  PLOT MCA DATA
C
      CALL VECTORS
      IF (MODE.EQ.0) CALL POINTS
      DO 600 I=1,500
      X = I
      Y = IY(I)
      CALL PLOT (X,Y,1,MARK)
600   CONTINUE
C
C  LABEL X AXIS TICS
C
      Y = -0.35/YFACT
      DO 650 I=1,5
      X = 100*I - 8.
      CALL SYMBOL (X,Y,0.,0.16,4,NUMB(I),
650   CONTINUE
C
C  LABEL Y AXIS TIC
C
      ENCODE (8,655,TIKY) YHI
655   FORMAT (E8.1)
      X = -3/XFACT
      CALL SYMBOL (X,YHI,0.,0.16,8,TIKY)
C
C  WRITE LEGEND
C
      Y = -.8/YFACT
      X = 0.
      CALL SYMBOL (X,Y,0.,0.16,60,LEGEND)
      CALL PLOTENO
C
C  MORE PLOTS^
C
      IF (INQUIREA(M7)) GOTO 100
      CALL EXIT
      END
```

```
      PROGRAM REFORM
C
C     PROGRAM REFRMATS DATA OF INOTECH 500 CHANNEL DUMP
C        FROM SAVED FILE FNAME
C            (9A8)
C            3 NULL LINES
C            (6X,5(4X,I7)) X 100
C
C        TO LUNOUT FOR USE BY CYBER PROGRAMS
C            (9A8)
C            (10I7) X 50
C     FNAME SHOULD CONTAIN PAPERTAPE OUTPUT FROM *TCOPY,
C     WITH QUESTION MARKS EDITED OUT USING SAR,,/^/,//.
C
      LUNOUT IS INTERNALLY EQUIPPED TO 10, 11, 12, .. .
      DIMENSION HEAD(9), KOUNT(10)
      DATA (BLANK=8H              )
   10 FORMAT (9A8,///)
   12 FORMAT (9A8)
   14 FORMAT (6X,5(4X,I7),/,6X,5(4X,I7))
   16 FORMAT (10I7)
   18 FORMAT (* INPUT FILENAME*)
   20 FORMAT (* *, A8, * LUN *, I2, *--*, 4A8)
      LUNOUT =9
      LUNIN = 9
  100 CONTINUE
      LUNOUT=LUNOUT+1
      WRITE (61,18)
      READ (60,12) FNAME
      IF (FNAME.EQ.BLANK) STOP
      CALL UNEQUIP (LUNIN)
      CALL UNEQUIP (LUNOUT)
      CALL EQUIP (LUNIN,FNAME)
      CALL EQUIP (LUNOUT,3HFILE          )
      READ (LUNIN,10) HEAD
      WRITE (LUNOUT,12) HEAD
      WRITE (61,20) FNAME,LUNOUT,(HEAD(J),J=1,4)
      J1=1
      J2=10
      DO 200 I=1,50
      READ (LUNIN,14) (KOUNT(J),J=J1,J2)
      WRITE (LUNOUT,16) (KOUNT(J),J=J1,J2)
  200 CONTINUE
      GO TO 100
      END
```

```
      PROGRAM CALIB
C     PROGRAM TO ANALYZE AND PLOT DETECTOR
C     CALIBRATION DATA.
C
C     THESE FILES MUST BE EQUIPPED BEFORE EXECUTION:
C        10=PLOT
C        45=LP
C        15=FIRST DATA FILE
C        16=SECOND DATA FILE
C        ... ETC.
C
C     TO EXECUTE:
C        LOAD,CALBIN,L=PLTLIB
C        RUN
C
C
C     HEAD          DATA FILE ID (16A4)
C     XF,XL         FIRST AND LAST CALIBRATION POSITIONS
C     XD            POSITION INCREMENT
C     POINTS=NP     NUMBER OF CALIBRATION POINTS
C     C(I)          CHANNEL CENTROID OF PEAK I
C     X(I)          POSITION (MM) OF PEAK I
C     Y(I)          INTEGRAL OF PEAK I
C     CPM(I)        CHANNELS/MM AT PEAK I
C     Z(J)          COUNT OF CHANNEL J IN CALIBRATION SUM
C
      INTEGER HEAD(16)
      DIMENSION C(500), X(500), Y(500), CPM(500)
      DIMENSION Z(500),CHAN(500),CM(2),FWHM(100)
      DIMENSION LA81(3),LA82(3),LA83(3),LA84(3),LA85(3),LA86(3)
      DIMENSION NAME(4),YN(500)
      DATA (LA81=12HCHANNEL                    )
      DATA (LA82=12HPOSITION(MM)               )
      DATA (LA83=12HINTEGRAL                   )
      DATA (LA84=12HCHANNELS/MM                )
      DATA (LA85=12HCOUNTS                     )
      DATA (LA86=12HFWHM(MM)                   )
   10 FORMAT(* HOW MANY DATA SETS*  *)
   11 FORMAT(* PLOTS* 1.0=YES,  0.0=NO.   *)
   13 FORMAT(* PLOT WIDTH:   *)
   14 FORMAT(* PLOT HEIGHT:   *)
   19 FORMAT (F5.0)
   20 FORMAT(16A4)
   22 FORMAT(4(F5.0,/) /)
   24 FORMAT(/,3X,F7.2,17X,F9.0,/)
   26 FORMAT(*1*,16A4,/)
   30 FORMAT (//)
   29 FORMAT(1X,2F10.2,F10.0,2F10.3)
   32 FORMAT (6X,3F11.0)
   34 FORMAT(*0  POSITION  CENTROID  INTEGRAL      YCPM  *,
     1     *CHANNELS*,6X,*FWHM* / 7X,*(MM)    CHANNEL*,
     2     5X,*COUNT      COUNT     PER MM       (MM)*  )
   36 FORMAT(1X,2F10.2,F10.0,3F10.3)
   40 FORMAT(*0MEAN*,16X,F10.0,3F10.3)
   42 FORMAT(* STANDARD DEV*,8X,F10.0,3F10.3)
   44 FORMAT(* RELATIVE DEV*,8X,4F10.2)
   46 FORMAT(* CENTER/END*,30X,F10.3)
      DO 100 J=1,500
      CHAN(J)=FLOAT(J)
  100 CONTINUE
      WRITE (61,10)
      READ(60,18) SETS
      WRITE (61,11)
      READ (60,19) PLT
      NSETS=IFIX(SETS)
      IPLT=IFIX(PLT)
      IF(IPLT.NE.0) GO TO 105
      GO TO 110
  105 CONTINUE
      WRITE (61,13)
      READ (60,18) A8IN
      WRITE (61,14)
```

```
      READ (60,18) ORIN
      CALL SYMBOL(0.,0.,0.,0.,0.,16,NAME)
  110 CONTINUE
      LUN=14
C     LUN IS DATA INPUT.
      DO 350 NN=1,NSETS
      LUN=LUN+1
      I2=I500=1
C     I2        FLAG FOR (XO.GE.2.0)
C     I500      FLAG FOR FULL 500 CHANNEL INPUT
C     IBOTH     (I2) AND (I500)
      READ (LUN,20) HEAD
      READ(LUN,22) XF,XL,XO,POINTS
      IF (XO.LT.2.0) I2=0
      NP=IFIX(POINTS)
      NP1=NP-1
      NP2=NP-2
      NPO=NP/2
      NPT=NPO*2
      XO2=XO*2.0
      DO 120 I=1,3
      READ(LUN,24) C(I), Y(I)
  120 CONTINUE
      CA=C(1)
      CB=C(2)
      CC=C(3)
      CPM(1)=0.0
      CPM(NP)=0.0
      CPM(2)=(CC-CA)/XO2
      DO 140 I=4,NP
      READ (LUN,24) C(I), Y(I)
      CA=CB
      CB=CC
      CC=C(I)
      CPM(I-1) = (CC-CA)/XO2
  140 CONTINUE
      READ (LUN,30)
      IF (EOF(LUN)) I500=0
      IBOTH=I2*I500
      IF (I500.EQ.0) GO TO 150
      READ (LUN,32) (Z(J),J=1,500)
  150 CONTINUE
      X(1)=XF
      XX=XF
      DO 160 I=2,NP
      XX=XX+XO
      X(I)=XX
  160 CONTINUE
      CALL MEAN(Y,NP,Y1,Y2,Y3)
      DO 165 I=1,NP
      YN(I)=Y(I)/Y1
  165 CONTINUE
      CALL MEAN(YN,NP,YN1,YN2,YN3)
      CALL MEAN(CPM(2),NP2,CPM1,CPM2,CPM3)
      DENOM=CPM(2) + CPM(NP2)
      IF (NPT.EQ.NP) 170,180
  170 CE=(CPM(NPO)+CPM(NPO+1))/DENOM
      GO TO 190
  180 CE=2.0*CPM(NPO+1)/DENOM
  190 CONTINUE
      WRITE(45,25) (HEAD(I), I=1,16)
      IF (IBOTH.EQ.1) GO TO 200
      WRITE (45,35)
      WRITE(45,28) X(1), C(1), Y(1),YN(1)
      WRITE(45,28) (X(I),C(I),Y(I),YN(I),CPM(I), I=2,NP1)
      WRITE(45,28) X(NP), C(NP), Y(NP),YN(NP)
      WRITE(45,40) Y1,YN1,CPM1
      WRITE(45,42) Y2,YN2,CPM2
      WRITE(45,44) Y3,YN3,CPM3
      WRITE(45,46) CE
  200 CONTINUE
      IF (IBOTH.EQ.0) GO TO 270
C
CC    FIND FWHM OF PEAKS Z(I) CORRESPONDING TO CENTROIDS
C
      DO 260 I=2,NP1
C     FIND PEAK VALUE
      JCENT=IFIX(C(I))
      PMAX=Z(JCENT)
      JA=JCENT-2
      JB=JCENT+2
      DO 205 J=JA,JB
      IF (Z(J).GT.PMAX) GO TO 203
      GO TO 205
```

```
  203 JCENT=J
      PMAX=Z(J)
  205 CONTINUE
      HMAX=0.5*PMAX
C
C     FIND CHANNELS FOR HALF MAX--CH(M)
C     M=1   BELOW CENTROID
C     M=2   ABOVE CENTROID
C
      DO 230 M=1,2
      JINC=(-1)**M
      J1=JCENT
      J2=J1+JINC
      Z1=Z(J1)
      Z2=Z(J2)
      DO 210 JJ=1,12
      IF (Z2.LE.HMAX) GO TO 220
      J1=J2
      J2=J2+JINC
      Z1=Z2
      Z2=Z(J2)
  210 CONTINUE

  220 FJ2=FLOAT(J2)
      FJ1=FLOAT(J1)
      CH(M)=TERP(Z2,HMAX,Z1,FJ2,FJ1)
  230 CONTINUE
      FWHM(I)=(CH(2)-CH(1))/CPM(I)
  260 CONTINUE
      CALL MEAN(FWHM(2),NP2,FWHM1,FWHM2,FWHM3)
      WRITE (45,34)
      WRITE(45,36) X(1),C(1),Y(1),YN(1)
      WRITE(45,36) (X(I),C(I),Y(I),YN(I),CPM(I),FWHM(I), I=2,NP1)
      WRITE(45,36) X(NP),C(NP),Y(NP),YN(NP)
      WRITE(45,40) Y1,YN1,CPM1,FWHM1
      WRITE(45,42) Y2,YN2,CPM2,FWHM2
      WRITE(45,44) Y3,YN3,CPM3,FWHM3
      WRITE(45,46) CZ
  270 CONTINUE
      IF (IPLT.EQ.0) GO TO 350
C
C     DO PLOTS
C
      CSIZ=0.0
      IF (ABIN.LE.0.0) ABIN=11.0
      IF (ORIN.LE.0.0) ORIN=8.5
      ABLO=ORLO=0.0
      ABHI=600.0
      ABT=50.0
      LABT=0
      LINTAB=2
      LORT=0
      LINTOR=-1
      MARK=4
      ICODE=0
C
C     PLOT X VS C
C
      CALL AUTO(XL,1,ZAP,ORHI,ORT)
      CALL SETUP(ABIN,ORIN,ABLO,ABHI,ORLO,ORHI)
      CALL NEWAX(ABT,LABT,LINTAB,ORT,LORT,LINTOR)
      CALL GRAPH(C,X,NP,MARK,ICODE)
      CALL GLABEL(HEAD,LAB1,LAB2,CSIZ)
C
C     PLOT Y VS C
C
      CALL AUTO(Y,NP,ZAP,ORHI,ORT)
      CALL SETUP(ABIN,ORIN,ABLO,ABHI,ORLO,ORHI)
      CALL NEWAX(ABT,LABT,LINTAB,ORT,LORT,LINTOR)
      CALL GRAPH(C,Y,NP,MARK,ICODE)
      CALL GLABEL(HEAD,LAB1,LAB3,CSIZ)
C
C     PLOT CPM VS C
C
      CALL AUTO(CPM(2),NP2,ZAP,ORHI,ORT)
      CALL SETUP(ABIN,ORIN,ABLO,ABHI,ORLO,ORHI)
      CALL NEWAX(ABT,LABT,LINTAB,ORT,LORT,LINTOR)
      CALL GRAPH(C,CPM(2),NP2,MARK,ICODE)
      CALL GLABEL(HEAD,LAB1,LAB4,CSIZ)
C
C     PLOT Z VS CHANNEL
C
      IF (ISOO.EQ.0) GO TO 320
      MARK=17
```

```
      ICODE=1
      CALL AUTO(Z,500,ZAP,ORHI,ORT)
      CALL SETUP(ABIN,ORIN,ABLO,ABHI,ORLO,ORHI)
      CALL NEWAX(ABT,LABT,LINTAB,ORT,LORT,LINTOR)
      CALL GRAPH(CHAN,Z,500,MARK,ICODE)
      CALL GLABEL(HEAD,LAB1,LAB5,CSIZ)
C
CCC   PLOT FWHM VS X
C
      IF (IBOTH.EQ.0) GO TO 320
      ORHI=1.0
      ORT=0.2
      LINTAB=1
      LABT=0
      MARK=4
      ICODE=0
      CALL AUTO(XL,1,ZAP,ABHI,ABT)
      CALL SETUP(ABIN,ORIN,ABLO,ABHI,ORLO,ORHI)
      CALL NEWAX(ABT,LABT,LINTAB,ORT,LORT,LINTOR)
      CALL GRAPH(X,FWHM(2),NP2,MARK,ICODE)
      CALL GLABEL(HEAD,LAB2,LAB6,CSIZ)
  320 CONTINUE
      CALL PLOTEND
  350 CONTINUE
      CALL PLOTEND
      STOP
      END
```

```
      PROGRAM MCAPLT
C
C     ROBERT LYTZ
C     OREGON STATE UNIVERSITY OS3 SYSTEM
C     15 DECEMBER 1976
C
C     PROGRAM PLOTS 500 DATA POINTS FROM FILE.
C     TTY EXECUTION, USING CONMODE.
C
C     DATA INPUT---
C     CARD 1          LEGEND  (15A4)
C     CARD 2          IGNORED
C     CARD 3          IGNORED
C     CARD 4-104      500 DATA POINTS  (6X,5(1X,I10))
C
C
C     HOLLERITH OR COSY DATA ACCEPTED FROM  LUN OR SAVED
C     FILE, CONTAINING ONE 500-POINT DATA SET.  SAVED FILE
C     INTERNALLY EQUIPPED TO LUN 49.  ALL DATA FILES REWOUND
C     DURING EXECUTION AND BEFORE READING.
C
C     AUTOSCALE IS OPTIONAL DURING EXECUTION.
C
C     SEVERAL PLOTS MAY BE DONE DURING ONE EXECUTION,
C     BUT ONLY IF EACH DATA SET IS ON A SEPARATE FILE.
C
C     COMPLOT SUBPROGRAMS AND CONMODE TTY I/O
C     SUBPROGRAMS ARE USED.  THESE RESIDE ON
C     THE *ARAND LIBRARY.
C
C
C     ***  TO EXECUTE  ***
C       EQUIP,10=PLOT
C       LABEL,10/YOUR NAME
C       LOAD,OBJECTDECK,LIB=*ARAND
C       RUN
C
C
      DIMENSION M1(5),M2(5),M3(5),M4(5),M5(5),M6(5),M7(5)
      DIMENSION M8(5),M9(5)
      DIMENSION IY(500), LABEL(7), LEGEND(15), NAME(3), NUMB(6)
      EQUIVALENCE (LABEL(4),NAME(1))
      DATA (FIL =8H        )
      DATA (NUMB=24H100 200 300 400 500 600  )
      DATA (LEGEND=15(4H    ))
      DATA (M2 =#DATA ON SAVED FILE^$#)
      DATA (M3 =#LUN =                $#)
      DATA (M4 =#FILE NAME =          $#)
      DATA (M5 =#AUTOSCALE^           $#)
      DATA (M6 =#ORDINATE MAX =       $#)
      DATA (M7 =#MORE PLOTS^          $#)
      DATA (M8 =#MARK=                $#)
      DATA (M9 =#MODE=                $#)
  100 CONTINUE
      WRITE (61,110)
  110 FORMAT(#-#)
      MARK=DECINA(M8)
      MODE=DECINA(M9)
      IF (INQUIRE^(M2)) GOTO 200
C
CC    READ MCA DATA FROM LUN TO IY
C
      LUN = DECINA(M3)
      REWIND LUN
      READ (LUN,120) LEGEND
  120 FORMAT (15A4,///)
      READ (LUN,150) (IY(J),J=1,500)
  150 FORMAT (6X, 5(1X,I10))
      GOTO 300
  200 CONTINUE
C
C     READ MCA DATA FROM SAVED FILE TO IY
C
      KK = INCHARA(FIL,M4)
      CALL UNEQUIP(49)
      CALL EQUIP (49,FIL)
      REWIND 49
      READ (49,120) LEGEND
      READ (49,150) (IY(J),J=1,500)
  300 CONTINUE
      WRITE (61,320) LEGEND
  320 FORMAT (5X,15A4)
C
C     AUROSCALE^
```

```
C
      IF (INQUIREA(M5)) GOTO 400
C
C  AUTOSCALE NOT SELECTED. READ YHI.
C
      YHI = DECINA(M6)
      CHAR = 0.0
      GOTO 500
400   CONTINUE
C
C  AUTOSCALE SELECTED. CALCULATE YHI.
C
      IYHI = IY(1)
      DO 420 J=2,500
      II = IY(J)
      IF (II . GT. IYHI) IYHI = II
420   CONTINUE
      YHI = IYHI
      YLOG = ALOG10(YHI)
      ILOG = YLOG
      DIG = YLOG - ILOG
      DIG = 10.**DIG
      IG = DIG
      CHAR = 10.**ILOG
      YHI = FLOAT(IG + 1)*CHAR
      WRITE (61,450) IYHI,YHI
450   FORMAT (' HI DATA =',I6, '     AUTOSCALE =', E8.1)
500   CONTINUE
C
CC  DETERMINE FACT (= INCHES/GRAPH UNITS)
CC  AND PLOT AXIS
C
      CALL SIZE (12.,12.)
      YFACT = 6./YHI
      XFACT = 10./500.
      CALL SCALE (XFACT,YFACT,1.,4.,0.,0.)
      CALL AXIS (0.,500.,0.,0.,YHI,0.,100.,CHAR,4,0)
C
CC  PLOT MCA DATA
C
      CALL VECTORS
      IF (MODE.EQ.0) CALL POINTS
      DO 600 I=1,500
      X = I
      Y = IY(I)
      CALL PLOT (X,Y,1,MARK)
600   CONTINUE
C
CC  LABEL X AXIS TICS
C
      Y = -0.35/YFACT
      DO 650 I=1,5
      X = 100*I - 8.
      CALL SYMBOL (X,Y,0.,0.16,4,NUMB(I))
650   CONTINUE
C
CC  LABEL Y AXIS TIC
C
      ENCODE (8,655,TIKY) YHI
655   FORMAT (E8.1)
      X = .3/XFACT
      CALL SYMBOL (X,YHI,0.,0.16,8,TIKY)
C
CC  WRITE LEGEND
C
      Y = -.8/YFACT
      X = 0.
      CALL SYMBOL (X,Y,0.,0.16,60,LEGEND)
C
CC  PUT BOX AROUND GRAPH
C
      Y = -2./YFACT
      X = -.5/XFACT
      CALL PLOT (X,Y,3,0)
      X = 10.5/XFACT
      CALL PLOT (X,Y,1,0)
      Y = 6.5/YFACT
      CALL PLOT (X,Y,1,0)
      X = -.5/XFACT
      CALL PLOT (X,Y,1,0)
      Y = -2./YFACT
      CALL PLOT (X,Y,1,0)
      CALL PLOTEND
C
CC  MORE PLOTS^
C
      IF (INQUIREA(M7)) GOTO 100
      CALL EXIT
      END
```

```
C     LIBRARY PLTLIB
CCCCC CONTENTS:
CCCCCCC   GRAPH
CCCCCCC   QLABEL
CCCCCCC   LABEL
CCCCCCC   NEWAX
CCCCCCC   SETUP
CCCCCCC   TECP
CCCCCCC   AUTO
CCCCCCC   MEAN
C
      SUBROUTINE GRAPH(X,Y,N,MARK,I)
      COMMON/CCC/XIN,YIN,XLO,XHI,YLO,YHI,BL,BR,BB,BT,XS,YS,XF,YF,CS
      DIMENSION X(1),Y(1)
      CALL WINDOW(XLO,YLO,XHI,YHI)
      IF (I.EQ.0) GO TO 10
      CALL VECTORS
      GO TO 20
   10 CALL POINTS
   20 CONTINUE
      CALL PLOT (X(1),Y(1),3,3)
      DO 300 J=1,N
      CALL PLOT(X(J),Y(J),1,MARK)
  300 CONTINUE
      CALL SIZE(XS,YS)
      RETURN
      END
C
CC
      SUBROUTINE QLABEL(LEGEND,LABX,LABY,CSIZ)
      DIMENSION LEGEND(1),LABX(1),LABY(1)
      JPOS=7
      CALL LABEL(JPOS,CSIZ,12,LEGEND)
      JPOS=3
      CALL LABEL(JPOS,CSIZ,12,LABX)
      JPOS=15
      CALL LABEL(JPOS,CSIZ,12,LABY)
      RETURN
      END
C
CC
      SUBROUTINE LABEL(I,CSIZ,NCHAR,TEXT)
      COMMON /CCC/ XIN,YIN,XLO,XHI,YLO,YHI,BL,BR,BB,BT,XS,YS,XF,YF,CS
      INTEGER TEXT(1)
      IF (I.LT.1) RETURN
      IF (I.GT.16) RETURN
      CZZ=CSIZ
      IF (CZZ.EQ.0.0) CZZ = CS
      CSY=CZZ/YF
      CSY2=2.*CSY
      CSY3=3.*CSY
      CSY4=4.*CSY
      CSX=CZZ/XF
      CSX2=2.*CSX
      CSX3=3.*CSX
      CSX4=4.*CSX
C
CC    DETERMINE WHERE LABEL IS PUT, ACCORDING TO ARGUMENT I
C
      GO TO (1,2,3,4,5,6,7,8,9,10,11,12,13,14,15,16)  I
    1 X=XLO
      Y=YLO-CSY3
      GO TO 200
    2 X=XLO
      Y=-CSY3
      GO TO 200
    3 X=CSX4
      Y=-CSY3
      GO TO 200
    4 X=XLO
      Y=CSY
      GO TO 200
    5 X=CSX4
      Y=CSY
      GO TO 200
    6 X=XLO
      Y=YHI-CSY2
      GO TO 200
    7 X=CSX4
      Y=YHI
      GO TO 200
    8 X=XLO
      Y=YHI+CSY
      GO TO 200
```

```
 9    RETURN
10    RETURN
11    X=XLO-CSX2
      Y=YLO+CSY2
      GO TO 200
12    X=XLO+CSX2
      Y=YLO+CSY2
      GO TO 200
13    X=-CSX2
      Y=YLO+CSY2
      GO TO 200
14    X=CSX2
      Y=YLO+CSY2
      GO TO 200
15    X=-CSX2
      Y=CSY2
      GO TO 200
16    X=CSX2
      Y=CSY2
      GO TO 200
200   CONTINUE
      ANGLE=0.0
      IF(I.GT.10) ANGLE=90.0
      CALL SYMBOL(X,Y,ANGLE,CZZ,NCHAR,TEXT)
      RETURN
      END
C
C
      SUBROUTINE NEWAX(XT,LXT,LINTX,YT,LYT,LINTY)
      COMMON/CCC/ XIN,YIN,XLO,XHI,YLO,YHI,BL,BR,BB,BT,XS,YS,XF,YF,CS
      CALL PLOTEND
      CALL VECTORS
C
CCC   DRAW BOX
C
      CALL PLOT(BL,BB,0,0)
      CALL PLOT(BR,BB,1,0)
      CALL PLOT(BR,BT,1,0)
      CALL PLOT(BL,BT,1,0)
      CALL PLOT(BL,BB,1,0)
      XORG=YORG=0.0
      CALL AXISL(XLO,XHI,XORG,YLO,YHI,YORG,XT,YT,LXT,LYT,LINTX,
     1   LINTY,1.,1.,CS)
      RETURN
      END
C
C
      SUBROUTINE SETUP(XINCH,YINCH,XL,XH,YL,YH)
      COMMON /CCC/ XIN,YIN,XLO,XHI,YLO,YHI,BL,BR,BB,BT,XS,YS,XF,YF,CS
      X90R=0.5
      Y90R=0.5
      XMARF=0.10
      YMARF=0.10
      YLABF=0.15
      XLO=XL
      YLO=YL
      XHI=XH
      YHI=YH
      XIN=XINCH
      YIN=YINCH
      XDIF=XH-XL
      XMAR=XDIF*XMARF
      XF=XINCH/(XDIF + 2.0*XMAR)
      XS=XINCH + 2.0*X90R
      X9IAS=X90R + (XF*XMAR)
      YDIF=YH-YL
      YMAR=YMARF*YDIF
      YLAB=YLABF*YDIF
      YF=YINCH/(YDIF+YLAB+2.0*YMAR)
      YS=YINCH + 2.*Y90R
      Y9IAS=Y90R + YF*(YMAR+YLAB)
      BL=XL-XMAR
      BR=XH+XMAR
      BB=YL-YLAB-YMAR
      BT=YH+YMAR
      CALL SIZE(XS,YS)
      CALL SCALE(XF,YF,X9IAS,Y9IAS,XL,YL)
C     CHARACTER SIZE SCALED ACCORDING TO YIN
      CS=0.09*FLOAT(1+IFIX(YIN/3.0))
      RETURN
      END
C
C
```

```
      FUNCTION TERP(A1,A2,A3,B1,B3)
      TERP = B1 + (B3-B1)*(A2-A1)/(A3-A1)
      RETURN
      END
C
C
      SUBROUTINE AUTO(A,N,AHI,AMAX,DECADE)
C
CCC   A(I)      ARRAY TO BE SCALED.  ALL A .GE.0.0
CCC   N         NUMBER OF ELEMENTS IN A
CCC   AHI       LARGEST A(I)
CCC   EXAMPLE:  IF AHI = 7231.0, THEN
CCC   AMAX=8000.0 AND DECADE=1000.0
C
      DIMENSION A(1)
      AHI=A(1)
      DO 30 I=1,N
      IF (A(I).LT.0.0)GO TO 50
      IF (A(I).GT.AHI) AHI=A(I)
   30 CONTINUE
      IF (AHI.EQ.0.) GO TO 70
      ALOG = ALOG10(AHI)
      ICHAR=IFIX(ALOG)
      AMANT=ALOG-FLOAT(ICHAR)
      DECADE=10.0**ICHAR
      FIG=10.0**AMANT
      AMAX=FLOAT(IFIX(FIG)+1) * DECADE
      RETURN
   50 CONTINUE
C
CCC   ERROR MESSAGE
C
      WRITE (45,60) I, A(I)
   60 FORMAT (// * ERROR IN AUTO--NEGATIVE NUMBER.*
     1    /  * ARRAY(*, I3, *) = *, F8.1  )
      RETURN
   70 WRITE (45,80)
   80 FORMAT (*0 ERROR IN AUTO- ALL ELEMENTS ZERO*)
      RETURN
      END
C
C
      SUBROUTINE MEAN(Y,N,AVG,STDEV,RELDEV)
      DIMENSION Y(1)
      FN=FLOAT(N)
      AVG=0.0
      DO 10 K=1,N
      AVG=AVG+Y(K)
   10 CONTINUE
      AVG=AVG/FN
      SD=0.0
      DO 30 I=1,N
      DIF=AVG-Y(I)
      SD=SD+DIF*DIF
   30 CONTINUE
      SD=SD/(FN-1.0)
      STDEV=SQRT(SD)
      RELDEV=100.*STDEV/AVG
      RETURN
      END
```